Response to comments of referee #1

General Comments

The main objective of this field study is to assess the impact of new particle formation (NPF) and secondary aerosol on the cloud condensation nuclei (CCN) budget in the summertime Arctic troposphere. To this end, a physico-chemical characterization of newly formed particles, their nucleation process and growth constituted the scaffolding of this work. The authors succeeded to run a formidable state of the art equipment onboard RV Polarstern during an Arctic research cruise. The presented results and conclusions are predicated on an in-depth and sound data evaluation. The authors clearly state assumptions and shortcomings (e.g. the lack of gaseous H2SO4 or in situ organic carbon measurements, which would have been beneficial to constrain nucleation and growth mechanism). Nevertheless, the presented outcome of this work is a considerable progress in understanding aerosol-cloud interaction and its climatic consequences during Arctic summertime. In my opinion, the authors organized their manuscript straightforward and their conclusions are widely comprehensible. Without doubt, the topic addresses the scientific scope of ACP and I recommend a final publication after some minor revisions I specified below.

REPLY:

We are contented that referee #1 sees the value of such studies. We also sincerely thank to referee #1 for his/her time, comments, and suggestions, which will indeed improve the manuscript. In the following, we would like to address the detailed comments step-by-step.

DETAILED COMMENTS

1. Chapter 2.1.1: I think you should better move the whole section to the corresponding places in the "Results" chapter, because it is reasonable to present this auxiliary information along with the described NPF events. In the present form, part of the information given now in chapter 2.1.1 are just repeated in chapter 3.

REPLY:

We agree with the referee #1 that information presented in chapter 2.1.1 can be moved to chapter 3. We also realized that part of the auxiliary information is truly repeated in chapter 3. Thus, we reviewed the mentioned chapters, dissolved chapter 2.1.1, and updated chapter 3 accordingly. Thank you for the insightful suggestion.

We have also noticed that chapter 3.1.3 shall indicate 26 June, and not 28. Changes are highlighted in yellow.

3.1.1 NPF 1: 1 June

The first NPF event with a subsequent particle growth was observed from around 6 am onwards on 1 June, 2017. The RV Polarstern reached the marginal ice zone at 11 am and entered the pack ice at around 3 pm on 31 May, 2017 (note that all times in this study are given in UTC). This can be seen from the air and water temperature profiles (Fig. 2). The temperature of air and water decreased from approx. +5 °C to -5 °C (air) and -2 °C (water). In this area, the ice was broken up by leads, which facilitated the passage of the vessel towards the north. Around 8 pm a region with more densely packed ice was reached, which obstructed the movement of the ship (Nicolaus, 2018). On these occasions, due to frequent reverse-forward ship movement, pollution highly affected the measurements on-board (see PNSDs in Fig. 1). On 1 June, the vessel could once again pass through open leads in the pack ice, allowing for contamination-free scans for the time period from 4 am to 8 pm. During this time, RV Polarstern moved 26 km (from 80.39°N 7.58°E to 80.62°N 7.94°E) in mostly cloud-free conditions. From 6 pm to 8 pm, a thin ice cloud was present in over 8 km altitude. Also, over a short period from 2 to 3 pm, intermittent low-level liquid clouds were present, which however did not decrease the global radiation significantly. For a more detailed description of local and associated large scale weather patterns during PS106 refer to Knudsen et al. (2018).

Before the NPF event, the average particle number concentration in a size range from 10 to 50 nm (PNC_{10-50}), was 50 particles cm^{-3}.

…

3.1.2 NPF 2: 18 June

On 17 June, the ship was moving southward through packed ice area, breaking floes and navigating through polynyas (Nicolaus, 2018). Over the complete day of 17 June, low-level stratocumulus clouds were present, which were broken up occasionally between 7 am and 1 pm, and 4 to 10 pm. Between 11 pm on 17 June and 1 am on 18 June, measured visibility decreased, accompanied by an increase in relative humidity (RH), indicating fog. This low-level cloud layer was present until approximately 8 am on 18 June, when RV Polarstern left the packed ice entering the marginal ice zone. This resulted in water and air temperature increase from -1.9 °C to approx. 2 and 0.5 °C above zero, respectively. At the same time, local wind speed decreased from 5 to 2 m s^{-1}. During the following hours, until 6 pm, no clouds were present except for a very thin, high ice cloud at 8 km from approximately 11:30 am to 12 pm. This period of high incident radiation was only briefly interrupted by a short fog event from 3 to 3:30 pm. During this whole time, RV Polarstern moved through open water, but was always surrounded by floating ice. Starting at 6 pm, a thin low-level cloud layer was present above the ship, which decreased the global radiation significantly. This cloud layer was present until the next day, 19 June, at approximately 12 pm. During 19 June, RV Polarstern was moving through open water and ice along the west coast of Spitsbergen Island (Fig. 1). From approximately 12:30 pm to 3 pm another short cloud-free period led to high global radiation. At 4 pm at approx. 3 km altitude a cloud moved in decreasing the global radiation once again.

The PNC_{10-50} and $PNC_{100-800}$ from 17 June prior to the NPF event were rather stable, with an average value of approx. 30 cm^{-3}.

…

3.1.3 NPF 3: 26 June

The third, least intensive NPF event occurred during the second leg of the expedition, 26 June, when RV Polarstern was at the marginal ice zone, around 200 km east of Svalbard, moving towards the North. Areas dominated by open water were passed by the vessel, as well as ice-covered water (Nicolaus, 2018). However, the ice was never very densely packed and the transit of the ship did not require breaking the ice. Low-level clouds and fog were present during all of 25 June to 27 June; on 28 of June a short period of cloud-free conditions was observed from around 4 to 6 am. There were two short floe stations, one on 25 June from around 5 pm until midnight and the other on 27 June from around midnight to 3 am.

The formation and growth of particles was already observed on both 24 and 25 June during less pronounced NPF events (not shown), when the ship was approx. 100 km South of Svalbard coast.

…

3.1.4 NPF 4: 2 July

From midnight of 1 July to 4 July, RV Polarstern was moving northwards from 81.64°N 32.62°E to 82.16°N 32.87°E. This region was mostly ice-covered with some open leads, through which the vessel could pass without having to break the ice. At this time of the expedition, melt ponds were observed frequently on the ice floes. On 1 July, there was a thick (up to 3 km altitude) low-level cloud layer present until 2 pm associated with some snow fall. After 1 pm, the cloud bottom height increased steadily; however, some intermittent fog was still present at sea level. A single fogbow was observed between 6:20 and 7 pm. The fog dissolved at midnight on 2 July. Almost throughout the entire day of 2 July, no clouds were present except for optically thin cirrus clouds, allowing for high solar irradiation.

On 2 July, the RV Polarstern ventured further into the Arctic ice, more than 300 km from the coasts of Svalbard and Prince George Land (81.51°N, 32.97°E).
…

2. Chapter 2.2.3, line 204 & 205: Please briefly specify in which way you determine particle hygroscopicity (I guess kappa is derived from CCNC data?).

REPLY:

Thank you for your question. The hygroscopicity parameter kappa was derived from VH-TDMA measurements (when instrument was running in H-TDMA mode). To specify this, we have included the following description to chapter 2.2.3:

The particle hygroscopicity parameter kappa (κ) was derived from VH-TDMA data following the κ-Köhler theory by Petters and Kreidenweis (2007):

$$\kappa = (GF^3 - 1) \cdot \left[\frac{1}{\mathrm{S}} \exp\left(\frac{4\sigma_\mathrm{s} \mathrm{M_W}}{\mathrm{RT}\rho_\mathrm{W} \mathrm{D_d} GF}\right) - 1\right] \tag{1}$$

where S is the saturation ratio; σ_s - the surface tension of the solution; M_W - the molecular weight of water; R - the universal gas constant; T - the temperature; ρ_W - the density of water; and D_d – particle dry diameter.

Since the new equation (Eq. 1) was introduced, we re-numbered the following equations accordingly.

3. Page 10, lines 283 to 287: Contamination control: Did you entirely rely on the CNC data or did you also include relative wind direction and velocity from the ships weather station?

REPLY:

Thank you for your question. A separate condensation particle counter (CPC) was used to measure total particle number concentration (PNC) with time resolution of 2 seconds (please note that in the text, chapter 3, time resolution was said to be 1 s, which is not correct). An exemplary data of PNC is presented in Fig. R1. It can be clearly seen that ship pollution heavily affects the momentary PNC. Even during NPF event, the maximum particle number concentration did not exceed 5000 particles cm^{-3}. Meanwhile, ship pollution resulted in order of magnitude higher concentrations. It is obvious that such increase must be related to ship exhaust pollution. Moreover, we have also compared PNC increase with a signal from Single Particle Soot Photometer (SP^2, operated inside the aerosol container by scientist from Alfred Wegener Institute. Data is not presented in the manuscript). After comparing the results from both SP^2 and CPC, we came to conclusion that CPC recorded sharp increase in PNC is a good indicator for ship-related pollution. Therefore, for online measurements only CPC and SMPS data was used for contamination inspection.

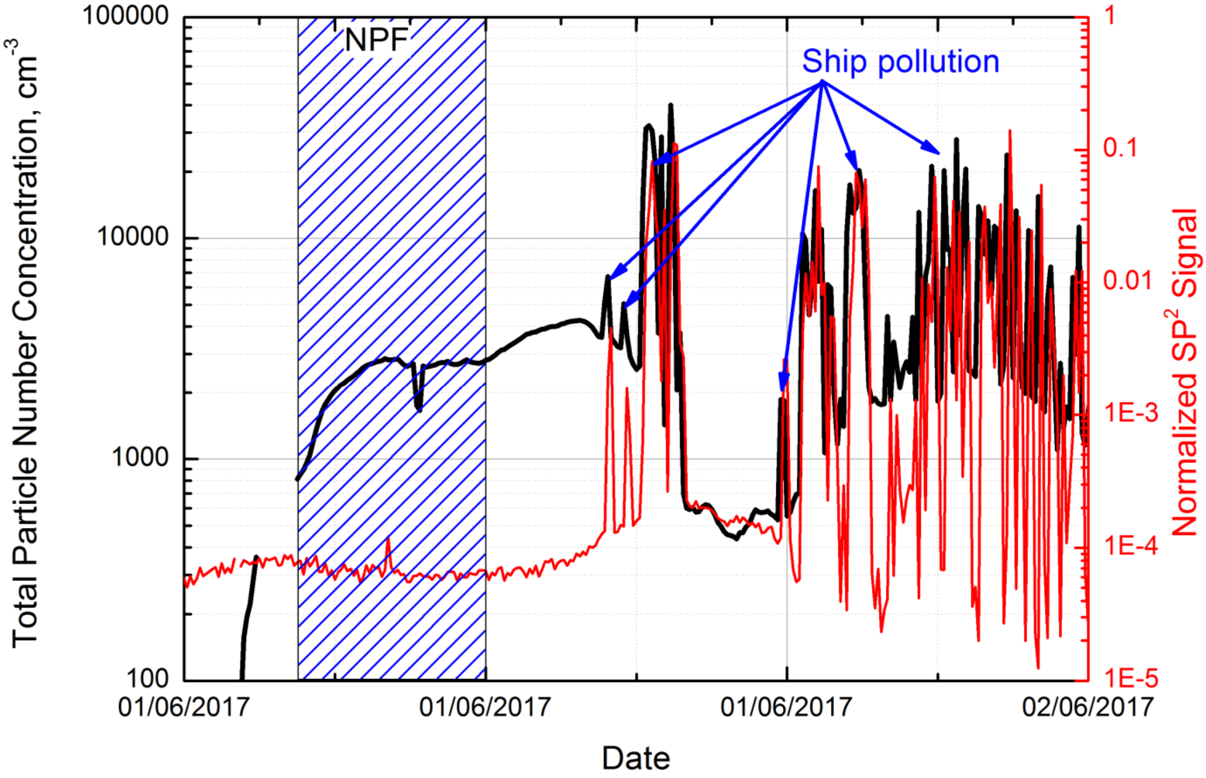

Fig. R1. Total particle number concentration during new particle formation event and contamination from ship.

That being said, automatic system (to measure relative wind direction) was installed together with high volume sampler to stop the pumps when wind came from a specific direction (related to ship exhaust). Similar approach was used by Huang et al. (2018), who performed her measurements inside same TROPOS measurement container onboard RV Polarstern. Berner impactor, on the other hand, did not have such system to prevent samples from contamination. However, in our work we did not use samples, which had high elemental carbon concentrations, indicating ship exhaust pollution.

Huang, S., Wu, Z., Poulain, L., van Pinxteren, M., Merkel, M., Assmann, D., Herrmann, H., and Wiedensohler, A.: Source apportionment of the organic aerosol over the Atlantic Ocean from 53° N to 53° S: significant contributions from marine emissions and long-range transport, Atmos. Chem. Phys., 18, 18043–18062, https://doi.org/10.5194/acp-18-18043-2018, 2018.

4. Page 10, lines 289 to 291: Data from Zeppelin Mountain Observatory: If these data are significant for your evaluation, I miss a more detailed discussion along with your results.

REPLY:

Thank you for your comment. Data from both Villum Research Station and Zeppelin Mountain Observatory was used only for supplementary information (to confirm whether NPF is a regional phenomenon) regarding NPF observed at RV Polarstern (as indicated in line 290: "data for visual inspection …"). We refrained ourselves from more detailed discussion, because we did not obtain/possess full data set regarding the NPF events. More detailed discussion would require a deeper look into data sets from Zeppelin Mountain Observatory and Villum Research Station, discuss the results with station responsible personnel/scientists etc., which is out of the scope of this study.

5. Page 18, lines 535 to 540: Estimating gaseous H2SO4 concentrations is crucial in order to describe nucleation and growth mechanism. If I understand aright, you used the tables and the given interpolation method presented by Yu (2010), where the basic input parameter is the observed nucleation rate (and not the growth rate)? Please clarify. In addition, you assume that because of the measured hygroscopicity parameter, only the binary system H2SO4-H2O is in the running and particularly not the tenary H2SO4-NH3-H2O system. In my view, it may still be worthwhile to envisage the latter option by comparison (see Napari et al., 2002).

REPLY:

Thank you for your comment/suggestion. For gaseous H2SO4 concentration, we reached out to Fangqun Yu (UAlbany), who was kind to introduce us to FORTRAN routine, which we used to estimate the assumed gas participating in NPF. The H2SO4 concentration was obtained by matching our calculated nucleation rate with corresponding modeled nucleation rate by varying H2SO4 concentration. When preparing the manuscript, we were also intended to use ternary nucleation mechanism to investigate our observed nucleation rates, however, Prof. Yu unfortunately did not have look up tables for ternary nucleation. Thus, we are grateful to referee #1, who pointed us to a valuable source of information, which we previously missed.

Based on our observed formation rates and Napari et al. (2002) parametrization, we estimated the concentrations of H2SO4 and NH3 (Fig. R2), which ranged from 1 x 10^4 to 5 x 10^6 cm^{-3}, and 0.1 to 100 ppt, respectively. Assuming Napari et al. (2002) used ppt as pptv for NH3, we see that such concentrations of ammonia can be indeed found in Artic region (Wentworth et al., 2016). In manuscript (Lines 560 – 570), we provided some sort of discussion regarding ammonia involvement in nucleation, which we expanded based on new results from the parametrization of ternary system, as suggested by referee #1. We have included the following text into manuscript:

Some studies (e.g. Croft et al., 2016; Köllner et al., 2017) identified that certain nitrogen-containing species such as ammonia and amines are linked to particle growth in the Arctic region. To test this, we investigate the formation rate of critical clusters using a parametrization of the ternary H_2SO_4-NH_3-H_2O system, presented by Napari et al. (2002). That is, we adjust the concentrations of H_2SO_4 and NH_3 until we get the formation rate close to that of observed value. The estimated concentrations of H_2SO_4 and NH_3 varied from 1 x 10^4 to 5 x 10^6 cm^{-3} and 0.1 to 100 ppt, respectively (see supplementary material). According to Wentworth et al. (2016), such concentrations of NH_3 can be indeed found in the Artic region. There is evidence that H_2SO_4-NH_3-H_2O clusters are only partly neutralized under atmospheric conditions (e.g. Kurtén et al., 2007; Schobesberger et al., 2015). On the other hand, Asmi et al. (2010) reported that Aitken mode particles are somewhat more neutralized. Now, if we assume that the newly formed particles were partly neutralized by ammonia (as suggested by Giamarelou et al., 2016), we would expect particle hygroscopicity to be close to that of ammoniated sulfates. However, our observed HGF of 20 and 30 nm particles during both events were somewhat lower (e.g. 1.46 versus 1.64, Asmi et al., 2010).

References:

Asmi, E., Frey, A., Virkkula, A., Ehn, M., Manninen, H.E., Timonen, H., Tolonen-Kivimäki, O., Aurela, M., Hillamo, R. and Kulmala, M.: Hygroscopicity and chemical composition of Antarctic sub-micrometre aerosol particles and observations of new particle formation. Atmospheric Chemistry and physics, 10, 4253-4271, 2010.

Kurtén, T., Torpo, L., Sundberg, M.R., Kerminen, V.M., Vehkamäki, H. and Kulmala, M.: Estimating the NH3:H2SO4 ratio of nucleating clusters in atmospheric conditions using quantum chemical methods. Atmospheric Chemistry and Physics, 7, 2765-2773, 2007.

Schobesberger, S., Franchin, A., Bianchi, F., Rondo, L., Duplissy, J., Kürten, A., Ortega, I.K., Metzger, A., Schnitzhofer, R., Almeida, J. and Amorim, A.: On the composition of ammonia–sulfuric-acid ion clusters during aerosol particle formation. Atmospheric Chemistry and Physics, 15, 55-78, 2015.

Wentworth, G. R., Murphy, J. G., Croft, B., Martin, R. V., Pierce, J. R., Côté, J.-S., Courchesne, I., Tremblay, J.-É., Gagnon, J., Thomas, J. L., Sharma, S., Toom-Sauntry, D., Chivulescu, A., Levasseur, M., and Abbatt, J. P. D.: Ammonia in the summertime Arctic marine boundary layer: sources, sinks, and implications. Atmospheric Chemistry and Physics, 16, 1937–1953, 2016.

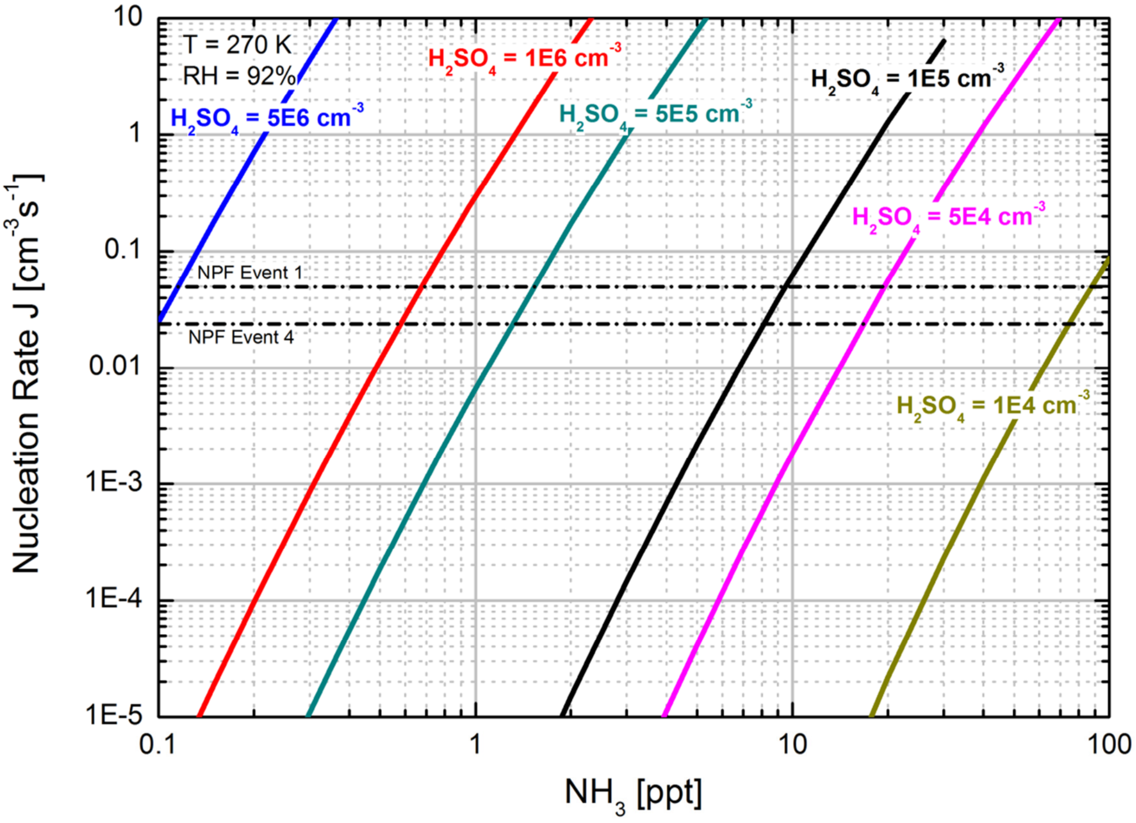

Fig. R2. Nucleation rate as a function of ammonia mixing ratio at T= 270 K and RH= 92% (according to parametrization by Napari et al. (2002). Total sulfuric acid concentration (in molecules per cm^3) is indicated for each curve. Dash-dot lines show the observed formation rate limits.

We have also included Fig. R2 to supplementary material.

6. Page 19, line 559: Sorry for nagging, but being a chemist, I have to note that ammonia is not an organic species (though it could be biogenic, if you mean this).

REPLY:

Thank you for your remark on this chemical incorrectness. Nagging is accepted. It is true that ammonia is not an organic species. However, ammonia is not exclusively biogenic either, even though biogenic sources are considered the biggest contributors for the Arctic atmosphere. Taking all into consideration, we changed the text in line 559 as follows:

Some studies (e.g. Croft et al., 2016; Köllner et al., 2017) identified that certain nitrogen-containing species such as ammonia and amines are linked to particle growth in the Arctic region.

7. Page 22, line 655 and eq. (7): The CCN increase due to NPF is defined as the difference between the CCN formed under background aerosol with diameter >100 nm and the CCN resulting from NPF. I do not understand why you used a cut-off of 100 nm defining background conditions. First, the model handles a bi-modal size distribution with geometric mean diameter and geometric standard deviation as input. Secondly, during all NPF events to be considered (referring to Fig. 2), particles did not grow above 50 nm. Thus, if at all, it would be reasonable defining a cut-off at around 50 nm instead of 100 nm for the background case. Please clarify!

REPLY:

Thank you for your comment. We agree that the definition of the CCN increase is somewhat not clear. In the following, we would like to clarify the line of thought when calculating the CCN increase due to NPF:

1. We calculate CCN number concentration resulting from parcel model using input values presented in Table 3. That is, we use those PNSDs, which is a result of new particle formation and subsequent growth. Model then outputs the CCN number concentration resulting from each mode (smaller particle mode at 13 to 44 nm; and larger particle mode at 101 to 194 nm). Total CCN number concentration is then a sum of CCN number from each mode. Please note that we calculate CCN number concentration resulting from 2 modes.
2. We then take total CCN number concentration (resulting from bi-modal size distribution, influenced by NPF) and divide it by the number of CCN resulting only from uni-modal distribution of >100 nm particles (from a different parcel model run, including only accumulation mode particles). We called these (>100 nm) particles as background aerosol, because from our observations it seems that it is always present in the Arctic atmosphere. In figure 2, one can see that average PNSD (PNSDs were taken from the cleanest episodes observed onboard RV Polarstern: 31 May 15:00 to 1 June 06:00; 14 June 15:00 to 15 June 15:00; 1 July 15:00 to 2 July 03:00; 5 July 21:00 to 6 July 12:00; 8 July 00:00 to 8 July 12:00) is indeed composed of two modes with geometric mean diameters at 22 and 132 nm.

   It might sound reasonable to calculate the increase in CCN number concentration with the reference to average background PNSD (which includes two modes). However, if looked at overall campaign PNSDs (not shown in the manuscript; available at request), in many cases the smaller particle mode is a result of new particle formation that happened either in the past days, or different location (and were transported to measurement site). Moreover, during NPF at 1 June, mode at <50 nm was not present at all. Another way would be to use PNSDs recorded just before each NPF event (Fig. R3). However, in this case, <50 nm particle mode is also frequently a result of the past NPFs. Therefore, it would be not entirely correct to include <50 nm mode if we want to estimate the increase in CCN number concentration due to NPF.

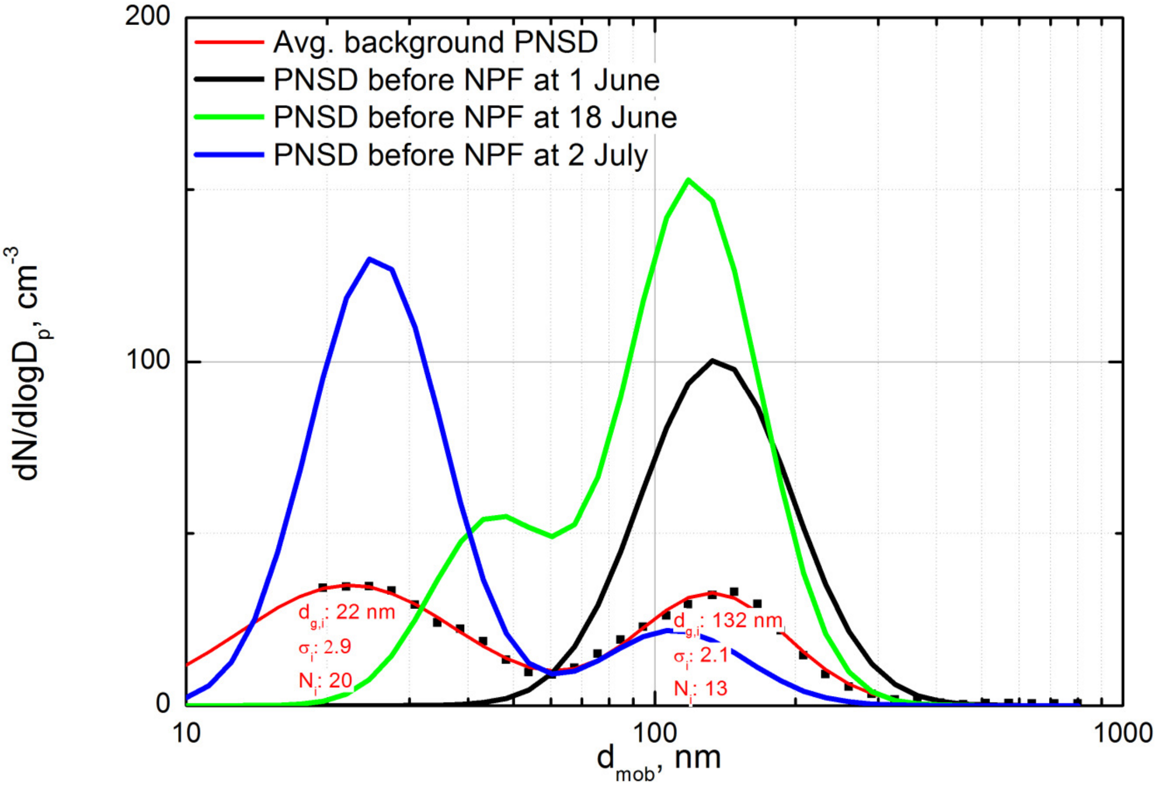

Fig. R3. Particle number size distributions (PNSD) measured prior new particle formation and campaign average PNSD (derived from the clean episodes). Please note that the mode at geometric mean diameter > 100 nm is present in all the cases, which cannot be said about ultrafine particle mode (PNSD before NPF at 1 June).

That being said, we have re-analyzed the increase in CCN number concentration in two different ways: 1) using the CCN number concentration resulting from campaign average PNSD (PNSD only from clean episodes); and b) using the CCN number concentration resulting from PNSD measured just before the NPF. Because we did not measure the hygroscopicity parameter kappa of 20 nm particles continuously, we used kappa value of 0.28 (average kappa value of 16-25 nm particles, measured during NPF). For accumulation mode particles, we assumed kappa of 0.33 (campaign average). In case 1, the number concentration of CCN (resulting from campaign average background PNSD) was 17 and 28 cm^{-3}, for updraft wind speeds of 0.1 and 3.2 m s^{-1}, respectively. This gave us the CCN number increase by 2 to 11 fold (versus 2 to 5 if old calculation from manuscript is used) for updraft wind speed of 0.1 m s^{-1}. For updraft wind speed of 3.2 m s^{-1}, the increase in CCN number was even higher – from 8 to 51 fold (versus 4 to 32 if old calculation from manuscript is used)

For case 2, the number concentration of CCN (resulting from PNSD just before NPF) depends on a specific PNSD, which was measured before every NPF event. Let us start with 1 June. The CCN number concentration, resulted from PNSD measured during 1 June (Fig. R3, black line) was 35 (for 0.1 m s^{-1} updraft wind) and 40 (for 3.2 m s^{-1} updraft wind) cm^{-3}. For lower updraft wind speed, parcel model did not show any increase in CCN number. However, for higher updraft wind, the CCN increase was 29 fold (versus 10 fold if old calculation method is used). For 18 June, the CCN increase was from 2 to 4 fold (same as in our old calculations) and from 6 to 20 fold (versus 6 to 32 fold in our old calculations) for updraft wind speeds of 0.1 and 3.2 m s^{-1}, respectively. And finally for 2 July, the CCN concentration increase was 5 fold in both updraft wind speed cases (same as in our old calculation). Please note that we did not include here calculations for 26 June NPF, because PNSD prior NPF was strongly affected by NPF on 24 and 25 June.

The main conclusions from such an exercise could be as follows:

1. Aerosol particle mode at geometric mean diameter of >100 nm was always present during the measurement campaign.
2. This cannot be said about <50 nm particle mode (see Fig. R3, PNSD before 1 June NPF).
3. It may seem sensible to use campaign averaged PNSD from clean episodes to define background PNSD, however, from our measurements, we noticed that in most cases the smaller particle mode is a result of NPF (either past days or transported from different location). Thus, it is not very precise to include nucleation mode particles in background aerosol definition when we try to estimate the increase in CCN number due to NPF.
4. Another approach could be using PNSD before NPF event to define background aerosol (same problem as in point 3).
5. We have calculated the increase in CCN concentration using two different PNSDs: for case one, campaign clean episode average PNSD; and PNSD recorded just before NPF event (point 3 and point 4 of these conclusions). We found that in case campaign average PNSD is assumed as background aerosol, the CCN increase is even higher (up to 11 fold (versus 5 fold; for updraft wind speed of 0.1 m s^{-1}). In case the PNSD prior NPF event was assumed as background aerosol, there was almost no difference compared to the results obtained using the methodology presented in the manuscript.
6. In both cases, we were able to show the CCN increase due to NPF.

Therefore, we tend to believe that our methodology to estimate the CCN number increase is correct (least wrong; we do not want to include <50 nm mode particles in the calculation, because most of the time these particles were the result of NPF during previous days). Nevertheless, we agree with referee #1 that some clarification is needed in the manuscript. For this, in the manuscript we have changed the following:

We define the CCN number concentration (N_{CCN}) increase due to particles created in the nucleation process as:

$$Increase\ of\ N_{CCN} = \frac{(N_{CCN,bp} + N_{CCN,NPF})}{N_{CCN,bp}}, \qquad (8)$$

where $(N_{CCN,bp} + N_{CCN,NPF})$ is the number concentration of CCN resulting from the particles created in NPF event (calculated from bi-modal PNSD using parcel model; see Table 3 for simulation parameters) and $N_{CCN,bp}$ is the CCN number concentration resulting entirely from accumulation mode particles present during the NPF event (newly formed particle mode is suppressed in parcel simulation). For more detailed discussion about CCN increase calculation, please refer to supplementary materials.

Moreover, we included the above discussion to supplementary material.

8. Figure 2: This series of figures show a wealth of information that I could not really decipher in the present printed version. A magnification of the on-line version is necessary, but the resolution of the figures are somewhat poor. I would therefore recommend remedying this point.

REPLY:

Thank you for your recommendation. We realized that the quality of on-line version of figure 2 is truly poor. This may have happened due to the following: we have prepared the manuscript using MS Word. Meaning, Fig. 2 was imported and had to be resized to fit A4 format. Later, for submission to ACP, MS Word document was converted to pdf. We did not upload Fig. 2 as a separate vector graphics picture, resulting in poor resolution. We will make sure that in final version of manuscript, the highest quality figure will be included. For the moment, we attach Fig. 2 once again (in landscape orientation to maximize the resolution).

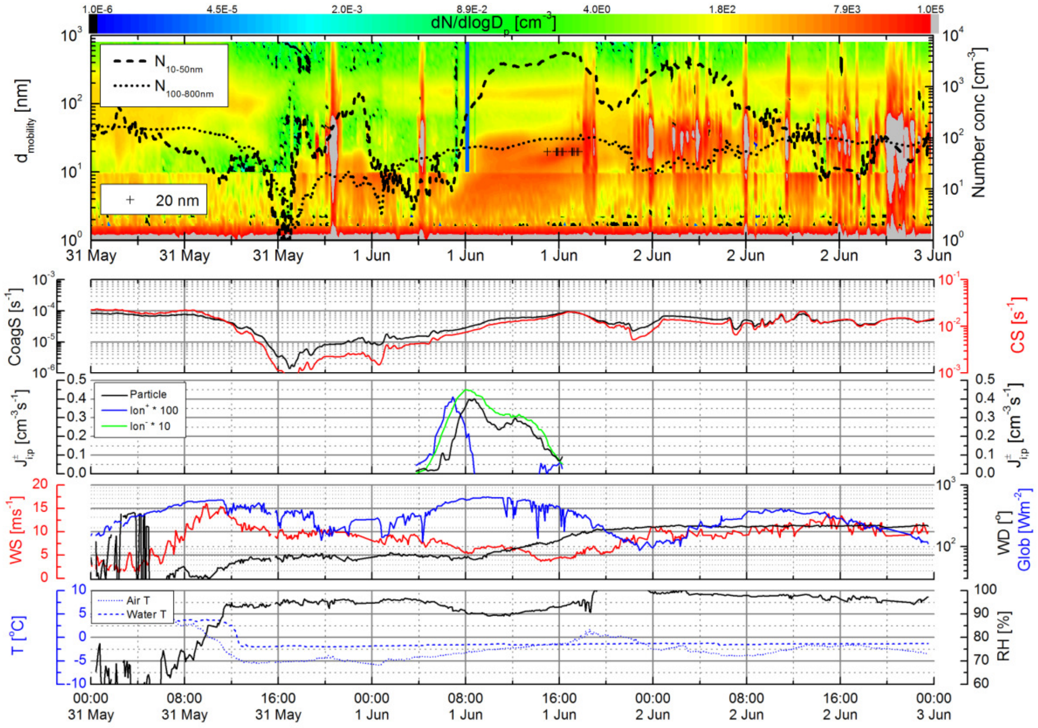

dN/dlogD$_p$ [cm^{-3}]
1.0E-6
4.5E-5
2.0E-3
8.9E-2
4.0E0
1.8E2
7.9E3
1.0E5
d$_{mobility}$ [nm]
Number conc [cm^{-3}]
N$_{10-50nm}$
N$_{100-800nm}$
+ 20 nm
31 May
1 Jun
2 Jun
3 Jun
CoagS [s^{-1}]
CS [s^{-1}]
J$^{\pm}_{i,p}$ [cm^{-3}s^{-1}]
Particle
Ion^{+} * 100
Ion^{-} * 10
WS [ms^{-1}]
WD [°]
Glob [Wm^{-2}]
T [°C]
RH [%]
Air T
Water T
00:00 31 May
08:00 31 May
16:00 31 May
00:00 1 Jun
08:00 1 Jun
16:00 1 Jun
00:00 2 Jun
08:00 2 Jun
16:00 2 Jun
00:00 3 Jun

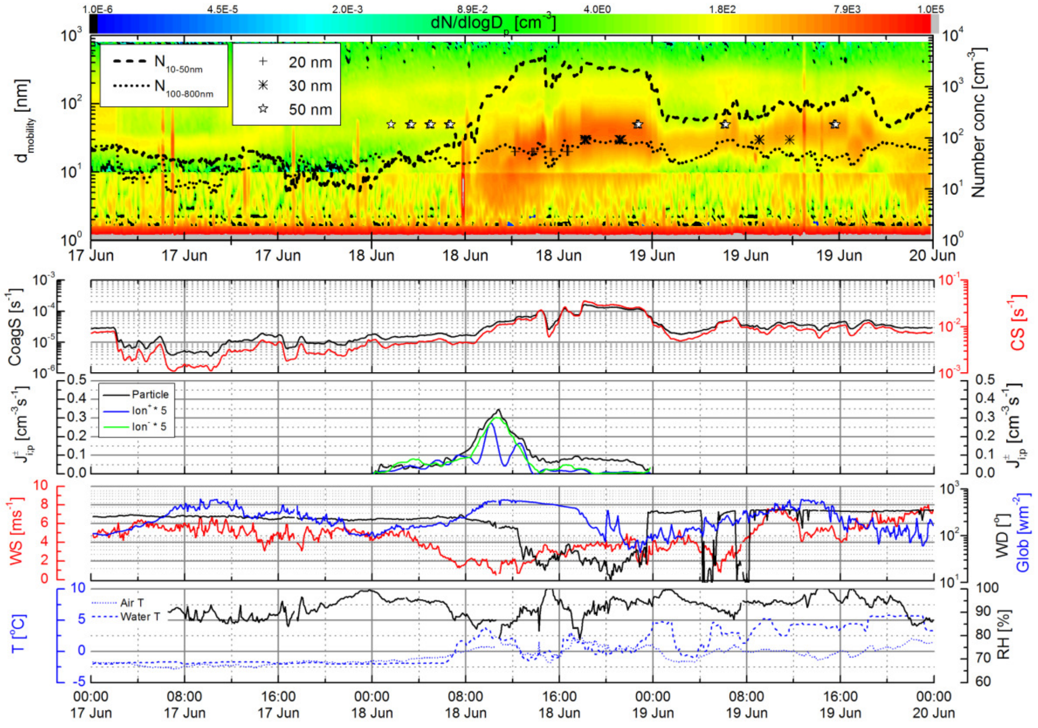

dN/dlogD$_p$ [cm^{-3}]
1.0E-6
4.5E-5
2.0E-3
8.9E-2
4.0E0
1.8E2
7.9E3
1.0E5
d$_{mobility}$ [nm]
Number conc [cm^{-3}]
N$_{10-50nm}$
N$_{100-800nm}$
+ 20 nm
✳ 30 nm
☆ 50 nm
17 Jun
18 Jun
19 Jun
20 Jun
CoagS [s^{-1}]
CS [s^{-1}]
J$^{\pm}_{i,p}$ [cm^{-3}s^{-1}]
Particle
Ion^{+} * 5
Ion^{-} * 5
WS [ms^{-1}]
WD [°]
Glob [Wm^{-2}]
T [°C]
RH [%]
Air T
Water T
00:00 17 Jun
08:00 17 Jun
16:00 17 Jun
00:00 18 Jun
08:00 18 Jun
16:00 18 Jun
00:00 19 Jun
08:00 19 Jun
16:00 19 Jun
00:00 20 Jun

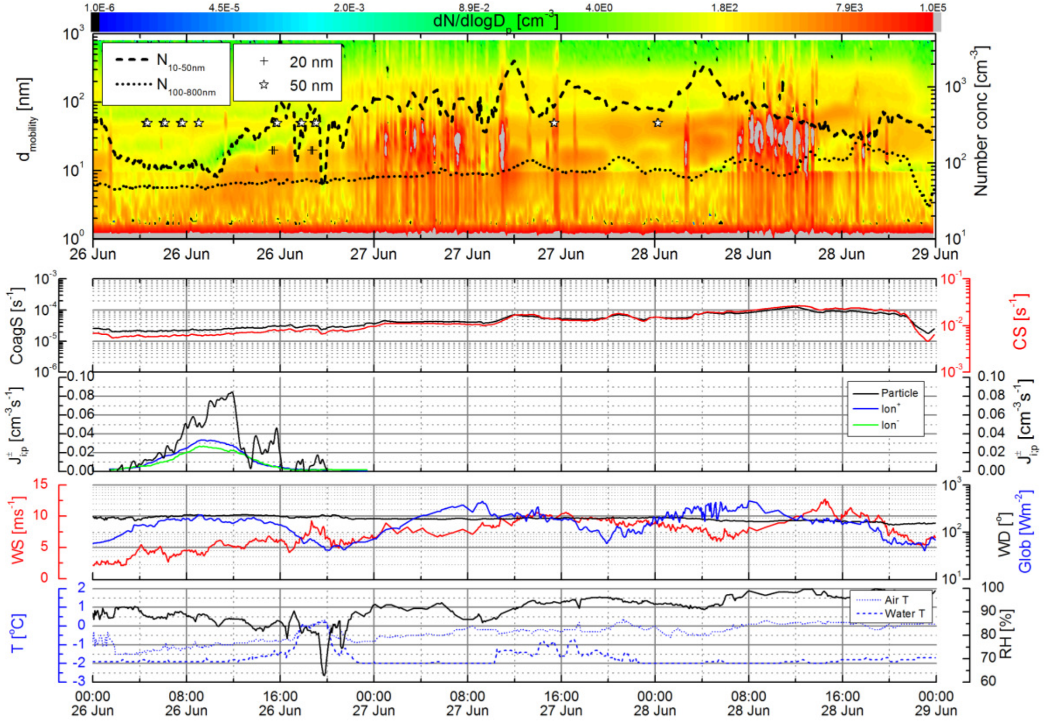

dN/dlogD$_p$ [cm^{-3}]
1.0E-6
4.5E-5
2.0E-3
8.9E-2
4.0E0
1.8E2
7.9E3
1.0E5
d$_{mobility}$ [nm]
Number conc [cm^{-3}]
N$_{10-50nm}$
N$_{100-800nm}$
+ 20 nm
☆ 50 nm
26 Jun
27 Jun
28 Jun
29 Jun
CoagS [s^{-1}]
CS [s^{-1}]
J$^{\pm}_{i,p}$ [cm^{-3}s^{-1}]
Particle
Ion^{+}
Ion^{-}
WS [ms^{-1}]
WD [°]
Glob [Wm^{-2}]
T [°C]
RH [%]
Air T
Water T
00:00 26 Jun
08:00 26 Jun
16:00 26 Jun
00:00 27 Jun
08:00 27 Jun
16:00 27 Jun
00:00 28 Jun
08:00 28 Jun
16:00 28 Jun
00:00 29 Jun

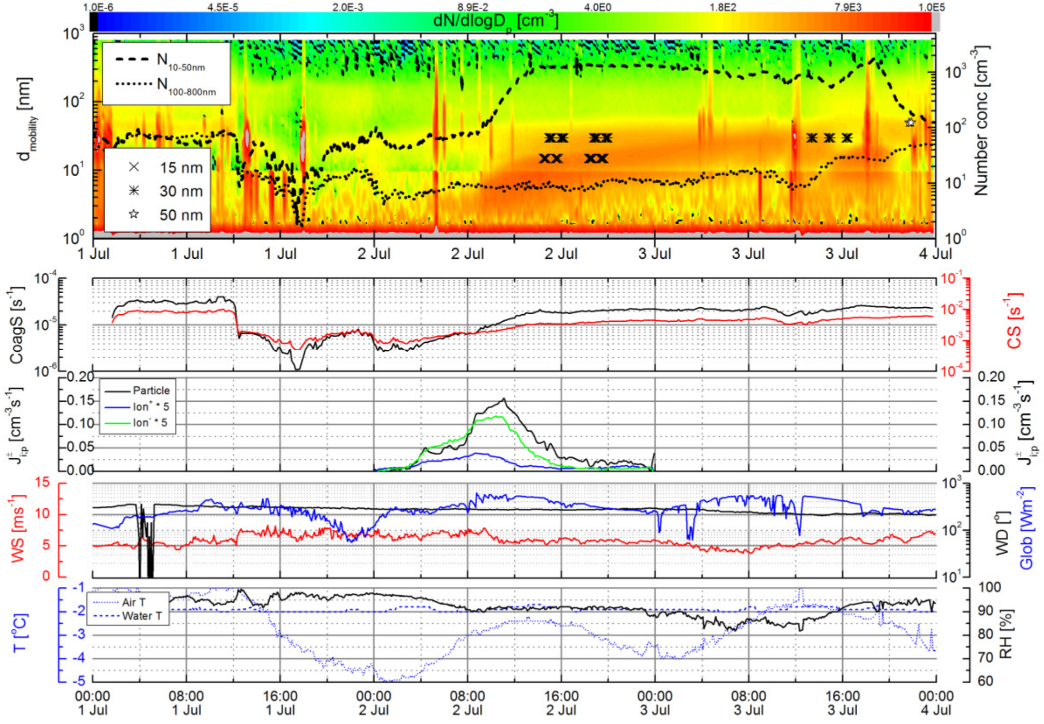

dN/dlogD$_p$ [cm^{-3}]
1.0E-6
4.5E-5
2.0E-3
8.9E-2
4.0E0
1.8E2
7.9E3
1.0E5
d$_{mobility}$ [nm]
Number conc [cm^{-3}]
N$_{10-50nm}$
N$_{100-800nm}$
× 15 nm
✳ 30 nm
☆ 50 nm
1 Jul
2 Jul
3 Jul
4 Jul
CoagS [s^{-1}]
CS [s^{-1}]
J$^{\pm}_{i,p}$ [cm^{-3}s^{-1}]
Particle
Ion^{+} * 5
Ion^{-} * 5
WS [ms^{-1}]
WD [°]
Glob [Wm^{-2}]
T [°C]
RH [%]
Air T
Water T
00:00 1 Jul
08:00 1 Jul
16:00 1 Jul
00:00 2 Jul
08:00 2 Jul
16:00 2 Jul
00:00 3 Jul
08:00 3 Jul
16:00 3 Jul
00:00 4 Jul

9. Figure 4: Fine, but what is about sea salt (Na+ and/or Cl-) data? These results are equally of some interest. For instance, a correlation with OC could give a hint whether part of the OC is primary aerosol that may be generated in conjunction with sea spray (just a mere suggestion for my part).

REPLY:

Thank you for the suggestion. We agree that looking at sea salt data is worthwhile, thus, we added a size-resolved sodium data to Figure 4 (see below). Sodium was mainly found on aerosol particles on Berner stages 3-5, while the majority of OM was determined on the submicron particles (Berner stages 1-3).

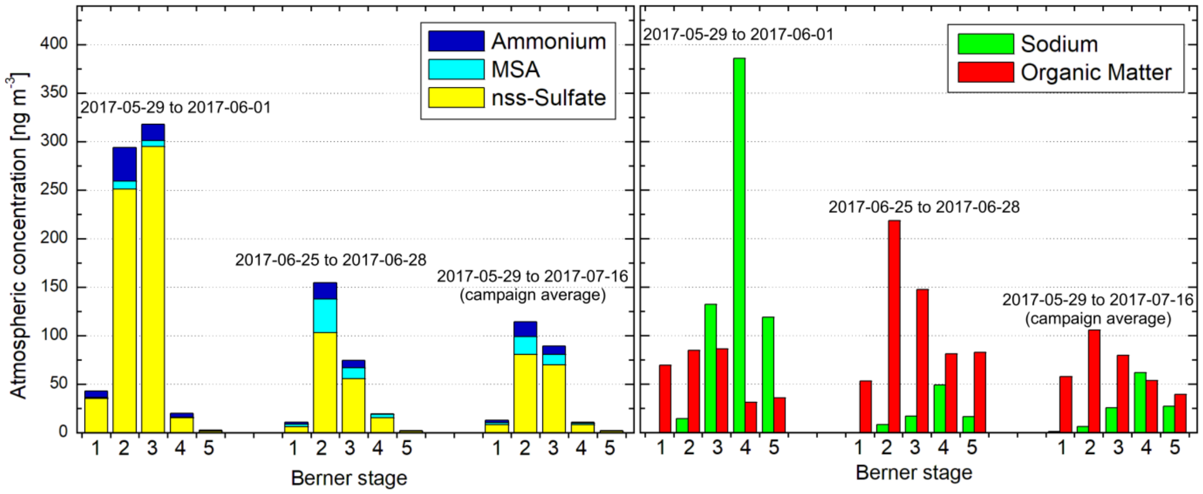

Figure 4: Size-resolved atmospheric concentrations for ammonium, MSA, nss-sulfate, sodium, and OM for two sampling periods and the whole campaign average.

Accordingly, we added this aspect to the text in the manuscript (Lines 435-447):

Sodium was mainly found on Berner stages 3 – 5. The sodium values for the sampling period from 25 to 28 June (Berner stage 4: 49 ng m-3) were quite similar to the average values, while the impactor samples from 29 May to 1 June showed much higher atmospheric concentrations (Berner stage 4: 386 ng m-3). This agrees well to previous studies, which show that atmospheric sea salt is mostly present in super-micron particles, while OM contributes strongly to the submicron particle composition (e.g. Müller et al., 2010). Previous works also suggest that OM is strongly enriched during the bubble bursting process (compared to sea salt) and therefore OM and sea salt are not transferred to the same extend from seawater to the aerosol particles (Keene et al., 2007; Quinn et al., 2015; Van Pinxteren et al., 2017). It is possible that increased sodium and OM, observed during NPF 1, is a result of sea spray, however, due to low sampling time resolution of Berner cascade impactor, we restrict ourselves from such conclusion. Moreover, please note that the increased values of sodium during this time period may be related to ship's proximity to open water (RV Polarstern reached the marginal ice zone only on 31 May), while the increase in OM could have happened later (e.g. 1 June), yet, included in the same sample. In chemical sample analysis, we did not find any positive correlation between OM/OC and sodium, concerning the different aerosol size classes. A more detailed chemical characterization of the aerosol particles during PS 106 cruise will be addressed in a separate publication.

Further changes:

We noticed that we missed to give a direct link between the Berner stages and their corresponding particle size. We fix this by including the following text into manuscript section 2.2.5:

The sampling of aerosol particles was conducted using five-stage low-pressure Berner impactors (Hauke, Austria) with a flow rate of 75 L min^{-1}, which was installed on the top of the observation deck facing the ocean at a height of ca. 25 m. Particles were collected in the size ranges 0.05 – 0.14 µm (stage 1), 0.14 – 0.42 µm (stage 2), 0.42 – 1.2 µm (stage 3), 1.2 – 3.5 µm (stage 4), and 3.5 – 10 µm (stage 5) aerodynamic particle diameter (50% cut-off) on aluminum foils as impaction substrates, which had been heated at 350 °C for at least 2 hours to reduce blank levels prior to sampling.

10. Page 16, line 453: It should be 5.4 nm h-1 (not 5.4 h-1).

REPLY:

Thank you. We fixed the noted typo.

11. Page 23, line 678: ...it can be concluded (not conclude).

REPLY:

Thank you. We fixed the noted typo.

Response to comments of referee #2

This manuscript describes an interesting and valuable set of measurements made aboard Polarstern in the region near Svalbard, during May to July 2017. The authors report measurements of neutral and charged clusters particle size (together covering a size range on <1 - 800nm), particle hygroscopicity and cloud condensation nuclei. Measurements of nucleation mode particle size and charged/neutral cluster abundance have been rarely made in Arctic regions, making this a unique and valuable data set that indirectly furthers our knowledge on the identity of species responsible for Arctic nucleation and initial growth of particles to Aitken mode sizes. The manuscript is well written and largely well organized. The following comments are intended to improve an already very good manuscript.

REPLY:

We thank to referee #2 for understanding the value of such studies. We also appreciate referee for his/her time, comments, and suggestions, which are intended to improve the manuscript. In the following, we would like to address the comments step-by-step.

General Comments

12. L65-73: This is an important section of the introduction, and at present is missing several of the relatively small amount of studies that exist. Since so few data sets exist, it is reasonable to cite them even if they are not all discussed in detail. Some that should be included are listed here: Freud et al, doi:10.5194/acp-17-8101-2017; Nguyen et al, doi: 10.5194/acp-16-11319-2016; Dall'Osto et al, doi: 10.5194/acp-19-7377-2019; Burkart et al, doi: 10.5194/acp-17-5515-2017; Burkart et al, doi: 10.1002/2017gl075671; Collins et al., doi: 10.5194/acp-17-13119-2017; Leaitch et al., doi: 10.12952/jour-nal.elementa.000017; Tremblay et al., doi: doi.org/10.5194/acp-19-5589-2019; These and others were recently reviewed in doi: 10.1029/2018rg000602.

REPLY:

Thank you for the comment. We have included the suggested references to manuscript. We have also re-wrote introduction to briefly overview the main findings of mentioned studies. Changes in introduction can be seen in yellow in a new manuscript version.

13. The discussion of ship deck observations in Section 2.1.1 may serve the reader better if they were incorporated into the larger discussion of NPF events in Section 3.1

REPLY:

Thank you for your suggestion. We merged Section 2.1.1 into Section 3.1. We agree that ship deck observations serve the reader better if they are incorporated into the discussion. Also, we noticed that some of the information is redundant. Changes are highlighted in yellow.

3.1.1 NPF 1: 1 June

The first NPF event with a subsequent particle growth was observed from around 6 am onwards on 1 June, 2017. The RV Polarstern reached the marginal ice zone at 11 am and entered the pack ice at around 3 pm on 31 May, 2017 (note that all times in this study are given in UTC). This can be seen from the air and water temperature profiles (Fig. 2). The temperature of air and water decreased from approx. +5 °C to -5 °C (air) and -2 °C (water). In this area, the ice was broken up by leads, which facilitated the passage of the vessel towards the north. Around 8 pm a region with more densely packed ice was reached, which obstructed the movement of the ship (Nicolaus, 2018). On these occasions, due to frequent reverse-forward ship movement, pollution highly affected the measurements on-board (see PNSDs in Fig. 1). On 1 June, the vessel could once again pass through open leads in the pack ice, allowing for contamination-free scans for the time period from 4 am to 8 pm. During this time, RV Polarstern moved 26 km (from 80.39°N 7.58°E to 80.62°N 7.94°E) in mostly cloud-free conditions. From 6 pm to 8 pm, a thin ice cloud was present in over 8 km altitude. Also, over a short period from 2 to 3 pm, intermittent low-level liquid clouds were present, which however did not decrease the global radiation significantly. For a more detailed description of local and associated large scale weather patterns during PS106 refer to Knudsen et al. (2018).

Before the NPF event, the average particle number concentration in a size range from 10 to 50 nm (PNC_{10-50}), was 50 particles cm^{-3}.

…

3.1.2 NPF 2: 18 June

On 17 June, the ship was moving southward through packed ice area, breaking floes and navigating through polynyas (Nicolaus, 2018). Over the complete day of 17 June, low-level stratocumulus clouds were present, which were broken up occasionally between 7 am and 1 pm, and 4 to 10 pm. Between 11 pm on 17 June and 1 am on 18 June, measured visibility decreased, accompanied by an increase in relative humidity (RH), indicating fog. This low-level cloud layer was present until approximately 8 am on 18 June, when RV Polarstern left the packed ice entering the marginal ice zone. This resulted in water and air temperature increase from -1.9 °C to approx. 2 and 0.5 °C above zero, respectively. At the same time, local wind speed decreased from 5 to 2 m s^{-1}. During the following hours, until 6 pm, no clouds were present except for a very thin, high ice cloud at 8 km from approximately 11:30 am to 12 pm. This period of high incident radiation was only briefly interrupted by a short fog event from 3 to 3:30 pm. During this whole time, RV Polarstern moved through open water, but was always surrounded by floating ice. Starting at 6 pm, a thin low-level cloud layer was present above the ship, which decreased the global radiation significantly. This cloud layer was present until the next day, 19 June, at approximately 12 pm. During 19 June, RV Polarstern was moving through open water and ice along the west coast of Spitsbergen Island (Fig. 1). From approximately 12:30 pm to 3 pm another short cloud-free period led to high global radiation. At 4 pm at approx. 3 km altitude a cloud moved in decreasing the global radiation once again.

The PNC_{10-50} and $PNC_{100-800}$ from 17 June prior to the NPF event were rather stable, with an average value of approx. 30 cm^{-3}.

…

3.1.3 NPF 3: 26 June

The third, least intensive NPF event occurred during the second leg of the expedition, 26 June, when RV Polarstern was at the marginal ice zone, around 200 km east of Svalbard, moving towards the North. Areas dominated by open water were passed by the vessel, as well as ice-covered water (Nicolaus, 2018). However, the ice was never very densely packed and the transit of the ship did not require breaking the ice. Low-level clouds and fog were present during all of 25 June to 27 June; on 28 of June a short period of cloud-free conditions was observed from around 4 to 6 am. There were two short floe stations, one on 25 June from around 5 pm until midnight and the other on 27 June from around midnight to 3 am.

The formation and growth of particles was already observed on both 24 and 25 June during less pronounced NPF events (not shown), when the ship was approx. 100 km South of Svalbard coast.

…

3.1.4 NPF 4: 2 July

From midnight of 1 July to 4 July, RV Polarstern was moving northwards from 81.64°N 32.62°E to 82.16°N 32.87°E. This region was mostly ice-covered with some open leads through which the vessel could pass without having to break the ice. At this time of the expedition, melt ponds were observed frequently on the ice floes. On 1 July, there was a thick (up to 3 km altitude) low-level cloud layer present until 2 pm associated with some snow fall. After 1 pm, the cloud bottom height increased steadily; however, some intermittent fog was still present at sea level. A single fogbow was observed between 6:20 and 7 pm. The fog dissolved at midnight on 2 July. Almost throughout the entire day of 2 July, no clouds were present except for optically thin cirrus clouds, allowing for high solar irradiation.

On 2 July, the RV Polarstern ventured further into the Arctic ice, more than 300 km from the coasts of Svalbard and Prince George Land (81.51°N, 32.97°E).

…

14. A detailed description of how pollution influence from the ship was reproducibly removed from the data set needs to be included in the Methods section. Was the influence quantified with a specific measurement (e.g., rapid variability in particle concentrations in a certain size range?)? Or, was a specific wind sector removed from the data? "Abrupt and short increases in particle number concentration recorded by a CPC" as cited in L286 as the method for filtering ship stack pollution; this should be elaborated in the methods section and detail is needed on how the authors determined that "most of the cases when the particle number increased tenfold" could be attributed to NPF. I strongly discourage the authors from including periods of ship pollution in Figure 2 (noted in L374-375). I disagree that "better representation of particle growth" (L1031-1032) warrants this.

REPLY:

Thank you for the comment. We would like to split the answer to referee #2 into several parts.

a. *Was the influence quantified with a specific measurement (e.g., rapid variability in particle concentrations in a certain size range?)?…"Abrupt and short increases in particle number concentration recorded by a CPC" as cited in L286 as the method for filtering ship stack pollution; this should be elaborated in the methods section and detail is needed on how the authors determined that "most of the cases when the particle number increased tenfold" could be attributed to NPF.*

REPLY:

Indeed, the pollution influence from the ship was quantified with a rapid variability in total particle number concentration. A separate condensation particle counter (CPC) was used to measure total particle number concentration (PNC) with time resolution of 2 seconds (please note that in the text, chapter 3, time resolution was said to be 1 s, which is not correct). An exemplary data of PNC is presented in Fig. R1. It can be clearly seen that ship pollution heavily affects the momentary PNC. Even during NPF event, the maximum particle number concentration did not exceed 5000 particles cm^{-3}. Meanwhile, ship pollution resulted in order of magnitude higher concentrations. It is obvious that such increase must be related to ship exhaust pollution. Moreover, we have also compared PNC increase with a signal from Single Particle Soot Photometer (SP^2, operated inside the aerosol container by scientist from Alfred Wegener Institute. Data is not presented in the manuscript). After comparing the results from both SP^2 and CPC, we came to conclusion that CPC recorded sharp increase in PNC is a good indicator for ship-related pollution. Therefore, for online measurements only CPC and SMPS data was used for contamination inspection.

Different methods exist to clean ambient background aerosol measurements from pollution plumes. For example, Kivekäs et al. (2014) used rolling window percentile to extract background concentrations from particle number size distributions effected by ship plumes. In our previous works, we used rolling window minimum method (see Kecorius et al., 2017). Nevertheless, in this work, we cleaned the online measurements by hand keeping 2 second time resolution CPC data as a reference. This way we are 100% certain that our analyzed results are ship contamination free. Software used to clean up the data was "Dafit" by Ries (2013).

b. *Or, was a specific wind sector removed from the data?*

REPLY:

Automatic system (to measure relative wind direction) was installed together with high volume sampler to stop the pumps when wind came from a specific direction (related to ship exhaust). Similar approach was used by Huang et al. (2018), who performed measurements inside same TROPOS measurement container onboard RV Polarstern. Berner impactor, on the other hand, did not have such system to prevent samples from contamination. However, we only used those samples, which had same order of OC with Digitel PM_1 samples. More detailed discussion regarding OC measurements using Digitel and Berner samplers will be provided in separate work. In the text, we addressed this limitation and added the following in chapter 3.4:

It must also be noted that there was no action taken (e.g. sampling interrupt dependent on specific wind sector) to reduce ship contamination for the size-segregated aerosol particle measurements. Thus, the contamination from the ship exhaust cannot be ruled out completely. However, the high concentrations of biogenic compounds like MSA and the presence of sodium on the aerosol particles suggested a strong marine influence to the particle composition.

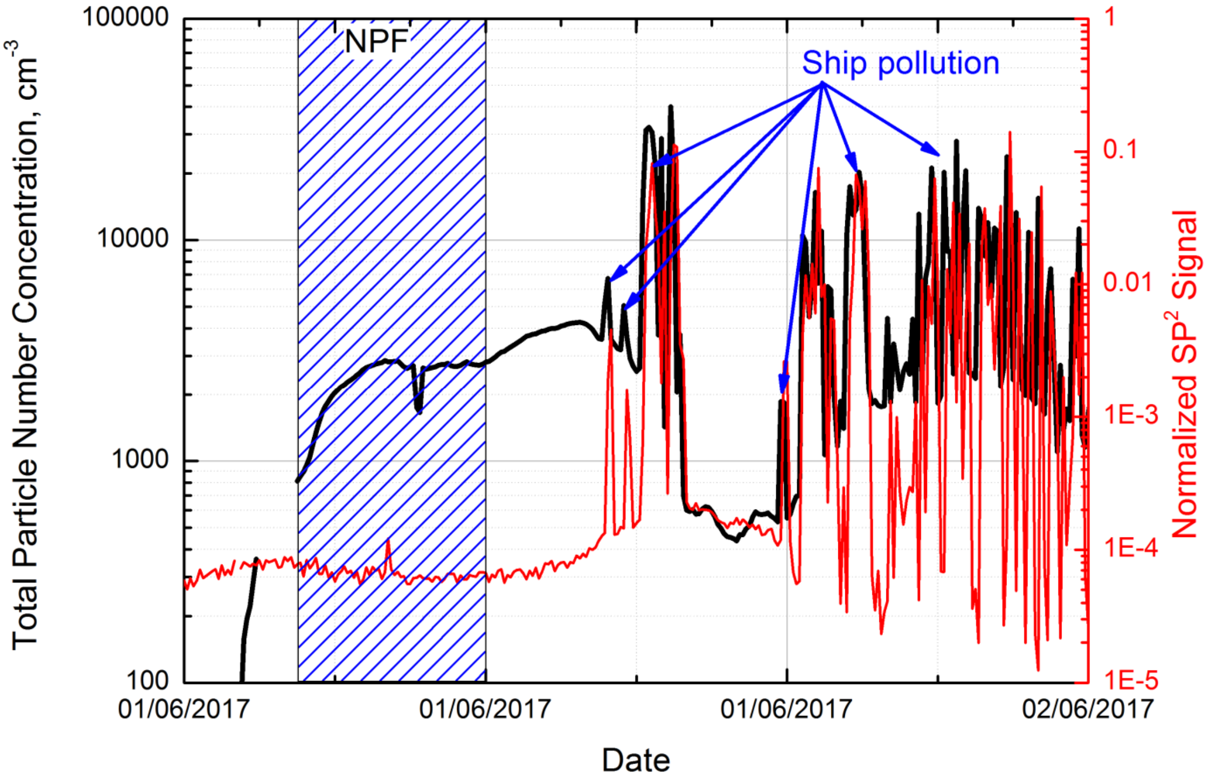

Fig. R1. Total particle number concentration during new particle formation event and contamination from ship.

c. *I strongly discourage the authors from including periods of ship pollution in Figure 2 (noted in L374-375). I disagree that "better representation of particle growth" (L1031-1032) warrants this.*

REPLY:

Ship pollution was included only for visual representation. The data discussed in the manuscript is pollution free. Moreover, by removing data from Fig. 2 that is influenced by ship pollution, we would introduce blank gaps in contour plots. This would greatly diminish the visibility of particle new formation and subsequent growth, which is extended over time period of several days. The inclusion of pollution episodes in Fig. 2 does not obstruct the reader from seeing the processes happening during measurements.

To note the ship pollution influence onto our results, we have included a new section, 2.5 Contamination from ship exhaust, into the manuscript.

Huang, S., Wu, Z., Poulain, L., van Pinxteren, M., Merkel, M., Assmann, D., Herrmann, H., and Wiedensohler, A.: Source apportionment of the organic aerosol over the Atlantic Ocean from 53° N to 53° S: significant contributions from marine emissions and long-range transport, Atmos. Chem. Phys., 18, 18043–18062, https://doi.org/10.5194/acp-18-18043-2018, 2018.

Kecorius, S., Madueño, L., Vallar, E., Alas, H., Betito, G., Birmili, W., Cambaliza, M.O., Catipay, G., Gonzaga-Cayetano, M., Galvez, M.C. and Lorenzo, G., 2017. Aerosol particle mixing state, refractory particle number size distributions and emission factors in a polluted urban environment: Case study of Metro Manila, Philippines. Atmospheric environment, 170, pp.169-183.

Kivekäs, N., Massling, A., Grythe, H., Lange, R., Rusnak, V., Carreno, S., Skov, H., Swietlicki, E., Nguyen, Q.T., Glasius, M. and Kristensson, A., 2014. Contribution of ship traffic to aerosol particle concentrations downwind of a major shipping lane. Atmospheric Chemistry and Physics, 14(16), pp.8255-8267.

Ries, L.C., 2013. Dafit-a new work flow oriented approach for time efficient data preparation, validation and flagging of time series data from environmental monitoring. In EnviroInfo (pp. 651-656).

15. Further to comment (3) above, for the offline chemical analysis the sampling time was 72-144 hours (L223); how was sampling pollution from the ship minimized or avoided (e.g., by a wind switch)? The presence or absence of any such precautions should be stated, and if they were absent the possible implications should be discussed.

REPLY:

Thank you for the comment. As stated above, to note the ship pollution influence onto our results, we have included a new section, 2.5 Contamination from ship exhaust, into the manuscript.

16. A slightly more descriptive title might be helpful. For example, "during PS106 cruise" could be replaced by a few words describing the region of measurements. This would be helpful for readers not familiar with the region covered by the cruise.

REPLY:

Thank you for the suggestion. We agree with referee #2 that more descriptive title would benefit the reader. We have updated the title to "New particle formation and its effect on CCN abundance in the summer Arctic: a case study in Fram Strait and Barents Sea".

Specific Comments

1. L44: This statement might be best attributed to a paper such as Croft et al., Nature Communications, 2016, that makes a more direct connection to radiative forcing.

REPLY:

Thank you for the comment. We have included mentioned citation to manuscript.

2. L60-62: This statement is more attributable to Willis et al., Reviews of Geophysics, 2018 (https://agupubs.onlinelibrary.wiley.com/doi/full/10.1029/2018RG000602) and Abbatt et al., ACP, 2019 (https://www.atmos-chem-phys.net/19/2527/2019/acp-19-2527-2019.html).

REPLY:

Thank you for the comment. We have included mentioned citation to manuscript.

3. L63: Dall'Osto et al., Scientific Reports, 2018 corroborates these results for different regions and multiple stations (https://www.nature.com/articles/s41598-017-17343-9 and https://www.nature.com/articles/s41598-018-24426-8)

REPLY:

Thank you for the comment. We have included mentioned citation to manuscript.

4. L206: I assume that the CCN measurements were made on poly disperse aerosol, but this is not explicitly stated.

REPLY:

Thank you for the comment. Yes, CCN measurements were made only for poly disperse aerosol. Now we have included this statement in the manuscript.

5. L218-219: A large fraction of the organic aerosol may be semivolatile (e.g., Burkart et al, GRL, 2017). How might the semivolatile fraction be impacted by both heating of the inlet and long sampling times? Possibly biases introduced into these measurements should be discussed.

REPLY:

Thank you for the comment. Aerosol inlet for online measurements was heated to 30 °C to prevent ice formation and blockage of the inlet. Only very tip of the inlet was heated. Here, the residence time of aerosol in this heated area was 0.06 s. That is considerably shorter than aerosol spends inside instruments itself before being measured. For offline measurements, on the other hand, residence time is much higher – approx. 1.2 s (for Berner sampler). However, as stated in the text (Lines 219-220): The temperature difference between the ambient air at the impactor inlet and the sampled air after the conditioning unit did not exceed a value of 9 K. Taking into account the low outside temperatures, we do not expect a significant loss of semi volatiles due to this conditioning process (the maximum temperature that tube was heated to was 7 °C). The aerosol particles on the aluminum foils were not exposed to heating and sampled at the (cold) outside temperatures. We added this information in the manuscript (Line 193):

The losses due to evaporation of semi volatile compounds are expected to be minimal.

Furthermore, during sample transportation, samples were stored at -20 °C, thus, we do not expect losses during this stage.

6. L390-391: This is a very interesting observation and is in agreement with Tremblay et al., 2018 (doi above), could these data be included in the Supplement?

REPLY:

Thank you for the comment. We do not possess the observational data neither from Villum Research Station nor Zeppelin mountain Observatory. Nevertheless, for comparison purposes, particle number size distributions can be freely obtained from EBAS, developed and operated by the Norwegian Institute for Air Research (NILU, http://ebas.nilu.no/).

7. L425-429: Burkart et al., 2017 (doi above) came to similar conclusions.

REPLY:

Thank you for the comment. We have included mentioned citation.

8. L431-441 and Figure 4: Rather than referring to the stage number here I suggest the authors refer to the corresponding size range.

REPLY:

Thank you for the comment. We have updates the text and Fig. 4 as suggested by referee #2.

9. Related to comment (8), are any accumulation mode particle present during growth events? Do these larger modes also grow during NPF? Is sea salt present in accumulation mode sizes? Collins et al., 2017 (doi above) and Burkart et al., 2017 (doi above) observed growth of multiple modes at different rates showing that the species responsible for growing the larger mode was more semi volatile. If this is the case can the composition of the larger modes be connected to what is growing the smallest particles?

REPLY:

Thank you for the questions, which we would like to answer step-by-step:

1. *are any accumulation mode particle present during growth events?*

   From figure 2 (in manuscript) and figure R2 (see below), it can be seen that indeed there is an accumulation mode particles present during both particle formation and growth events.

2. *Do these larger modes also grow during NPF?*

   In three of four analyzed NPF events, we did not observe accumulation particle growth. Some accumulation particle growth could be seen during NPF event on 18 June. On 17 June, geometric mean diameter of accumulation mode particles was approx. 100 nm. In 32 hours (from 17 June 08:00 to 18 June 16:00), accumulation mode particle geometric mean diameter grew to 120 nm, that is 0.6 nm h^{-1}. Burkart et al. (2017) observed Aitken mode particle growth to sizes above 100 nm in parallel with nucleation particles. The growth rate was estimated to be 3.4 nm h^{-1}.

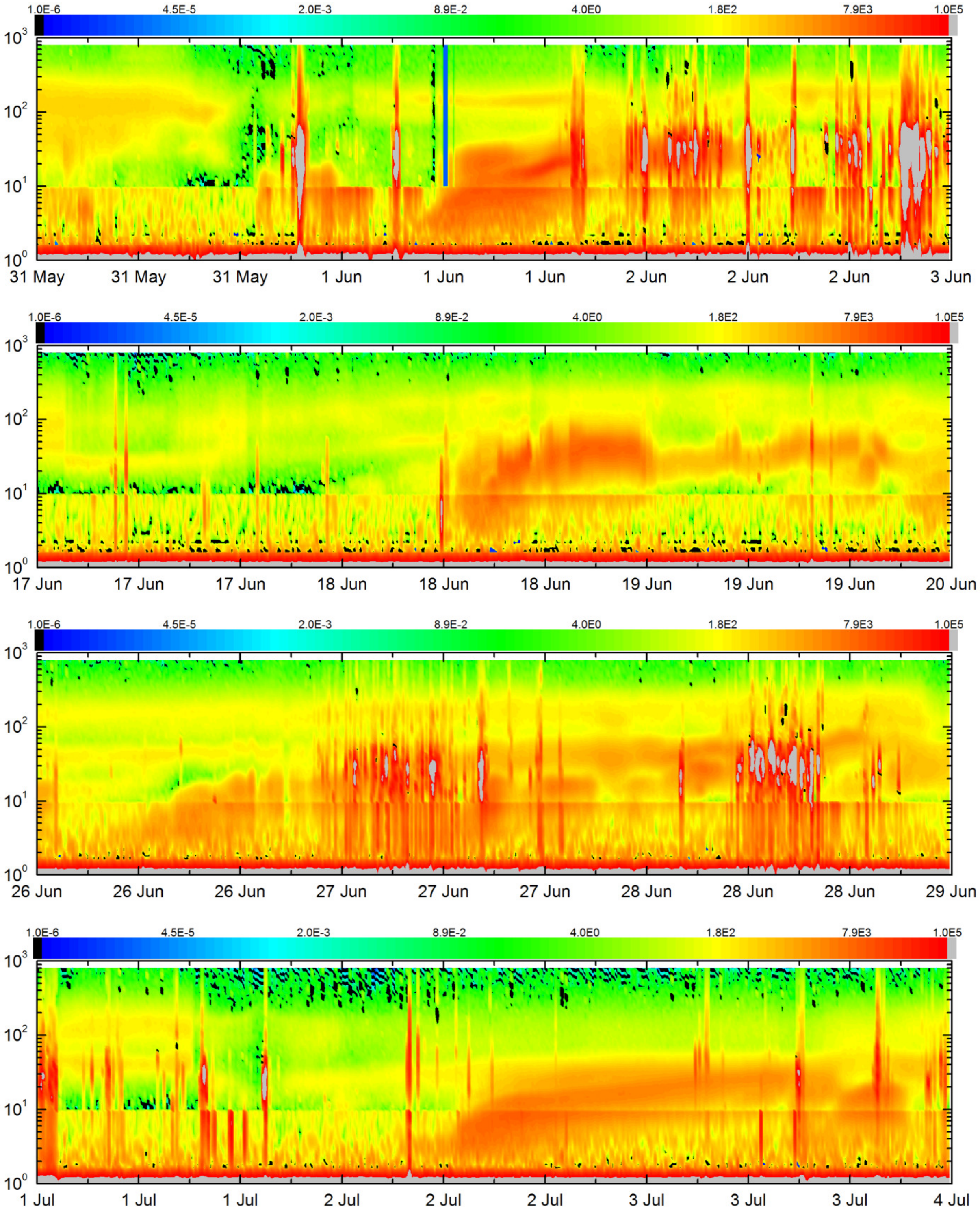

Fig. R2. Particle number size distribution during the new particle formation and growth events. Y-axis – mobility diameter (in nm), X-axis – time, color represents normalized particle concentration ($dN/dlogD_p$, cm^{-3}).

References:

Burkart, J., Hodshire, A.L., Mungall, E.L., Pierce, J.R., Collins, D.B., Ladino, L.A., Lee, A.K., Irish, V., Wentzell, J.J., Liggio, J. and Papakyriakou, T., 2017. Organic condensation and particle growth to CCN sizes in the summertime marine Arctic is driven by materials more semivolatile than at continental sites. *Geophysical Research Letters*, *44*(20), pp.10-725.

3. *Is sea salt present in accumulation mode sizes?*

   Unfortunately, we were not able to investigate chemical composition of aerosol particles for NPF event on 18 June. This is because the high volume and Berner samplers did not overlap with the measurement period, during which NPF was observed.

4. *Collins et al., 2017 (doi above) and Burkart et al., 2017 (doi above) observed growth of multiple modes at different rates showing that the species responsible for growing the larger mode was more semi volatile. If this is the case can the composition of the larger modes be connected to what is growing the smallest particles?*

   As mentioned above, on most of the cases we did not observe the accumulation mode particle growth during NPF events. The exception is 18 June, when a slight accumulation mode particle growth can be noticed. The particles grew from approx. 100 to 120 nm (geometric mean diameter) with a rate of 0.6 nm h^{-1}. Because chemical composition of aerosol particles was not possible to determine, we cannot neither confirm nor deny the resemblance of such observation with previous studies.

10. L444-446: This sentence described a very unique aspect of this study which could be highlighted more, for example in the abstract or at the end of the introduction.

REPLY:

Thank you for the comment. The methodology to observe new particle formation events is well defined in scientific literature, as well as frequently used in various environments (including Antarctica). We do not consider the used instrumentation to be unique in those terms. Therefore, although there are not many studies with same instruments in the Arctic region, we prefer not to highlight the uniqueness of the instruments, but rather focus on the scientific conclusions. Instruments are only the tools.

11. L450-460: Comparison to other Arctic studies that report growth rates might be more appropriate here, though I do not dispute the value of comparing to Antarctic studies. Collins et al., 2017 (doi above) report growth rates for events in the Canadian Arctic during two summers. Nieminen et al., ACP 2018 (doi: 10.5194/acp-18-14737-2018) include growth rates from Alert. Available observations were reviewed by Willis et al., 2018 (doi above).

REPLY:

Thank you for the comment. We have compared our results to the studies suggested by referee #2. The comparison was included into manuscript as well.

12. L567-569: Describing the experiments (i.e., the information in brackets) might be more useful than using experiment numbers for those readers not closely familiar with the CLOUD experiments.

REPLY:

Thank you for the comment. We have updated the manuscript as suggested by referee #2.

13. L572-573: If the measured Aitken mode particles were all organic, how much OM mass would you expect and how does that compare with the measured masses? Also, if the material is largely semivolatile how much do you expect that losses during sampling would impact this assessment?

REPLY:

Thank you for the question. To answer it, requires a mass closure between physical and chemical measurements of the atmospheric aerosol particles. Such an exercise is a great idea and could easily result in a publication itself; however, it is beyond the scope of this study. Multiple assumptions (e.g. Aitken mode particle density and shape; losses in Berner sampling lines; sampling efficiency; etc.) must be made to convert mobility particle diameter to volume equivalent particle diameter. Moreover, as can be seen from contour plots of particle number size distribution (Fig. 2; Fig. R2), pollution had a noticeable impact on measured particle number concentration. This may have effect on estimating particle shape and density, thus, affecting the final closure results (as Berner samplers were not stopped during pollution events). We could certainly provide a number here, however, without an extensive investigation and discussion on possible errors it would be meaningless.

To answer second part of the question: as stated above, we cannot account for losses of semivolatile organic matter during the sampling procedure. However, the samples were not exposed to heating (in fact they were cooled and experienced outside temperature) and they were immediately frozen after the sampling. We don´t expect significant losses of OM.

14. L619-620: The authors of Willis et al., 2016 provide reasonable evidence for a marine source. For example, that the organic and MSA driven growth was only observed in a shallow marine inversion layer and not aloft. Burkart et al., ACP, 2017 corroborate a marine source of NPF precursors.

REPLY:

Thank you for the comment. We have rephrased the text in manuscript to account for evidence or marine sources in NPF.

15. L634-636: The cited observations, as well as Collins et al., 2017, do demonstrate some growth into sizes above 50nm. The same work also demonstrates frequent simultaneous growth of multiple modes, and a resulting strong impact on CCN.

REPLY:

Thank you for the comment. In this work we were able to show that newly formed and slightly grown particles do not need to grow beyond 50 nm to act as CCN. This, however, does not mean that particles do not/cannot grow beyond these sizes. The increase in CCN number concentration due to none-NPF related particle growth was not the scope of this study.

16. L660-670: This is a useful analysis, and I don’t suggest that the authors make substantial changes here. However, I do wonder if updraft the most appropriate way to assess this for summer Arctic low level clouds directly impacted by marine sources? Advection from warmer to colder surfaces in a shallow boundary layer might be another mechanism for CCN to active in low altitude clouds, suggested by Leaitch et al., 2016. Marine influence was significantly less for the upper level clouds observed in Leaitch 2016 (see Bozem et al., ACPD, 2019 doi: 10.5194/acp-2019-70).

REPLY:

Thank you for the comment. The referee #2 is right wondering if updraft is the most appropriate way to assess NPF influence onto Arctic low level clouds. We do not state that this method is the most appropriate way to do so. We used the zero-dimensional, adiabatic cloud parcel model due to its availability and ease of use. More sophisticated model accounting for advection from warmer to colder surfaces (as suggested by referee #2) as well as topography influence may be a good starting point to answer this question in the future.

17. L706: Will these data be made publicly available in the future?

REPLY:

Thank you for the question. Making data publicly available requires it to be submitted to specific data base, which in turn necessitates the data to be in a specific format (e.g. NASA-Ames). At the moment, the data was analyzed, formatted and reformatted multiple times to serve the manuscript preparation. It is thus much easier to make data available on request. If referee #2 has an interest in specific data set, we may be able to provide a temporal data download link. This way the reviewer anonymity can be sustained.

Technical Corrections

1. L144: “0 am” typo?

REPLY:

Thank you for the notification. The typo was corrected.

2. L471: “is” to “are”

REPLY:

Thank you for the notification. The typo was corrected.

3. Supplement Figure S1: typo in the y-axis label? [m] to [nm]?

REPLY:

Thank you for the notification. The typo was corrected.

New particle formation and its effect on CCN abundance in the summer Arctic: a case study in Fram Strait and Barents Sea

Simonas Kecorius[1], Teresa Vogl[1,4], Pauli Paasonen[2], Janne Lampilahti[2], Daniel Rothenberg[3], Heike Wex[1], Sebastian Zeppenfeld[1], Manuela van Pinxteren[1], Markus Hartmann[1], Silvia Henning[1], Xianda Gong[1], Andre Welti[1], Markku Kulmala[2], Frank Stratmann[1], Hartmut Herrmann[1], and Alfred Wiedensohler[1]
[1]Leibniz Institute for Tropospheric Research (TROPOS), 04318 Leipzig, Germany
[2]Department of Physics, University of Helsinki, P. O. Box 64, 00014 Helsinki, Finland
[3]ClimaCell, Inc., Boston, 02210 Massachusetts, USA
[4]Institute for Meteorology, University of Leipzig, D-04103 Leipzig, Germany

Correspondence to: Simonas Kecorius (kecorius@tropos.de)

Abstract. In a warming Arctic the increased occurrence of new particle formation (NPF) is believed to originate from the declining ice coverage during summertime. Understanding the physico-chemical properties of newly formed particles, as well as mechanisms that control both particle formation and growth in this pristine environment is important for interpreting aerosol-cloud interactions, to which the Arctic climate can be highly sensitive. In this investigation, we present the analysis of NPF and growth in the high summer Arctic. The measurements have been done on-board Research Vessel Polarstern during the PS106 Arctic expedition. Four distinctive NPF and subsequent particle growth events were observed, during which particle (diameter in a range 10-50 nm) number concentrations increased from background values of approx. 40 up to 4000 cm^{-3}. Based on particle formation and growth rates, as well as hygroscopicity of nucleation and the Aitken mode particles, we distinguished two different types of NPF events. First, some NPF events were favored by negative ions, resulting in more-hygroscopic nucleation mode particles and suggesting sulfuric acid as a precursor gas. Second, other NPF events resulted in less-hygroscopic particles, indicating the influence of organic vapors on particle formation and growth. To test the climatic relevance of NPF and its influence on the cloud condensation nuclei (CCN) budget in the Arctic, we applied a zero-dimensional, adiabatic cloud parcel model. At an updraft velocity of 0.1 m s^{-1}, the particle number size distribution (PNSD) generated during nucleation processes resulted in an increase of the CCN number concentration by a factor of 2 to 5, compared to the background CCN concentrations. This result was confirmed by the directly measured CCN number concentrations. Although particles did not grow beyond 50 nm in diameter and the activated fraction of 15-50 nm particles was on average below 10%, it could be shown that the sheer number of particles produced by the nucleation process is enough to significantly influence the background CCN number concentration. It implies that NPF can be an important source of CCN in the Arctic. However, more studies should be conducted in the future to understand mechanisms of NPF, sources of precursor gases and condensable vapors, as well as the role of the aged nucleation mode particles on Arctic cloud formation.

1 Introduction

Atmospheric new particle formation (NPF), during which particles with diameters from 1 to 2 nm are formed, is a phenomenon observed in many different environments around the world (Kerminen et al., 2018). Initial steps involved in particle formation and subsequent growth are usually clustering and condensation of both organic and inorganic vapors (Schobesberger et al., 2013). Ions are also known to be involved in the nucleation process (e.g. Jokinen et al., 2018). If newly formed particles are not lost due to coagulation (Lehtinen, et al., 2007), and manage to grow to sizes >50 nm, they can act as cloud condensation nuclei (CCN, Kerminen et al., 2012). Under the presence of sufficient water vapor, CCN activate to form cloud droplets (Köhler, 1936). Atmospheric NPF is estimated to be a substantial source of the world's CCN budget (Merikanto et al., 2009). Thus, in a highly sensitive atmosphere such as the Arctic, where CCN number concentration is usually low (< 100 cm^{-3}, Mauritsen et al., 2011), NPF may be an important phenomenon controlling the radiative forcing (Allan et al., 2015; Croft et al., 2016).

During the last decade, Arctic regions have experienced remarkable changes. Here, the near-surface temperature has increased at least twofold compared to the Northern Hemisphere (a phenomenon known as Arctic amplification, Overland et al., 2011; Jeffries and Richter-Menge, 2012). In parallel, a substantial decline in multiyear sea ice cover (e.g. Bi et al., 2018), an increase in sea ice mean speed and deformation (Rampal et al., 2009), development of melt ponds (Polashenski et al., 2017), etc., was also observed. Such changes do not only reflect in the dynamics of the Arctic ecosystem (Meier et al., 2014), but are also predicted to impact mid-latitude climate (Serreze and Barry, 2011; Cohen et al., 2014; Walsh, 2014).

Recent studies suggest that the amplified warming in the Arctic and related changes are a result of a complex interaction between different feedback mechanisms including parameters such as temperature (Pithan and Mauritsen, 2014), surface albedo (e.g. Screen and Simmonds, 2010; Taylor et al., 2013), water vapor (Graversen and Wang, 2009), cloud (Vavrus, 2004), and the lapse-rate (Bintanja et al., 2012). Additionally, variations in atmospheric and oceanic heat transport were also identified as active players in the changing Arctic climate (Spielhagen et al., 2011; Alexeev and Jackson, 2013). Increase in latent heat and moisture transport towards the poles may drive the low-cloud formation, and thus, Arctic surface warming (Praetorius et al., 2018). And while the mechanisms of lapse rate, surface albedo, temperature and water vapor feedbacks are rather well understood, the net cloud feedback still retains one of the largest uncertainties (Zhang et al., 2018).

The multi-year analysis of particle number size distributions from the sites around the Arctic Ocean revealed frequent new particle formation, occurring either locally or at higher elevations and prevailing mostly during spring and summer months (Freud et al. 2017; Nguyen et al., 2016; Dall'Osto et al., 2019). In near future, the frequency of atmospheric NPF occurrences is expected to increase due to Arctic sea ice melt (Dall'Osto, et al., 2017; 2018a; 2018b). This makes measurements of the ultrafine particle physico-chemical properties in the Arctic increasingly valuable, if aerosol-cloud-climate interactions need to be understood (Willis et al., 2018; Abbatt et al., 2019). Contrary to scientific interest, such studies in this remote environment still remains limited, mainly because of logistic challenges in the region (e.g. Willis et al., 2017; Wendisch et al., 2018). The following are studies, which focus on nucleation mode particles in Arctic. Wiedensohler et al. (1996) reported the occurrence of ultrafine particles in the Arctic as a result of NPF. However, no correlation with potential precursor gases has been found. Karl et al. (2012) found that a sulfuric acid nucleation mechanism best explains the observed growth of nucleation mode particles over the central Arctic Ocean. In another study by Karl et al. (2013), marine granular nanogels were proposed as a novel route to atmospheric nanoparticles in the high Arctic. Furthermore, NPF in the Arctic region was associated with marine biological processes, such as the seasonal cycle of the gel-forming phytoplankton by Heintzenberg et al. (2017). From the results of volatility measurements, Giamarelou et al. (2016) have proposed that particles during NPF events in the high Arctic exist in the form of partly or fully neutralized ammoniated sulfates. Iodine from coastal macro algae was detected in the growing particles (Allan et al., 2015; Sipilä et al., 2016), suggesting the iodine as a nucleation precursor. A large body of studies comes from the Canadian Arctic region. For example, Croft et al. (2016) showed that ammonia from seabird-colony guano is a key factor contributing to bursts of newly formed particles at Alert, Nunavut, Canada. Aerosol particle growth in the Canadian Arctic Archipelago during summer was correlated with organic species, trimethylamine, and methanesulfonic acid (MSA), suggesting an important marine influence (Leaitch et al., 2013; Willis et al., 2016, Abbatt et al., 2019). Park et al. (2017) provided a compelling evidence of the contribution of marine biogenic dimethyl sulfide (DMS) to the formation of aerosol particles. Collins et al. (2017) also reported frequent ultrafine particle formation and growth in Canadian Arctic marine and coastal environments. Authors emphasized that the low condensation sink, high solar radiation, low sea ice concentration, and marine microbial processes all contribute to a higher frequency of particle formation and growth. Most recently, Tremblay et al. (2019) correlated particle formation and growth events with the melting of the sea ice. Authors indicated that besides oxidation of DMS to produce particle-phase sulfate, other gas-phase organic compounds are important for particle growth.

Compared to NPF research in Arctic environment, studies on whether nucleation mode particles (diameter of 20 nm) can act as CCN are even scarcer. Leaitch et al. (2016) investigated effects of 20–100 nm particles on liquid clouds in the clean summertime Arctic and found that particles as small as 20-50 nm can activate to cloud droplets. This was also confirmed by Burkart et al. (2017b), who found that in the Canadian high Arctic marine boundary layer, newly formed particles (approx. 30 nm in diameter) are capable of being involved in cloud activation. Suggesting that in the pristine environment, where cloud radiative forcing is limited by CCN available (Mauritsen et al., 2011), information about aerosol sources is crucial in understanding the link between sea ice melt and low altitude clouds.

In this investigation, we analyzed four cases of NPF and a subsequent growth from a perspective of particle physical (number concentration, number size distribution, and formation and growth rates) and indirect-chemical (hygroscopicity) properties. Our main goal here is to test the hypothesis that NPF and secondary aerosol production can influence the CCN budget in the summertime Arctic. The study is structured as follows. After a short description of materials and methods in section 2, we proceed by describing each NPF event separately (section 3). This includes specification of the meteorological conditions during which NPF occurred, characterization of particle formation and growth rates, followed by the observed hygroscopicity of newly formed particles, and the measured CCN concentrations during NPF events. We start the discussion of the results (section 4) with general overview of our observations, putting the results into perspective of other studies. This leads to section 4.1, where we discuss the indirect evidence of the composition of newly formed particles. Here, we reflect on our observational data as well as various techniques to gain information on particle formation mechanisms, possible sources of precursor gasses, etc. The discussion session is closed by investigating the implication of NPF for cloud formation. This is done by using zero-dimensional parcel model to examine, whether newly formed and slightly grown particles can become CCN. Model results are compared to measured number concentration of CCN during the NPF events. Main results are summarized at the end of the work, general conclusions are also provided.

2 Materials and methods

2.1 Description of observations

The data used in this study were obtained during two legs of an expedition of the German Research Vessel Polarstern (PS 106/1 and PS 106/2): the "Physical feedbacks of Arctic boundary layer, Sea ice, Cloud and AerosoL (PASCAL, PS 106/1)" and " Survival of Polar Cod in a Changing Arctic Ocean (SiPCA, PS 106/2)" (Macke and Flores, 2018; Wendisch et al., 2018). Both expeditions took place in the vicinity of Svalbard (Norway) from May to July, 2017. PASCAL was performed in the framework of the ArctiC Amplification: Climate Relevant Atmospheric and SurfaCe Processes, and Feedback Mechanisms $(AC)^3$ project and was designed to explore cloud properties, aerosol impact on clouds, atmospheric radiation and turbulent-dynamical processes. During the first leg of the trip (PS 106/1, PASCAL), the RV Polarstern reached approx. 82 degrees north where an ice-floe camp was established (5 – 14 June). The first leg of the expedition ended at Longyearbyen, Svalbard by the 21 June. On the 22 June, RV Polarstern left Svalbard for the SiPCA expedition. On second expedition leg aerosol particle measurements were performed until 16 July. The cruise track and the ice-drift are shown in Fig. 1.

2.2 Measurement setup and equipment

To measure aerosol particle physico-chemical properties, a temperature controlled measurement container, prepared and operated by the Leibniz Institute for Tropospheric Research, Leipzig, Germany, was installed on the observation deck of RV Polarstern. The aerosol container was air-conditioned to 24 °C and the aerosol inlet head was heated to 30 °C to ensure the stability of aerosol instrumentation and prevent icing, respectively. The aerosol inlet was made of 6 m length stainless steel tubing, with an inner tube diameter of 40 mm. It was placed on top of the measurement container with an angle of 45 degrees, pointing away from the ship. The aerosol flow in the 6 m long inlet was set to 40 l/min (Reynolds number <2000, laminar flow) to minimize particle losses. Inside the container, an isokinetic splitter was used together with short and vertical conductive tubes to feed the measurement instrumentation with an aerosol sample. Aerosol instrumentation (relevant to this study) included a neutral cluster and air ion spectrometer (NAIS), a mobility particle size spectrometer (MPSS), Volatility/Hygroscopicity-Tandem Differential Mobility Analyzer (VH-TDMA), and Cloud Condensation Nucleus Counter (CCNC) to measure aerosol particle number size distribution, volatility/hygroscopicity properties of aerosol particles, and the number concentration of CCN, respectively.

2.2.1 Neutral cluster and air ion spectrometer (NAIS)

Neutral cluster and air ion spectrometer (NAIS, Mirme and Mirme 2013) and guidelines by Kulmala et al. (2012) were used to study early stages of NPF and subsequent growth (including NPF event classification, formation (J) and growth rate (GR) calculation). NAIS measures number size distribution of neutral particles in the diameter range of approx. 2 – 40 nm and charged particles and clusters in the size-range of approx. 0.8 – 40 nm. The instrument is an extended version of the air ion spectrometer (Mirme et al., 2007) and utilizes a sample preconditioning section to enable measurements of neutrally charged particles. Unipolar corona chargers are used for both charging and charge neutralization. Charged particle classification is carried out in the multichannel differential mobility analyzer (DMA) where 21 individual electrometers are used to record electric current carried by the charged particles. Due to high total flow of NAIS (60 L min^{-1}) a dedicated 1.3 m long copper inlet (3.5 cm in diameter) was installed to sample ambient air. Measurement data were inverted using the v14-lrnd inversion algorithm (Wagner et al., 2016). Particle losses due to diffusion were corrected before data processing.

2.2.2 Mobility particle size spectrometer (MPSS)

Particle number size distributions (PNSD), in a mobility size range from 10 to 800 nm, were measured with a TROPOS-type mobility particle size spectrometer (MPSS, Wiedensohler et al., 2012). The MPSS consisted of a Hauke-type DMA (effective length of 28 cm), condensation particle counter (CPC, model 3772, TSI Inc., USA, flow rate 1 L min^{-1}), a closed-loop sheath flow arrangement and a bipolar diffusion charger, assuring the bipolar charge equilibrium as described in Wiedensohler (1988). The sample flow rate was controlled by a CPC (1 L min^{-1}) and the sheath flow rate was 5 L min^{-1}. The time resolution of an up-and-down scan was 5 min. Electrical particle mobility distributions were inverted to PNSDs using the inversion algorithm presented by Pfeifer et al. (2014). The final PNSDs were corrected for transmission losses in the sampling lines using the method of equivalent length and CPC counting efficiencies (Wiedensohler et al., 1997). Sizing accuracy of MPSS was controlled using nebulized polystyrene latex spheres (PSL, Thermo Scientific™, Duke Standards™) of 203 nm (Wiedensohler et al., 2018). High voltage supply offset calibration, instrument flows and tests for leakage were performed on a regular basis (once per week).

2.2.3 Volatility/Hygroscopicity tandem differential mobility analyzer (VHTDMA)

Aerosol particle affinity to water and volatility properties (not discussed here) were measured using the TROPOS-type Volatility/Hygroscopicity tandem differential mobility analyzer (VHTDMA, Augustin-Bauditz et al., 2016). The instrument consists of a DMA-1 that selects chosen quasi-monodisperse particles, a thermodenuder (not used in this study), an aerosol humidification section that conditions the particles selected by the DMA-1, and a MPSS-equivalent closed-loop sheath flow unit inside the temperature controlled box, which is used to obtain the hygroscopic growth factor (HGF). The HGF is defined as the ratio between the measured particle electrical mobility diameter at a given RH as measured by the second DMA and the initially selected, dry diameter.

During the whole expedition, two constant aerosol particle sizes, 50 and 150 nm, were selected for the measurement of HGF at a target RH of 90%. Additionally, HGF of 15, 20 and 30 nm size particles were measured during NPF and growth events. The system RH, measured by a humidity sensor, was periodically calibrated by an automatic calibration unit, using pure ammonium-sulfate. Scans with RH ±2% from target RH were excluded from data analysis. Sizing accuracy, high voltage supply offset calibration, flow rates, and zero tests were performed regularly (once per week). In general, recommendations have been followed as described in Massling et al. (2011).

The VH-TDMA data was inverted using a TDMAinv routine (Gysel et al., 2009) to retrieve the Probability Density Functions of GF (GF-PDF). Scans with RH < 20% were used to calibrate size offset in the system, as well as to define the width of the transfer function (Gysel et al., 2009). The particle hygroscopicity parameter kappa (κ) was derived from VH-TDMA data following the κ-Köhler theory by Petters and Kreidenweis (2007):

$$\kappa = (GF^3 - 1) \cdot \left[\frac{1}{S}\exp\left(\frac{4\sigma_s M_W}{RT\rho_W D_d GF}\right) - 1\right] \quad (1)$$

where S is the saturation ratio; σ_s - the surface tension of the solution; M_W - the molecular weight of water; R - the universal gas constant; T - the temperature; ρ_W - the density of water; and D_d – particle dry diameter.

2.2.4 Cloud condensation particle counter (CCNC)

The CCNC (model CCN-100 from Droplet Measurement Technologies, Roberts & Nenes, 2005) measured CCN number concentrations, subsequently at six different supersaturations (0.1, 0.15, 0.2, 0.3, 0.5 and 1%), where each supersaturation was sampled for 10 minutes. Hence an hourly average concentration at each supersaturation is available. The instrument was calibrated before and directly following the campaign using pure ammonium sulfate particles of known sizes, based on the ACTRIS protocol (Gysel & Stratmann, 2013). Only poly-disperse aerosol was sampled by CCNC.

2.2.5 Offline chemical analysis

The sampling of aerosol particles was conducted using five-stage low-pressure Berner impactors (Hauke, Austria) with a flow rate of 75 L min^{-1}, which was installed on the top of the observation deck facing the ocean at a height of ca. 25 m. Particles were collected in the size ranges 0.05 – 0.14 µm (stage 1), 0.14 – 0.42 µm (stage 2), 0.42 – 1.2 µm (stage 3), 1.2 – 3.5 µm (stage 4), and 3.5 – 10 µm (stage 5) aerodynamic particle diameter (50% cut-off) on aluminum foils as impaction substrates, which had been heated at 350 °C for at least 2 hours to reduce blank levels prior to sampling. To avoid condensation of atmospheric water on the surface of these aluminum foils, a conditioning unit was mounted between the impactor inlet and the sampling unit consisting of a 3 m tube. By heating the sampled air, high relative humidity of the ambient air was reduced to 75-80% before the collection of the aerosol particles. The temperature difference between the ambient air at the impactor inlet and the sampled air after the conditioning unit did not exceed 9 K. Thus, the losses due to evaporation of semi volatile compounds are expected to be minimal.

After sampling, the aluminum foils were stored in aluminum boxes at -20 °C and transported in dry ice to the TROPOS laboratories in Leipzig, Germany. Field blanks were collected by loading the Berner impactor with the aluminum foils at the sampling site with no air drawn through it. Please note that the sampling time was set to 72 or 144 hours (to accumulate enough particle mass on the filters), thus, it does not exclusively comprise the discussed NPF events. For example, during NPF Event 1, chemical particle composition was determined from samples that were collected between 29 May (midday) and 1 June (approx. 8 am.). During the NPF Event 3, sampling was done between 25 June (11 am) to 28 June (9 am).

Particle mass determination was performed by weighing clean (blank) and particle-loaded filters using a microbalance UMT-2 (Mettler-Toledo, Switzerland). The concentrations of water-soluble methanesulfonic acid (MSA) and inorganic compounds relevant to this study (SO_4^{2-}, NH_4^+, Na^+) in filtered (0.45 µm syringe) aqueous extracts (50% of the filter in 2 mL) were determined using ion chromatography (ICS3000, Dionex, Sunnyvale, CA,USA), as described in Müller et al. (2010). Assuming that the ocean is the major source of the measured atmospheric sodium, sea salt sulfate (ss-sulfate) was calculated from the constant mass ratio ($\frac{SO_4^{2-}}{Na^+} = 0.251$) in bulk seawater (Galloway et al., 1993; Fomba et al., 2014). Non-sea salt sulfate (nss-sulfate) was calculated by subtracting ss-sulfate from the total sulfate concentration. The determination of total carbon (TC) as organic carbon (OC) and elemental carbon (EC) was carried out by a two-step thermographic method (C-mat 5500, Ströhlein, Germany) with nondispersive infrared sensor (NDIR) detection as described in Müller et al. (2010). Organic matter (OM) was calculated by considering OM as twice OC (OM=2 x OC) for remote aerosols (Turpin and Lim, 2001)

2.3 Analysis of PNSD measurements

Before NPF event classification, inverted and loss-corrected NAIS and MPSS PNSDs were merged together. For the smallest particle diameter, from 2 to 10 nm, exclusively NAIS data was chosen. This is because the MPSS used in this study was optimized to operate in a diameter range from 10 to 800 nm. The diffusional losses of sub-10 nm particles were too great to accurately recover the PNSD at initial steps of nucleation. Contrarily, uncertainties in the NAIS measured particle number concentration increases for particle diameters larger than 10 nm (Wagner et al., 2016). For these reasons, PNSDs from both NAIS and MPSS were merged at 10 nm diameter. No additional treatment (e.g. spline fit to smooth merging distributions) was performed on merged PNSDs.

Following the protocol by Kulmala et al. (2012), NPF events were visually identified from the merged PNSDs. Although different types of NPF were recorded (e.g. short bursts in the smallest particle number as e.g. described for the Arctic region by Heintzenberg et al., 2017 and Dall'Osto et al., 2017), in this work we will only focus on NPF events with subsequent particle growth. This type of event does not only include particle formation, but also includes later particle growth lasting for several hours, thus representing a more regional phenomenon (Ström et al., 2009). It also allows us to calculate GR of the particles, which would not be possible in the case of short nucleation mode particle bursts.

Different methods exist to determine the GR based on the measured PNSD. For example, maximum-concentration and log-normal distribution function methods were proposed by Kulmala et al. (2012). Tracking regions of PNSD and interpreting the change rate of the size-integrated general dynamic equation methods was suggested by Pichelstorfer et al (2018). In this work, we used try-error approach to find the best fit to determine GR by selectively applying all mentioned methods for certain NPF cases. The formation rate of particles of certain size (*J*) was calculated as described by Kulmala et al. (2012), based on the observed changes in particle concentrations, determined GR, and particle losses characterized by coagulation sink (CoagS).

2.4 Adiabatic cloud parcel model

To study the climatic relevance of NPF in the Arctic, we have used a zero-dimensional, adiabatic cloud parcel model. Thorough formulation of the model is given by Rothenberg and Wang (2016) and will not be discussed here. Model code is also freely available at https://pyrcel.readthedocs.io. Shortly, at the initial step, the model calculates an equilibrium wet-size distribution from the set of given parameters. This includes the description of the aerosol population and environmental specifications of temperature, pressure, relative humidity, parcel ascending velocity, and the height of the planetary boundary layer. The aerosol particle population, consisting of two modes, is described by the total number concentration, the geometric mean diameter, and the geometric standard deviation of the log-normal distribution. The hygroscopicity parameter κ following Petters and Kreidenweis (2007) is used to describe particle chemical composition. The evolution of the parcel supersaturation, temperature, pressure and, liquid/vapor water content are then integrated forward in time to describe the thermodynamic evolution of an adiabatically lifted, non-entraining parcel. In the model, the evolution of supersaturation S is:

$$\frac{dS}{dt} = \alpha(T,P) - \gamma(T,P)\frac{dw_c}{dt}, \qquad (2)$$

where α and γ are functions depending on temperature and pressure (Leaitch et al., 1986) and w_c is the liquid cloud water mass mixing ratio. Change in temperature is described as:

$$\frac{dT}{dt} = -\frac{gV}{c_p} - \frac{L}{c_p}\frac{dw_v}{dt}. \qquad (3)$$

V is the updraft velocity, g – gravity, c_p - is the specific heat of dry air at constant pressure, L is the latent heat of water, and w_v – water vapor mass mixing ratio. Water mass conservation is ensured as vapor condenses into cloud water. Pressure change within the ascending parcel can be written as:

$$\frac{dP}{dt} = -\frac{gVP}{R_d T_v}, \qquad (4)$$

where T_v is temperature, R_d- gas constant for dry air. The change in cloud water:

$$\frac{dw_c}{dt} = \frac{4\pi\rho_w}{\rho_a}\sum_{i=1}^{n} N_i r_i^2 \frac{G}{r_i}\left(S - S_{eq}\right). \qquad (5)$$

Here ρ_a and ρ_w is the density of air and water, respectively. N_i is a number concentration and r_i is radius in a size bin, S is environmental saturation, S_{eq} is the predicted equilibrium supersaturation under framework described by Petters and Kreidenweis (2007). G is a growth coefficient, which is a function of both the chemical and physical properties of particles.

2.5 Contamination from ship exhaust

During the cruise, ship exhaust occasionally disturbed measurements on board RV Polarstern This was mostly pronounced during the periods when ship was breaking the ice (rapid forward-backward direction change) and/or was drifting during sea experiments. Ship exhaust contamination can be seen in Fig. 2 contour plots as a sharp increase in particle number concentrations over the whole particle diameter range. The contamination from online measurements was removed manually. For this, we referred to total particle number concentration observed by separate CPC with 2 second time resolution. The comparison between total particle number concentration and the signal from single particle soot photometer (results are not shown here) confirmed that the total CPC indeed is able to observe sharp increase in particle number, which is related to ship exhaust (black carbon particles).

For off-line measurements, an automatic system (to measure relative wind direction) was installed together with high volume sampler to stop the pumps when the wind direction was associated with pollution sector. Similar approach was used by Huang et al. (2018). Berner impactor, on the other hand, did not have such system to prevent samples from contamination. To avoid measurement artefacts, only samples with the same order of organic carbon as from high volume samplers were used for data analysis and discussion.

3 Results

During the PS106 cruise, a number of instances were recorded whereby a total particle number concentration (integrated from MPSS between 10 to 800 nm) steadily increased from the background concentrations of several hundred to several thousand particles per cm3 (Fig. 1). After eliminating the contribution from the ship exhaust (by filtering abrupt and short increases in particle number concentration recorded by a total CPC with 2 second time resolution), these cases were associated with new particle formation (NPF) events. For further discussion, we have selected four NPF events with a subsequent particle growth, which represent the phenomenon on a regional scale (Ström et al., 2009). To gain information about the scale of NPF, also additional data of PNSD information from the Villum Research Station and Zeppelin mountain Observatory were taken into account (data for visual inspection were taken fromhttp://ebas.nilu.no/).

The geographic location of the observed NPF events can be seen in Fig. 1 (indicated with black rectangles and date of occurrence), and took place between 78.55 to 81.66 degrees North and 7.28 to 33.96 degrees East. The most intense event (NPF 1) occurred on 1 June 2017, with the total particle number concentration increasing from 100 to more than 4000 particles cm^{-3}. During the NPF event, the lateral distance between RV Polarstern and the nearest coast of Svalbard archipelago was 150 km. The least intensive NPF event (NPF 3) was recorded on 26 June during which the total particle number concentration increased from 160 to 700 particles cm^{-3}. Nevertheless, the subsequent particle growth from 3 nm to approx. 50 nm lasted for 3 days. All the events that were recorded during June (1st, 18th and 26th) took place in the vicinity of the marginal ice zone. The most northern event (NPF 4, 81.6 degrees North) was observed on 2 July, 2017. At this time, the RV Polarstern was further away from marginal ice zone. The average total particle number concentration before the NPF event was approx. 100 particles cm^{-3}, which increased to 1400 particles cm^{-3} during the event.

3.1 Overview of the NPF events

In this paragraph, a detailed overview of the events is presented with the focus on environmental conditions during which NPF occurred, as well as the formation and growth rates of newly formed particles.

3.1.1 NPF 1: 1 June

The first NPF event with a subsequent particle growth was observed from around 6 am onwards on 1 June, 2017. The RV Polarstern reached the marginal ice zone at 11 am and entered the pack ice at around 3 pm on 31 May, 2017 (note that all times in this study are given in UTC). This can be seen from the air and water temperature profiles (Fig. 2). The temperature of air and water decreased from approx. +5 °C to -5 °C (air) and -2 °C (water). In this area, the ice was broken up by leads, which facilitated the passage of the vessel towards the north. Around 8 pm a region with more densely packed ice was reached, which obstructed the movement of the ship (Nicolaus, 2018). On these occasions, due to frequent reverse-forward ship movement, pollution highly affected the measurements on-board (see PNSDs in Fig. 1). On 1 June, the vessel could once again pass through open leads in the pack ice, allowing for contamination-free scans for the time period from 4 am to 8 pm. During this time, RV Polarstern moved 26 km (from 80.39°N 7.58°E to 80.62°N 7.94°E) in mostly cloud-free conditions. From 6 pm to 8 pm, a thin ice cloud was present in over 8 km altitude. Also, over a short period from 2 to 3 pm, intermittent low-level liquid clouds were present, which however did not decrease the global radiation significantly. For a more detailed description of local and associated large scale weather patterns during PS106 refer to Knudsen et al. (2018).

Before the NPF event, the average particle number concentration in a size range from 10 to 50 nm (PNC_{10-50}), was 50 particles cm^{-3}. The particle number concentration in the size range from 100 to 800 nm ($PNC_{100-800}$) before the event decreased from 150 to as low as 2 particles cm^{-3}. This resulted in a sharp decrease in the coagulation sink for 3 nm particles from 7.6 × 10−5 s^{-1} to 8.6 × 10^{-6} s^{-1}. Condensation sink also decreased by one order of magnitude from 2.2 × 10^{-2} to 2.2 × 10^{-3} s^{-1}, creating favorable conditions for particles to form. The NPF event occurred when the RH was approx. 90% and particle formation rate peaked when the global radiation was approaching the maximum (600 W m^{-2}). The wind speed gradually decreased from average 8 on 31 May, 2017, to 5 m s^{-1} during the NPF event. As a result of the NPF, the number of ultrafine particles increased by almost 2 orders of magnitude.

The backward air mass trajectories (calculated for 200 and 2000 m above sea level, Draxler and Rolph, 2012) showed possible intrusion of air from higher altitudes, also that air was arriving at the ship following the 80 degrees North latitude, passing over the Prince George Land and North-East Svalbard archipelago (Fig. 1). This can be confirmed by the increase in ozone concentration at Zeppelin observatory (Aas et al., 2018; data available from http://ebas.nilu.no/). Following the NPF event on 1 June, the wind direction gradually changed from NE to SW, and brought in a sudden fog (at 7 pm , evident from a steep increase of ambient RH to 100% and a simultaneous decrease in visibility measured by the vessel's meteorology station). This can be seen as a sharp increase in both air temperature and RH (to over 100%) causing disruption in the PNSD (onwards from approx. 8 pm., 1 June). At the same time, further observations of the event were corrupted by the local pollution from ship exhaust.

Some parameters describing newly formed particles and ions are shown in Table 1. The particle GR in a size range from 3 to 7 nm was 1.2 nm h^{-1}. After the NPF event, subsequent particle growth lasted for about 12 hours, during which the particles were able to grow to approx. 30 nm in diameter (geometric mean diameter). The GR for 1.6 to 3 nm ions was somewhat more variable – 0.7 for negative and 1.4 nm h^{-1} for positive ions. Please note that we were not able to calculate the positive ion GR in a size range from 1.6 to 3 nm. Instead, the GR for a particle size range 1.6 to 4 nm was calculated. The formation rate of 3-nm (J_{3-}) sized neutral particles and negative ions (1.6-nm, $J_{1.6-}$) was approx. 0.4 and 0.045 cm^{-3} s^{-1}, respectively.

3.1.2 NPF 2: 18 June

On 17 June, the ship was moving southward through packed ice area, breaking floes and navigating through polynyas (Nicolaus, 2018). Over the complete day of 17 June, low-level stratocumulus clouds were present, which were broken up occasionally between 7 am and 1 pm, and 4 to 10 pm. Between 11 pm on 17 June and 1 am on 18 June, measured visibility decreased, accompanied by an increase in relative humidity (RH), indicating fog. This low-level cloud layer was present until approximately 8 am on 18 June, when RV Polarstern left the packed ice entering the marginal ice zone. This resulted in water and air temperature increase from -1.9 °C to approx. 2 and 0.5 °C above zero, respectively. At the same time, local wind speed decreased from 5 to 2 m s^{-1}. During the following hours, until 6 pm, no clouds were present except for a very thin, high ice cloud at 8 km from approximately 11:30 am to 12 pm. This period of high incident radiation was only briefly interrupted by a short fog event from 3 to 3:30 pm. During this whole time, RV Polarstern moved through open water, but was always surrounded by floating ice. Starting at 6 pm, a thin low-level cloud layer was present above the ship, which decreased the global radiation significantly. This cloud layer was present until the next day, 19 June, at approximately 12 pm. During 19 June, RV Polarstern was moving through open water and ice along the west coast of Spitsbergen Island (Fig. 1). From approximately 12:30 pm to 3 pm another short cloud-free period led to high global radiation. At 4 pm at approx. 3 km altitude a cloud moved in decreasing the global radiation once again.

The PNC_{10-50} and $PNC_{100-800}$ from 17 June prior to the NPF event were rather stable, with an average value of approx. 30 cm^{-3}. The corresponding coagulation (for 3 nm particles) and condensation sink was 1.2×10^{-5} and 2.8×10^{-3} s^{-1}, respectively. Analysis of backward trajectories showed that since midnight of 17 June, air masses were passing over the Arctic Ocean, and Greenland Sea. From the beginning of 18 June and onwards, air masses were already passing over the North-East coast area of Greenland (Fig. 1). The NPF event occurred when the global radiation reached its maximum at 570 W m^{-2} and the RH decreased to 85%. During the event, the PNC_{10-50} increased to 3200 cm^{-3}. Particle growth was slightly disturbed by a fog episode (can be seen in PNSD and as RH increase to 100% in Fig. 2) at around 3 pm and drizzle at 11 pm. Nevertheless, the particle growth remained observable until the evening of 19 June. During this time (after a period of 32 hours), newly formed particles grew to approx. 50 nm (geometric mean diameter).

The GRs for particles in the size range from 3 to 7 nm were in a range from 3.6 to 4.9 nm h^{-1}. The GR for 1.6 to 3 nm negative ions was 2.9 nm h^{-1}, and 4 to 9 nm positive ions 3.3 nm h^{-1}. The J_{3-} of particles was approx. 0.35 cm^{-3} s^{-1}. Formation rate for positive ($J_{1.6-}$) and negative (J_{4-}) ions were 0.05 and 0.06 cm^{-3} s^{-1}, respectively. If compared to Event 1, it can be seen that despite similar intensity of NPF, particle growth during the second event was approx. 2 times faster, and particles were able to grow to larger diameters (30 nm during event 1 versus 50 nm during Event 2).

3.1.3 NPF 3: 26 June

The third, least intensive NPF event occurred during the second leg of the expedition, 26 June, when RV Polarstern was at the marginal ice zone, around 200 km east of Svalbard, moving towards the North. Areas dominated by open water were passed by the vessel, as well as ice-covered water (Nicolaus, 2018). However, the ice was never very densely packed and the transit of the ship did not require breaking the ice. Low-level clouds and fog were present during all of 25 June to 27 June; on 28 of June a short period of cloud-free conditions was observed from around 4 to 6 am. There were two short floe stations, one on 25 June from around 5 pm until midnight and the other on 27 June from around midnight to 3 am.

The formation and growth of particles was already observed on both 24 and 25 June during less pronounced NPF events (not shown), when the ship was approx. 100 km South of Svalbard coast. New particle formation along the East coast of Svalbard can be seen in Fig. 1 as increase in total particle number concentrations, which were measured from 24 to 28 June, along a distance of more than 600 km. The daily average of PNC_{10-50} and PNC_{100-}

$_{800}$ from June 24 up to the NPF event (26 June) were approx. 600 and 50 cm^{-3}. As a result of NPFs on 24 and 25 June, an interesting pattern emerged in 26 June PNSD (Fig. 2). At the beginning of 26 June (midnight to 3 am), three distinctive modes with geometric mean diameters of 15, 40 and 150 nm can be seen. The smallest mode at 15 nm is a result of the NPF, which occurred on 25 June. These newly formed particles slowly grew in size and by 8 am 26 June, the mode at 40 nm emerged, which was in turn a result of NPF and subsequent particle growth observed on 24 June. Larger size particles (150 nm in diameter) seem to exist independently from the NPF events, and were present before, during, and after the NPF on 26 June. However, because we were not able to identify particle growth, the NPF events on 24 and 25 June was excluded from the result and discussion sections.

The event on 26 June started with relatively calm winds (2 m s^{-1}), which gradually increased to 10 m s^{-1} over a 3 day period (26 to 28 June) with a constant rate of 0.3 m s^{-1} h^{-1}. The direction of wind remained stable during the event, with prevailing winds from South-South West (190° to 200°) direction, and stagnant air masses coming from the marginal ice zone. At the beginning of the event, relative humidity was at around 87%, and remained below 95% during the whole 3 day period. Air and water temperature during the event were approx. -1.5 °C. During the described three day period, water temperature remained the same (with some short episodes of warmer water), while air temperature steadily increased to 0 °C. The NPF event occurred with a global radiation being at its maximum (200 W m^{-2}), however, this time solar radiation was at least two fold lower than observed during previous cases. This is due to the presence of a low-level cloud layer topped at 2 km during the whole day of 26 June. The corresponding coagulation and condensation sink just before the event was 2.2×10^{-5} and 6.0×10^{-3} s^{-1}, respectively.

The GR of 3 to 7 nm particles was in a range from 0.5 to 0.7 nm h^{-1}. The GR of negative (1.6 to 3 nm) and positive ions (2 to 6 nm) were accordingly 1.2 and 2.2 nm h^{-1}. Despite the noticeable pollution from ship exhaust, particle growth after the NPF event was observed over the period of three days (Fig. 2). During this time period, particles grew from several nanometers up to sizes of 50 nm (geometric mean diameter). The formation rate of positive (J_{2-}) and negative ($J_{1.6-}$) ions were 0.03 cm^{-3} s^{-1}, and the J_{3-} for particles was approx. 0.08 cm^{-3} s^{-1}.

3.1.4 NPF 4: 2 July

From midnight of 1 July to 4 July, RV Polarstern was moving northwards from 81.64°N 32.62°E to 82.16°N 32.87°E. This region was mostly ice-covered with some open leads, through which the vessel could pass without having to break the ice. At this time of the expedition, melt ponds were observed frequently on the ice floes. On 1 July, there was a thick (up to 3 km altitude) low-level cloud layer present until 2 pm associated with some snow fall. After 1 pm, the cloud bottom height increased steadily; however, some intermittent fog was still present at sea level. A single fogbow was observed between 6:20 and 7 pm. The fog dissolved at midnight on 2 July. Almost throughout the entire day of 2 July, no clouds were present except for optically thin cirrus clouds, allowing for high solar irradiation.

On 2 July, the RV Polarstern ventured further into the Arctic ice, more than 300 km from the coasts of Svalbard and Prince George Land (81.51°N, 32.97°E). The prevailing Western winds were rather stable during a 3 day period (from 1 to 4 June) at 6 m s^{-1}. The same was true for water temperature, which remained approx. 2 °C below zero during the whole event period. The air temperature, on the other hand, was varying between negative

1 and negative 5 °C. The calculated backward air mass trajectories indicated that before the midday of 1 July, air was coming from the direction of the Prince George Land. The average PNC_{10-50} and $PNC_{100-800}$ during this time was 60 and 70 cm^{-3}, respectively (Fig. 2). From 1 July onwards, air masses arriving at RV Polarstern passed closer and closer to the North-East coast of Greenland, however, did not pass over the land, as it was the case for Event 2 (Fig. 1). Effective wet removal of particles by fog could be observed during the afternoon hours of 1 July, leading to extremely low particle number concentrations prior to the NPF event. The PNC_{10-50} and $PNC_{100-800}$ respectively decreased to 40 and 10 cm^{-3}. The resulting coagulation and condensation sink became 4.5×10^{-6} and 1.0×10^{-3} s^{-1}, respectively. The NPF event started at 8 am on 2 July at an ambient RH of approx. 90%, and a maximum global radiation of 500 W m^{-2}. In parallel to RV Polarstern measurements, the formation of new particles was also observed at both Villum Research Station and Zeppelin Observatory, indicating a regional phenomenon.

The particle GR, in a size range from 3 to 7 nm, was 0.9 nm h^{-1}. After 40 hours of growth, the geometric mean diameter of particles reached 30 nm. The GR of negative ions was 1.5 nm h^{-1} (in a size range from 2 to 3 nm). Once again, it has to be noted that for ions, the GR in the 1.6 to 3 nm size range was difficult to obtain. Particle formation rate, J_{3-} was approx. 0.15 cm^{-3} s^{-1}. The formation rate of negative ions (J_{2-}) was 0.02 cm^{-3} s^{-1}. As in the case of Event 1, negative ions seemed to be more prominent than positive ones.

3.2 Particle hygroscopicity during NPF events

The size segregated HGF and hygroscopicity parameter κ during NPF events is presented in Table 2. Diameters and scan times of dry particles that were selected for HGF measurements are also indicated in Fig. 2. The HGF scans were performed following the growth of freshly formed particles from MPSS PNSD measurements. In most of the instances newly formed particles grew rather slowly and took between 2 and 7 hours to grow to diameters of 20 - 30 nm, when its HGF was measured. The HGF of 30 - 50 nm particles was measured between 20 to 40 hours after the initial NPF event. Despite the size of selected dry particles, the measured HGF distributions were exclusively mono-modal, indicating internal mixture of the aerosol particle. The highest HGF of nucleation mode particles (15 - 20 nm) was observed during Event 1 and Event 4. The HGF of 20 nm particles during Event 1 was measured 7 hours after the beginning of the NPF, and was 1.46±0.02 (± standard deviation (sd); κ = 0.41±0.02). At the time of Event 4, HGF of the 15 nm particles was 1.34±0.01 (κ = 0.33±0.02). The lowest HGF of 20 nm particles was observed throughout both Event 2 and Event 3, and was 1.17 (κ = 0.13±0.00) and 1.16 (κ=0.12±0.02), respectively. Hygroscopicity of slightly grown Aitken mode particle (30 to 50 nm) varied from 1.17±0.02 (κ = 0.11±0.00) to 1.55±0.01 (κ = 0.38±0.00). In general, the longer the particles aged, the more hygroscopic they became. For example, 8 hours after the new particles were formed during Event 2, the HGF of 20 nm particles was 1.17±0.02. After another 15 hours, these particles grew to sizes of approx. 30 nm, which HGF increased to 1.43±0.05 (κ = 0.36±0.08). Interestingly, the HGF of 50 nm particles was somewhat lower, 1.25±0.01 (κ = 0.16±0.04). Nevertheless, it followed the same pattern and with time increased to the values recorded before the NPF event.

3.3 Measured CCN concentrations during NPF events

Concentrations of CCN (N_{CCN}) measured during the four NPF events can be seen in Fig. 3. An increase in N_{CCN} during these events can be seen across all supersaturations. To determine the increase, measured data were fitted, visible as lines in Fig. 3. Data included in the fitting were taken from times on when formation rates of particles were noticeably increased (10% of the maximum signal) and go up to the time when the NPF event was interrupted by a change in air mass or fog formation. These periods span 10, 39.5, 44.5 and 29 hours for the NPF events 1 to 4, respectively. Independent of the duration of the event, the observed increase in N_{CCN} during these periods were mostly roughly a factor of two for supersaturations from 0.1 to 0.5% and roughly a factor of 3 to 6 at 1%. This larger increase at the highest supersaturation is related to the fact that the number concentrations of smaller particles, which are only activated at higher supersaturations, increased the strongest. During NPF event 2, the increase was somewhat lower, mostly below a factor of 2. These measurements clearly show that during NPF events not only new particles are generated, but also that particulate mass is gained on particles of all sizes, increasing their size and hence their ability to act as CCN at a given supersaturation. A similar observation was made in Antarctica (Herenz et al., 2019), where NPF events with increases in total particle number concentrations from a few hundred to thousands of particles per cm^3 were also accompanied by an increase in N_{CCN} of at least a factor of 2 at all examined supersaturations. Burkart et al. (2017b) came to similar conclusion. This is in agreement with modelling results by Merikanto et al. (2009), where CCN in Arctic regions were found to almost exclusively originate from NPF.

3.4 Chemical composition of size resolved particles

The size-resolved absolute atmospheric concentrations of ammonium, MSA, nss-sulfate, and sea salt (sodium) for the selected periods versus campaign average are shown in Fig. 4. On average, the highest concentrations of nss-sulfate (81 and 70 ng m^{-3}), MSA (18 and 10 ng m^{-3}), and ammonium (16 and 8.7 ng m^{-3}) were found in a size range 0.14 – 0.42 µm (impactor stage 2) and 0.42 – 1.2 µm (impactor stage 3), respectively. While the concentrations of nss-sulfate and ammonium on the impactor samples from 25 to 28 June were comparable to the average values, the impactor samples from 29 May to 1 June stood out with much higher values, especially in the accumulation mode (nss-sulfate: 251 and 295 ng m^{-3} and ammonium: 34 and 17 ng m^{-3} in size range 0.14 – 0.42 µm and 0.42 – 1.2 µm, respectively). Also for smaller particles (size range 0.05 – 0.14 µm, stage 1), nss-sulfate was found at a much higher concentration (35 ng m^{-3}) than the average (8.3 ng m^{-3}).

It must also be noted that no action was taken (e.g. sampling interrupt dependent on specific wind sector) to reduce ship contamination for the size-segregated aerosol particle measurements. Thus, the contamination from the ship exhaust cannot be ruled out completely. However, the high concentrations of biogenic compounds like MSA and the presence of sodium on the aerosol particles suggested a strong marine influence to the particle composition.

The highest organic matter (OM) mass concentration were found on stage 2 (106 ng m^{-3}) and lowest - on stage 5 (39 ng m^{-3}). OM mass concentration for the period from 25 to 28 June strongly exceeded the average concentration, especially in the accumulation mode (218 ng m^{-3} and 147 ng m^{-3} for stages 2 and 3, respectively). For a time period from 29 May to 1 June the OM mass concentration ranged close to the average values.

Sodium was mainly found on Berner stages 3 – 5. The sodium values for the sampling period from 25 to 28 June (Berner stage 4: 49 ng m-3) were quite similar to the average values, while the impactor samples from 29 May to 1 June showed much higher atmospheric concentrations (Berner stage 4: 386 ng m-3). This agrees well to previous studies, which show that atmospheric sea salt is mostly present in super-micron particles, while OM contributes strongly to the submicron particle composition (e.g. Müller et al., 2010). Previous works also suggest that OM is strongly enriched during the bubble bursting process (compared to sea salt) and therefore OM and sea salt are not transferred to the same extend from seawater to the aerosol particles (Keene et al., 2007; Quinn et al., 2015; Van Pinxteren et al., 2017). It is possible that increased sodium and OM, observed during NPF 1, is a result of sea spray, however, due to low sampling time resolution of Berner cascade impactor, we restrict ourselves from such conclusion. Moreover, please note that the increased values of sodium during this time period may be related to ship's proximity to open water (RV Polarstern reached the marginal ice zone only on 31 May), while the increase in OM could have happened later (e.g. 1 June), yet, included in the same sample. In chemical sample analysis, we did not find any positive correlation between OM/OC and sodium, concerning the different aerosol size classes. A more detailed chemical characterization of the aerosol particles during PS 106 cruise will be addressed in a separate publication.

4 Discussion

4.1 General overview

Although NPF events in the high Arctic were reported by several studies, there are no observations, which use the same or equivalent measurement equipment as in this study, able to observe the dynamic changes of the smallest particles (formation and growth of >1.6 nm clusters). Because of this, we have also calculated the rate at which new particles appear at larger diameter (10 nm, J_{10-}). The values of so called apparent nucleation rates are more frequently reported in the literature. For example, in a several studies from the Svalbard region, GRs for 5 to 25 nm particles were reported to be from 0.1 to 0.6 nm h^{-1}, but in general $\leq$1.0 nm h^{-1} (Ström et al., 2009; Giamarelou et al., 2016; Heintzenberg et al., 2017). The corresponding J_{10-} values were in a range from 0.1 to 1.4 cm^{-3} s^{-1}. Nieminen et al. (2018), on the other hand, reviewed NPF events based on long-term measurements and reported GRs for the Arctic region to be 1.1 – 1.2 nm h^{-1} (for June – August time period). The reported formation rates were somewhat lower, 0.008 – 0.032 cm^{-3} s^{-1}. In case of this study, GR for 5 - 25 nm and J_{10-} values varied correspondingly from 0.7 - 5.4 nm h^{-1} and 0.04 - 0.4 cm^{-3} s^{-1}, respectively. The GR of 5 - 25 nm size particles in this study was on average 0.9 nm h^{-1}. The GR of 5 - 25 nm particles on 18 June, however, outstands other NPF events with GR being significantly higher, 5.4 nm h^{-1}. During the same event, the J_{10-} was also higher, 0.4 cm^{-3} s^{-1}. Nevertheless, on average, the observed GR and J_{10-} values were in the same order as reported in other studies from Arctic region (e.g. Asmi et al., 2016; Nieminen et al., 2018). Some studies for similar environmental conditions also exist. Jokinen et al. (2018) provided a comprehensive study on the particle formation in coastal Antarctica. The growth and formation rates for 3 nm particles were found to be between 0.3 - 1.3 nm h^{-1}, and 0.03 - 0.14 cm^{-3} s^{-1}. It was concluded that ion-induced nucleation of sulfuric acid and ammonia is a major source of secondary aerosol particles in the pristine Antarctic environment. Kyrö et al. (2013) reported formation rates of negative clusters ($J_{1.6^-}$, 0.01 to 0.4 cm^{-3} s^{-1}) measured at the Finnish Antarctic Research Station, Aboa, in Dronning Maud Land. In addition, apparent nucleation rates of 10 nm particles at Aboa ranged from 0.003 to 0.3 cm^{-3} s^{-1}. In yet another Antarctic study, Weller et al. (2015) reported the average growth and formation rates (in a size range from 3 to 25 nm) to be 0.9 nm h^{-1} and 0.06 cm^{-3} s^{-1}, respectively. These authors also concluded that due to an insufficient amount of low volatile organic compounds, the particle growth was restricted to the nucleation mode. All of these studies showed some resemblance to the results observed in our study.

The question is what mechanism drives the nucleation and what are the condensable vapors responsible for the observed particle growth in the pristine high altitude environments. Most recent studies indicate the importance of semi volatile organics (Willis et al., 2016; Burkart et al., 2017a). The subsequent growth of newly formed particles was associated with organic precursors from meltwater ponds Kyrö et al. (2013), while Weller et al. (2015) speculated that low volatile organic compounds of marine origin governs the growth of newly formed particles in Antarctica. It was also shown that in a clean environment, sufficiently high sulfuric acid concentrations (10^7 molecules cm^{-3}) can fully explain particle growth (Jokinen et al., 2018). The GRs observed in our study are somewhat similar to those from akin environments, however, they remain difficult to compare because of case-to-case variability.

Insights on the chemical composition of nucleation mode particles and the climatic relevance of NPF can be drawn from the hygroscopicity measurements either at water vapor sub-saturation (measurements of HGF) or supersaturation (measurements of the number of CCN). While κ is a parameter that is independent of experimental conditions, HGF still depends on dry particle size and RH for which it was determined. Still, for the Arctic more data is available for HGF, so that we will use this parameter for comparison with literature in the following. Zhou et al. (2001) measured the HGF during the Arctic Ocean Expedition 1996. The HGF of nucleation mode particles (just after a NPF event, dry diameters of 15) was 1.38. The HGF of 35 nm particles was 1.56. After some time, the particles that grew to sizes of 50 nm were found to be less hygroscopic (HGF of 1.05). It was suggested that these particles were produced at the sea surface and not in the free troposphere. However, the authors could not derive the composition of those nucleation mode particles. Park et al. (2014) reported HGF values of 50 nm particles during enhanced number concentration of the Aitken mode to be 1.46. Sulfate and biogenic volatile organic species were identified to contribute to the Aitken mode particle formation. Compared to our measured HGF of 15 and 20 nm particles, we can see that during Events 1 and 4 values agree reasonably well to previously measured particle hygroscopicity. The HGF of nucleation mode particles during Events 2 and 3, on the other hand, are significantly lower. The hygroscopicity of the Aitken mode particles, measured during Event 4 was almost identical to that noted by Park et al. (2014). On the other instances, for example Event 2, the HGF of the Aitken mode particles was lower (1.33 versus 1.46) than previously reported values. It clearly indicates that different condensable vapors were driving the growth of newly formed particles into sizes of 30 to 50 nm.

Based on particle hygroscopicity, formation and growth rates of positive/negative ions and neutral clusters, and offline chemical analysis, our observed NPF events represent two different cases: 1) more hygroscopic particle formation favored by negative ions, events 1 and 4 (1 June and 2 July, respectively); and 2) relatively low hygroscopicity particle formation during events 2 and 3 (18 and 26 June, respectively), suggesting the presence of condensable organics in particle growth. Further, we would like to discuss event-specific particle growth/formation rates and hygroscopicity with respect to formation mechanism and condensable vapors.

4.2 Indirect evidence of the composition of newly formed particles

4.2.1 NPF 1 and 4

Occurrences of nucleation mode particles in the summer Arctic were associated with intrusion from higher altitudes and new particle production in upper layers of the marine boundary layer (MBL, e.g. Wiedensohler et al., 1996). It is possible that the NPF precursors can be brought from either open ocean or anthropogenic continental sources by air masses. Coupled with low condensation and coagulation sink and with plentiful global radiation it creates favorable conditions for new particles to be formed. However, in all of our observed NPF cases the particle formation started from nucleation of 1-2 nm clusters, suggesting that the NPF took place right at the sea level, rather than in upper layers of the MBL. In this study, unfortunately neither high-resolution online chemical composition of aerosol particles, nor relevant gases (e.g. SO_2, O_3) were directly measured on-board RV Polarstern. To gain some insights into the chemical composition of newly formed and slightly grown particles, as well as precursor gases, we used measured particle physico-chemical properties (e.g. hygroscopicity, growth rate, etc.) as well as satellite imagery.

It is known that Arctic phytoplankton contributes to the production of dimethyl sulfide (DMS), which is the main source of biogenic sulfur (Stefels et al., 2007; Levasseur, 2013 and reference therein). Released into the atmosphere, DMS can be involved in NPF through oxidation and creation of sulfuric acid (H_2SO_4) (Kulmala et al., 2001; Park et al., 2017). In a study by Nguyen et al. (2016), NPF and particle growth at a Station Nord, Greenland was found to be linked to O_3 most likely through creation of hydroxyl (OH) radical and oxidation of sulfur dioxide (SO_2) and volatile organic compounds. The satellite-derived chlorophyll-a mass concentration in surface seawater, as an indicator for phytoplankton biomass (Becagli et al., 2016) can be seen in Fig. 5 (left). It is evident that during all NPF events the RV Polarstern was in a close proximity to an area of increased biological activity in the Arctic Ocean. During Event 1, we also observed large ice-attached mats of the *Melosira arctica* (Fig. 5), which suggests the presence of DMS (Levasseur, 2013). It can also be seen from Fig. 5 that sea ice retreat is somewhat linked to increase in chlorophyll-a mass concentration in surface seawater. For example, on 26 June some ice coverage in the southern part of Prince George Land can still be visible, while on 2 July it is all gone, replaced by biological activity. This is most likely because the ice edge provides increased stability from the melt water, which facilitates the seasonal production of phytoplankton (Conover and Huntley, 1991).

An interesting feature was observed with respect to formation rates and the number size distributions of positive and negative ions during Events 1 and 4 (Fig. 2, see also Supplementary material SP-1). Firstly, it seems that the formation of ions occurred before that of neutral particles. The peak ion formation rate was observed approx. half an hour prior the formation of neutral particles. Although not in Polar Regions, similar behavior was noticed in several other studies suggesting the importance of ions in NPF events (Manninen et al., 2010; Jayaratne et al., 2016). The role of ions in NPF was investigated in both laboratory and field studies (e.g. Wagner et al., 2017; Jokinen et al., 2018). It was shown that ions enhance the nucleation and condensation of the vapor molecules by stabilizing the molecular clusters and/or are involved in charged cluster neutralization via recombination with oppositely charged clusters. The second interesting feature that was observed only during Events 1 and 4 was the absence of smallest (<1.6 nm) positive ions. Negatively charged ions seemed to be involved in the particle formation more favorably than the positive ones. This was also observed in previous studies (e.g. Hirsikko et al., 2007; Asmi et al., 2010; Jokinen et al., 2018) and was associated with sulfuric-acid nucleation. Although H_2SO_4 concentrations were not determined directly, the presence of negative clusters suggests that in case of Events 1 and 4, sulfuric acid was somewhat involved in observed NPF too.

From previous studies, it was shown that H_2SO_4 concentration of 10^7 molecules cm^{-3} are sufficient to explain the observed new particle GRs in coastal Antarctica (Jokinen et al., 2018). In our case, the hypothesis was tested that H_2SO_4 was involved in NPF Events 1 and 4 by using the look-up tables from an ion-mediated nucleation model for the H_2SO_4-H_2O binary system (Yu, 2010). At a given temperature (T_{Event1} = 268.8 K; T_{Event4} = 268.4 K), relative humidity (RH_{Event1} = 96.3%; RH_{Event4} = 96.23%), and surface area concentration of pre-existing particles (S_{Event1} = 2.9 μm^2 cm^{-3}; S_{Event4} = 0.5 μm^2 cm^{-3}), and assumed ionization rate (Q = 2 ion-pairs cm^{-3} s^{-1}) - the corresponding H_2SO_4 concentrations was calculated to be approx. 10^6 molecules cm^{-3}. If compared to study from Antarctica (Jokinen et al., 2018) or laboratory studies by Dunne et al. (2016) from the CERN CLOUD (Cosmics Leaving Outdoor Droplets) chamber, our calculated H_2SO_4 concentration is 10 to 30 times lower than that from previous studies. On the other hand, the results of this study are in agreement with a study by Ehn et al. (2007), who studied the relationship between particle hygroscopicity and sulfuric acid concentration in boreal forest. Authors reported that concentration of H_2SO_4, corresponding to 15 and 20 nm particle HGFs of 1.34 and 1.46, was in a range of 10^7 molecules cm^{-3}. Nevertheless, there were numerous instances when the same hygroscopic growth was also observed at lower H_2SO_4 concentrations ($<10^7$). Moreover, both in the Arctic and Antarctica, H_2SO_4 concentrations of 10^6 molecules cm^{-3} were associated with NPF by Croft et al. (2016) and Kyrö et al. (2013), respectively.

The fraction of the particle growth that can be explained by sulfuric acid can be found from the comparison of observed versus predicted particle growths. From Vakkari et al. (2015), the particle growth due to sulfuric acid can be found from the relation:

$$GR_{calc} = \frac{C_{H_2SO_4}}{A}, \qquad (6)$$

where coefficient A is equal to 1.58 x 10^7, 1.99 x 10^7, and 2.28 x 10^7 for particle growth in the size range from 1.5 to 3, 3 to 7, and 7 to 20 nm, respectively. Using our estimated concentration of H_2SO_4 we found that growth (in a size range from 1.5 to 3 nm) due to sulfuric acid alone accounts only from 4 to 10% of the observed growth during Event 4 and 1, respectively. The contribution to particle growth in a size range from 3 to 20 nm gets even lower, 4-5%. Our values are somewhat comparable to those observed in the Antarctica (Kyrö et al., 2013). It suggests that besides sulfuric acid, other vapors have to be present to reach the observed particle growth. From offline chemical analysis, we see that during Event 1, ammonium and nss-sulfate in accumulation and the Aitken mode particles were somewhat higher than campaign average (Fig. 4). Some studies (e.g. Croft et al., 2016; Köllner et al., 2017) identified that certain nitrogen-containing species such as ammonia and amines are linked to particle growth in the Arctic region. To test this, we investigate the formation rate of critical clusters using a parametrization of the ternary H_2SO_4-NH_3-H_2O system, presented by Napari et al. (2002). That is, we adjust the concentrations of H_2SO_4 and NH_3 until we get the formation rate close to that of observed value. The estimated concentrations of H_2SO_4 and NH_3 varied from 1 x 10^4 to 5 x 10^6 cm^{-3} and 0.1 to 100 ppt, respectively (see supplementary material). According to Wentworth et al. (2016), such concentrations of NH_3 can be indeed found in the Artic region. There is evidence that H_2SO_4-NH_3-H_2O clusters are only partly neutralized under atmospheric conditions (e.g. Kurtén et al., 2007; Schobesberger et al., 2015). On the other hand, Asmi et al. (2010) reported that Aitken mode particles are somewhat more neutralized. Now, if we assume that the newly formed particles were partly neutralized by ammonia (as suggested by Giamarelou et al., 2016), we would expect particle hygroscopicity to be close to that of ammoniated sulfates. However, our observed HGF of 20 and 30 nm particles during both events were somewhat lower (e.g. 1.46 versus 1.64, Asmi et al., 2010). Similar hygroscopicity of ultrafine particles (HGF = 1.38 for 15 nm particles) in the Arctic was observed by Zhou et al. (2001). However, authors excluded the water-sulfuric acid nucleation as a source of such particles because <50 nm particles did not appear to be composed neither of sulfuric acid nor ammonium sulfate. Kim et al. (2016) measured the hygroscopicity of nanoparticles produced from homogeneous nucleation in the CLOUD experiment. If compared to CLOUD experiment results, the measured hygroscopicity of 20 nm particles during Event 1 was closest to the results of experiment, during which sulfuric acid and dimethylamine (DMA) concentrations were 7.6x10^{6} molecules cm^{-3} and 23.8 ppt, respectively. With that being said, experiment with sulfuric acid (15.1x10^{6} molecules cm^{-3}) and organics produced from α-pinene ozonolysis (420 ppt) resulted in 15 nm particles with HGF = 1.33, which is identical to those observed during Event 4.

To conclude, one can only assume that during Events 1 and 4, the NPF was initiated by sulfuric acid. The involvement of ammonia in new particle formation although is possible, cannot be proved by this work. The organics of marine-origin could have been involved in particle growth to some extent. However, low (compared to campaign average) organic matter concentrations, observed by offline chemical analysis, oppose to aforesaid conclusion. The hypothesis that NPF is driven by sulfuric acid can be supported by the results of neutral cluster and ion number size distribution and hygroscopicity measurements of nucleation mode particles.

4.2.2 NPF 2 and 3

Following the same line of thought as in the previous section, we investigate to what extent sulfuric acid may have been involved in the NPF and growth during Events 2 and 3. From satellite imagery of chlorophyll-a (Fig. 5) we can see that RV Polarstern remained in close proximity to somewhat decreased, but still present biological activity in the Arctic ocean. In addition to that, some depletion in sea ice-cover close to Greenland, as well as increase in biological activity south of Svalbard was also observed (Fig. 5). Thus, it is safe to say that air masses arriving at RV Polarstern were passing over regions, which are a potential source of both DMS and organics of marine origin. Assuming a H_2SO_4-H_2O binary system, the H_2SO_4 concentrations corresponding to formation rates of those observed for Event 2 and 3 were from 15 to 50% higher, compared to Events 1 and 4. This is mainly because during Events 2 and 3 both, the condensation sink and temperature were higher too. Only between 1 and 3% of observed particle growth during Event 2 can be explained by H_2SO_4 alone. This fraction is somewhat higher on Event 3 (6-9%). At the initial states of nucleation mode particle growth, particle hygroscopicity on both events was rather low (HGF between 1.16 and 1.18). Such low hygroscopic particle growth, coupled with rather rapid increase in size (Event 2, from 3 to 20 nm, GR = 4.2 nm h^{-1}) suggest that in these events the organics must have played a much bigger role during initial particle growth than during Events 1 and 4. The observed particle hygroscopicity agrees rather well with less-hygroscopic particle values reported by Zhou et al. (2001). During Event 2, particle hygroscopicity did not change much when particles from nucleation mode grew into the Aitken mode, with HGF remaining between 1.16 and 1.18. Only after approx. 30 hours after the new particles were created, they grew to a diameter of 50 nm with slightly increased hygroscopicity, HGF =

1.33. Contrarily, on Event 3 the HGF of 50 nm particles (after approx. 40 hours after the nucleation) reached values of 1.55. It is expected that with time newly formed particle hygroscopicity will increase due to the process known as aging. From smog chamber experiments, Tritscher et al. (2011) showed that organic aerosol photochemical aging increases the particle hygroscopicity mainly due to O_3 induced condensation of organic molecules onto particles. The rate at which particle hygroscopicity parameter κ increases can be calculated from the change in κ over the time period ($\Delta\kappa/\Delta t$). We found that during events 2 and 3 κ changed with the rates of 0.0027 and 0.0067 h^{-1}, respectively. These values are surprisingly close to those observed by Tritscher et al. (2011), further supporting the evidence of organics participating in our observed particle growth.

Using our calculated formation rates (0.06 and 0.026 cm^{-3} s^{-1} during events 2 and 3, respectively) and sulfuric acid values from previous studies (5 x 10^6 molecules cm^{-3}, Croft et al., 2016) as a guideline, we calculate the extremely low-volatility organic compound concentration from the parameterization of particle formation rate as a function of sulfuric acid and EL-VOC concentration (Riccobono et al., 2014):

$$J = 3.27 \times 10^{-21} cm^{-6} s^{-1} \times [H_2SO_4]^2 \times (EL - VOC). \quad (7)$$

The resulting EL-VOC concentration for Event 2 was found to be approx. 8.0 x 10^6 molecules cm^{-3}. This is 40 times higher than what is expected from monoterpenes air-sea flux in Arctic Ocean (Croft et al., 2016). On the other hand, during Event 3, the estimated concentration of EL-VOC was in pair with results published by the same authors. The question is where the EL-VOC comes from? Kyrö et al. (2013) showed that NPF can be a result of precursor vapor emission from meltwater ponds. In Fig. 5, we can see that air masses during Event 2 is arriving from the coast of Greenland, with a pronounced sea-ice index change, indicating ice retreat. Moreover, measurements of PNSD at Villum Research Station also indicated the occurrence of NPF. However, it remains unclear if the ice and biological activity development at the coast of Greenland could have produced the organic vapors that participated in NPF observed at RV Polarstern. Yet another source of condensable organic vapor could be the aged phytoplankton blooms, presented as irregularities in chlorophyll-a spatial distribution, at the marginal ice zone, close to research vessel.

Atmospheric particulate methanesulfonic acid (MSA) and none-sea salt sulfate (nss-sulfate) are considered to be oxidation end products of DMS, which is released as a gas during biogenic processes and indicates the formation of secondary aerosol with biogenic origin (Leck et al., 2002; Miyazaki et al., 2010). MSA was shown to be involved in nucleation mode particle growth in the Arctic by Willis et al. (2016). Authors found that MSA and condensable organic species, originating from marine-derived biogenic volatile organic compounds, drive particle growth in a shallow marine inversion layer. Organic matter in Arctic submicron particles was found to be of both continental and biogenic marine origins (Kerminen et al., 1997; Chang et al., 2011). Orellana et al. (2011) showed that submicron OM can be composed of phytoplankton exudates in form of marine hydrogels. If we look at offline chemical analysis of aerosol sample, OM was found on all impactor stages, especially on the submicron particles between 0.14 and 1.2 µm. While submicron particles of the impactor samples for Episode 1 were mainly dominated by ammonium and nss-sulfate (see Fig. 4), higher concentrations of OM (together with MSA) were found for the sampling period between 25 to 28 June. These results corresponded to the observed differences between particle hygroscopicity during events 1 and 3.

To summarize, the rapid particle growth (Event 2), and the low but steadily increasing hygroscopicity (events 2 and 3) suggest that organics must have been involved in both NPF and subsequent particle growth. Although our observed results agree with previously made conclusions that particle growth in the Arctic is largely via organic condensation (Burkart et al., 2017a), due to a lack of measurements, we cannot specify which organic species may/or may not have been involved in these processes. We also cannot exclude neither the role of iodine (Allan et al., 2015) in the initial steps of NPF, nor other pathways for initial particle growth (e.g. aminium salts; Smith et al., 2010). In the future, measurements of chemical composition of naturally charged air ions and ion clusters and low-volatile aerosol precursor gases would greatly improve our understanding about NPF processes and particle growth in the Arctic.

4.3 Implication for CCN abundance

In the last section of this work, the climatic relevance of the newly formed particles in the Arctic is discussed. In several studies (e.g. Allan et al., 2015; Willis et al., 2016; Burkart et al., 2017b) it was reported that nucleated particles in the Arctic atmosphere rarely grow beyond the Aitken mode. It is the result of low organic vapor/precursor gas concentrations involved in NPF and subsequent growth, as well as particle lifetime (particles being scavenged by fog or precipitation, Karl et al., 2012). These findings are also comparable to those from Antarctica. Weller et al. (2015) reported that particle growth is governed by the deficit of availability of low volatility organic compounds of marine origin and made the conclusion that particles do not grow to a diameter range relevant for acting as CCN. On the other hand, some studies both from Arctic and Antarctica proved that particles do not have to grow beyond 50-60 nm in diameter to be able to act as CCN (Kyrö et al., 2013; Croft et al., 2016; Leaitch et al., 2016). This is because in the pristine Arctic environment the absence of larger particles may lower water uptake, which will increase supersaturation, enabling cloud water to condense on smaller particles (Leaitch et al., 2016).

To examine to which degree NPF may influence the CCN nuclei budget in the Arctic, we used an adiabatic non-entraining cloud parcel model (described in section 2.4). All the initial parameters and simulation results can be found in Table 3. The change in CCN number was calculated for two different updraft wind velocities, 0.1 and 3.2 m s^{-1}, representing the 75th percentile and maximum value, respectively. The measurements of vertical wind velocity was performed during the ice-drift station, as described by Egerer et al. (2019), and can also be found online (https://doi.pangaea.de/10.1594/PANGAEA.899803). We define the CCN number concentration (N_{CCN}) increase due to particles created in the nucleation process as:

$$Increase\ of\ N_{CCN} = \frac{(N_{CCN,bp} + N_{CCN,NPF})}{N_{CCN,bp}}, \tag{8}$$

where $(N_{CCN,bp} + N_{CCN,NPF})$ is the number concentration of CCN resulting from the particles created in NPF event (calculated from bi-modal PNSD using parcel model; see Table 3 for simulation parameters) and $N_{CCN,bp}$ is the CCN number concentration resulting entirely from accumulation mode particles present during the NPF event (newly formed particle mode is suppressed in parcel simulation). For more detailed discussion about CCN increase calculation, please refer to supplementary materials. It can be seen that for most of the cases (when RH>90%), the CCN number concentrations increased by a factor of 2 to 5 (at upward wind velocities of 0.1 m s^{-1}) and 4 to 32 (at upward wind velocities of 3.2 m s^{-1}). Although the activated number fraction in a size range from 15 to 20 nm was rather low (1.5 - 4%), the high number of nucleation mode particles resulted in a noticeable increase of total CCN. The CCN fraction was higher (30 - 50%) when 3.2 m s^{-1} updraft wind speed was assumed. For the Aitken mode particles, CCN fraction was approx. 12 and 80% for updraft wind speeds of 0.1 and 3.2 m s^{-1}, respectively. In some cases, the particles did not activate to CCN. This is because activation supersaturation was not reached during the parcel updraft. The maximum supersaturation achieved with an updraft velocity of 0.1 m s^{-1} was 0.17%. The updraft velocity of 3.2 m s^{-1} would represent although rare, however, not unlikely situation when supersaturations of 0.9% can be reached. It can be anticipated that an even higher fraction of CCN may result from nucleation mode particles when higher supersaturation values are reached. Measurements of CCN number concentration on-board RV Polarstern corroborate the results obtained by our modelling efforts, which all are in good agreement with previous works. For example, Croft et al. (2016) reported maximum supersaturation in the Arctic region of 0.15–0.25% for the updraft speed of 0.1 m s^{-1}. From a comprehensive study on the ultrafine particle effects on liquid clouds in the clean summertime Arctic, Leaitch et al. (2016) determined the supersaturation for low and high altitude clouds to be approx. 0.3 and 0.6%, respectively. In the Arctic environment with the lack of aerosol particles upon which clouds may form, even a small increase in aerosol loading can lead to cloud formation and thus influence the ice-covered Arctic surface (Mauritsen et al., 2011). From our results, we conclude that NPF in the Arctic can play a significant role in determining the future changes in this pristine and remote environment.

5 Summary and conclusion

Aerosol particle physico-chemical properties were determined in the summer Arctic on-board research vessel (RV) Polarstern from 26 May to 16 July 2017 as a part of the PASCAL/SiPCA campaign. Here, regional NPF events are analyzed and put into prospective of producing the CCN. From the measurements of neutral cluster and air ion number size distributions, it can be concluded that new particles were formed within the marine boundary layer and not mixed down from aloft. Therefore, the majority of particles in a size range up to 50 nm in diameter can be related to secondary aerosol production rather than primary emissions. Two different types of NPF were distinguished: a) NPF favored by negative ions, and more-hygroscopic nucleation mode particles; and b) NPF with subsequent rapid growth (Event 2), resulting in less-hygroscopic particles. From analysis of particle formation and growth rates, as well as the hygroscopicity of slightly grown particles, it seems that sulfuric acid-water ion-mediated nucleation is an acceptable mechanism explaining the observed NPF during events 1 and 4. Meanwhile, low particle hygroscopicity and rapid growth suggests that condensable organics were somewhat involved in particle growth during events 2 and 3. Although the imagery from satellite confirms the biological activity as a possible source of marine sulfur and organics, however, due to the lack of appropriate measurements we cannot provide quantitative information to what extent these precursor gases may have been involved in the observed particle formation and growth. For the same matter, we also cannot exclude other species (e.g. iodine) participating in NPF. To answer these questions, high temporal resolution measurements of nucleation and the Aitken mode particle chemical composition after the NPF is necessary, which remains a topic for the future research.

After the nucleation, in 12 to 56 hours newly formed particles grew to the Aitken mode sizes (approx. 30-50 nm). We have traced particle growth and measured particle hygroscopicity for dry diameters of 15, 20, 30, and 50 nanometers. Here, one of our main objectives was to test whether particles created in the Arctic marine boundary layer can act as CCN. To accomplish this task we have used a zero-dimensional, adiabatic cloud parcel model. Measured particle physico-chemical properties and ambient information (relative humidity, pressure, temperature) were used to simulate particle population activation to cloud droplets at two different updraft velocities of 0.1 and 3.2 m s^{-1}. Simulation results showed that although the activated fraction of nucleation mode particles were below 5% at an updraft wind velocity of 0.1 m s^{-1}, background CCN number concentration increased by up to a factor of 5. The Aitken mode particle activation was somewhat higher, approx. 12%. Such increase in CCN number concentrations was also confirmed by direct measurements for supersaturations from 0.1 to 1% on-board RV Polarstern. Our findings support previous observations suggesting that in pristine Arctic environment particles do not have to grow to sizes above 50 nm to act as CCN. We conclude that in a changing Arctic, NPF can be an important source of CCN. New particle formation and the Aitken mode particle ability to become CCN requires more in depth studies with the focus on mechanisms of NPF, chemical composition of the precursor gases and condensable vapors, as well as the identification of their sources and impact on Arctic clouds.

Data availability

Processed and raw data available on request from corresponding author.

Author contribution

SK – operated aerosol instrumentation on-board RV Polarstern, evaluated data, and wrote the manuscript.
TV – operated aerosol instrumentation on-board RV Polarstern and contributed to manuscript writing.
PP, JL, and MK – contributed to NAIS data evaluation, discussion and manuscript writing.
DR – contributed to the simulation of CCN.
HW – contributed writing the manuscript.
SZ and MP – collected samples for chemical analysis. Contributed writing the manuscript.
MH – operated the CCNC on-board RV Polarstern and evaluated CCNC data.
XG and AW – operated CCNC on-board RV Polarstern.
SH – calibrated the CCNC prior measurement campaign.
FS, HH, and AW – participated in fund raising for the measurement campaign.

Competing interests

The authors declare that they have no conflict of interest.

Special issue statement

This article is part of the special issue “Arctic mixed-phase clouds as studied during the ACLOUD/PASCAL campaigns in the framework of $(AC)^3$ (ACP/AMT inter-journal SI)”. It is not associated with a conference.

Acknowledgements

We gratefully acknowledge the funding by the Deutsche Forschungsgemeinschaft (DFG, German Research Foundation) – Projektnummer 268020496 – TRR 172, within the Transregional Collaborative Research Center "ArctiC Amplification: Climate Relevant Atmospheric and SurfaCe Processes, and Feedback Mechanisms (AC)³, as well as funding of the Polarstern cruise PS106 (expedition grant number AWI-PS-106-00) by AWI. Authors would also like to acknowledge a number of people, who were involved in this work. We acknowledge the discussions and support (H2SO4-H2O nucleation look-up tables) by Fangqun Yu (UAlbany). We also thank Sebastian Ehrhart (MPIC), Joachim Curtius (IAU), Steffen Münch (ETHZ), and Andreas Kürten (IAU) for the discussions concerning sulfuric acid-water nucleation. Ella-Maria Duplissy, Veli-Matti Kerminen, Jenni Kontkanen, Stephany N. Buenrostro Mazon from Helsinki University for their time, valuable suggestions, and discussions. Ulrike Egerer for providing the updraft wind velocities during the ice-drift station. Hannes Griesche, Ronny Engelmann and Martin Radenz for providing ship-based remote sensing data to characterize the cloud situations during the selected events. Peter Gege (DLR), Svenja Kohnemann (UniTrier), and Marcel Nicolaus (AWI) for sharing the ship-deck photos. Andreas Macke (TROPOS) and Hauke Flores (AWI), Chief Scientists of PS106 cruise, for the attitude and phenomenal attention to all our requests regarding scientific activities on-board RV Polarstern and on the ice. And finally, the RV Polarstern crew, staff members, numerous scientists, and Polar Bear guards and watchers, who made the expedition not only exceptional, but also a safe experience. Villum Research Station, Robert Lange, Andreas Massling, Henrik Skov, and Niels Bohse Hendriksen are acknowledged for providing PNSD data. We acknowledge Hartmut and Andrea Haudek for building the conditioning system for both aerosol inlet and the Berner impactor for these Arctic environmental conditions. Maik Merkel and Rene Rabe was a huge technical support for setting up the measurement container and Berner impactors. Susanne Fuchs performed the ion chromatography analysis and Anke Rödger the OC/EC thermographic analysis. We also acknowledge the use of imagery from the NASA Worldview application (https://worldview.earthdata.nasa.gov), part of the NASA Earth Observing System Data and Information System (EOSDIS). Also, this study has been conducted using E.U. Copernicus Marine Service Information (Arctic Chlorophyll Concentration from Satellite observations (daily average) Reprocessed L3 (ESA-CCI). We acknowledge two anonymous referees for their time, comments, and suggestions, which improved the final version of the manuscript.

References

Aas, W., Fiebig, M., Solberg, S. and Yttri, K.E.: Monitoring of long-range transported air pollutants in Norway, annual Report 2017, NILU rapport, 2018

Abbatt, J.P., Leaitch, W.R., Aliabadi, A.A., Bertram, A.K., Blanchet, J.P., Boivin-Rioux, A., Bozem, H., Burkart, J., Chang, R.Y., Charette, J. and Chaubey, J.P.: Overview paper: New insights into aerosol and climate in the Arctic. Atmospheric Chemistry and Physics, 19, 2527-2560, 2019.

Alexeev, V.A. and Jackson, C.H.: Polar amplification: is atmospheric heat transport important? Climate dynamics, 41, 533-547, 2013.

Allan, J.D., Williams, P.I., Najera, J., Whitehead, J.D., Flynn, M.J., Taylor, J.W., Liu, D., Darbyshire, E., Carpenter, L.J., Chance, R. and Andrews, S.J.: Iodine observed in new particle formation events in the Arctic atmosphere during ACCACIA. Atmospheric Chemistry and Physics, 15, 5599-5609, 2015.

Asmi, E., Frey, A., Virkkula, A., Ehn, M., Manninen, H.E., Timonen, H., Tolonen-Kivimäki, O., Aurela, M., Hillamo, R. and Kulmala, M.: Hygroscopicity and chemical composition of Antarctic sub-micrometre aerosol particles and observations of new particle formation. Atmospheric Chemistry and physics, 10, 4253-4271, 2010.

Asmi, E., Kondratyev, V., Brus, D., Laurila, T., Lihavainen, H., Backman, J., Vakkari, V., Aurela, M., Hatakka, J., Viisanen, Y. and Uttal, T.: Aerosol size distribution seasonal characteristics measured in Tiksi, Russian Arctic. Atmospheric chemistry and physics, 16, 1271-1287, 2016.

Augustin-Bauditz, S., Wex, H., Denjean, C., Hartmann, S., Schneider, J., Schmidt, S., Ebert, M. and Stratmann, F.: Laboratory-generated mixtures of mineral dust particles with biological substances: characterization of the particle mixing state and immersion freezing behavior. Atmospheric Chemistry and Physics, 16, 5531-5543, 2016.

Becagli, S., Lazzara, L., Marchese, C., Dayan, U., Ascanius, S.E., Cacciani, M., Caiazzo, L., Di Biagio, C., Di Iorio, T., Di Sarra, A. and Eriksen, P.: Relationships linking primary production, sea ice melting, and biogenic aerosol in the Arctic. Atmospheric environment, 136, 1-15, 2016.

Bi, H., Zhang, J., Wang, Y., Zhang, Z., Zhang, Y., Fu, M., Huang, H. and Xu, X.: Arctic Sea Ice Volume Changes in Terms of Age as Revealed From Satellite Observations. IEEE Journal of Selected Topics in Applied Earth Observations and Remote Sensing, 11, 2223-2237, 2018.

Bintanja, R., Van der Linden, E.C. and Hazeleger, W.: Boundary layer stability and Arctic climate change: A feedback study using EC-Earth. Climate dynamics, 39, 2659-2673, 2012.

Burkart, J., Hodshire, A.L., Mungall, E.L., Pierce, J.R., Collins, D.B., Ladino, L.A., Lee, A.K., Irish, V., Wentzell, J.J., Liggio, J. and Papakyriakou, T.: Organic condensation and particle growth to CCN sizes in the summertime marine Arctic is driven by materials more semivolatile than at continental sites. Geophysical Research Letters, 44, 10-725, 2017a.

Burkart, J., Willis, M. D., Bozem, H., Thomas, J. L., Law, K., Hoor, P., Aliabadi, A. A., Köllner, F., Schneider, J., Herber, A., Abbatt, J. P. D., and Leaitch, W. R.: Summertime observations of elevated levels of ultrafine particles in the high Arctic marine boundary layer. Atmos. Chem. Phys., 17, 5515–5535, 2017b.

Chang, R.W., Leck, C., Graus, M., Müller, M., Paatero, J., Burkhart, J.F., Stohl, A., Orr, L.H., Hayden, K., Li, S.M. and Hansel, A.: Aerosol composition and sources in the central Arctic Ocean during ASCOS, 2011.

Cohen, J., Screen, J.A., Furtado, J.C., Barlow, M., Whittleston, D., Coumou, D., Francis, J., Dethloff, K., Entekhabi, D., Overland, J. and Jones, J.: Recent Arctic amplification and extreme mid-latitude weather. Nature geoscience, 7, 627, 2014.

Collins, D. B., Burkart, J., Chang, R. Y.-W., Lizotte, M., Boivin-Rioux, A., Blais, M., Mungall, E. L., Boyer, M., Irish, V. E., Massé, G., Kunkel, D., Tremblay, J.-É., Papakyriakou, T., Bertram, A. K., Bozem, H., Gosselin, M., Levasseur, M., and Abbatt, J. P. D.: Frequent ultrafine particle formation and growth in Canadian Arctic marine and coastal environments. Atmos. Chem. Phys., 17, 13119–13138, 2017.

Conover, R.J. and Huntley, M.: Copepods in ice-covered seas—distribution, adaptations to seasonally limited food, metabolism, growth patterns and life cycle strategies in polar seas. Journal of Marine Systems, 2, 1-41, 1991.

Croft, B., Wentworth, G.R., Martin, R.V., Leaitch, W.R., Murphy, J.G., Murphy, B.N., Kodros, J.K., Abbatt, J.P. and Pierce, J.R.: Contribution of Arctic seabird-colony ammonia to atmospheric particles and cloud-albedo radiative effect. Nature communications, 7, 13444, 2016.

Dall, M., Beddows, D.C.S., Tunved, P., Krejci, R., Ström, J., Hansson, H.C., Yoon, Y.J., Park, K.T., Becagli, S., Udisti, R. and Onasch, T.: Arctic sea ice melt leads to atmospheric new particle formation. Scientific reports, 7, 3318, 2017.

Dall'Osto, M., Beddows, D.C.S., Asmi, A., Poulain, L., Hao, L., Freney, E., Allan, J.D., Canagaratna, M., Crippa, M., Bianchi, F. and De Leeuw, G.: Novel insights on new particle formation derived from a pan-european observing system. Scientific reports, 8, 1482, 2018a.

Dall, M., Geels, C., Beddows, D.C.S., Boertmann, D., Lange, R., Nøjgaard, J.K., Harrison, R.M., Simo, R., Skov, H. and Massling, A.: Regions of open water and melting sea ice drive new particle formation in North East Greenland. Scientific reports, 8, 6109, 2018b.

Dall'Osto, M., Beddows, D. C. S., Tunved, P., Harrison, R. M., Lupi, A., Vitale, V., Becagli, S., Traversi, R., Park, K.-T., Yoon, Y. J., Massling, A., Skov, H., Lange, R., Strom, J., and Krejci, R.: Simultaneous measurements of aerosol size distributions at three sites in the European high Arctic. Atmos. Chem. Phys., 19, 7377–7395, 2019.

Draxler, R.R. and Rolph, G.D.: HYSPLIT (HYbrid Single-Particle Lagrangian Integrated Trajectory), NOAA Air Resources Laboratory, Silver Spring, USA, 2012.

Dunne, E.M., Gordon, H., Kürten, A., Almeida, J., Duplissy, J., Williamson, C., Ortega, I.K., Pringle, K.J., Adamov, A., Baltensperger, U. and Barmet, P.: Global atmospheric particle formation from CERN CLOUD measurements. Science, 354, 1119-1124, 2016.

Egerer, U., Gottschalk, M., Siebert, H., Ehrlich, A., and Wendisch, M.: The new BELUGA setup for collocated turbulence and radiation measurements using a tethered balloon: First applications in the cloudy Arctic boundary layer, Atmos. Meas. Tech. Discuss., https://doi.org/10.5194/amt-2019-80, in review, 2019.

Ehn, M., Petäjä, T., Aufmhoff, H., Aalto, P., Hämeri, K., Arnold, F., Laaksonen, A. and Kulmala, M.: Hygroscopic properties of ultrafine aerosol particles in the boreal forest: diurnal variation, solubility and the influence of sulfuric acid. Atmospheric Chemistry and Physics, 7, 211-222, 2007.

Fetterer, F., Knowles, K., Meier, W. and Savoie, M.: Sea ice index. National Snow and Ice Data Center, Boulder, CO, digital media, accessed online http://nsidc. org/data/g02135. html, 25 May, 2019.

Fomba, K.W., Müller, K., Van Pinxteren, D., Poulain, L., Van Pinxteren, M. and Herrmann, H.: Long-term chemical characterization of tropical and marine aerosols at the Cape Verde Atmospheric Observatory (CVAO) from 2007 to 2011. Atmos. Chem. Phys., 14, 8883-8904, 2014.

Freud, E., Krejci, R., Tunved, P., Leaitch, R., Nguyen, Q. T., Massling, A., Skov, H., and Barrie, L.: Pan-Arctic aerosol number size distributions: seasonality and transport patterns. Atmos. Chem. Phys., 17, 8101–8128, 2017.

Giamarelou, M., Eleftheriadis, K., Nyeki, S., Tunved, P., Torseth, K. and Biskos, G.: Indirect evidence of the composition of nucleation mode atmospheric particles in the high Arctic. Journal of Geophysical Research: Atmospheres, 121, 965-975, 2016.

Galloway, J.N., Savoie, D.L., Keene, W.C. and Prospero, J.M.: The temporal and spatial variability of scavenging ratios for NSS sulfate, nitrate, methanesulfonate and sodium in the atmosphere over the North Atalantic Ocean. Atmospheric Environment. Part A. General Topics, 27, 235-250, 1993.

Graversen, R.G. and Wang, M.: Polar amplification in a coupled climate model with locked albedo. Climate Dynamics, 33, 629-643, 2009.

Gysel, M., McFiggans, G.B. and Coe, H.: Inversion of tandem differential mobility analyser (TDMA) measurements. Journal of Aerosol Science, 40, 134-151, 2009.

Gysel, M., and Stratmann, F.: WP3 – NA3: In-situ chemical, physical and optical properties of aerosols, Deliverable D3.11: Standardized protocol for CCN measurements, Tech. rep., accessed online http://www.actris.net, 25 May, 2019.

Heintzenberg, J., Tunved, P., Galí, M. and Leck, C.: New particle formation in the Svalbard region 2006--2015. Atmospheric Chemistry and Physics, 17, 2017.

Herenz, P., Wex, H., Mangold, A., Laffineur, Q., Gorodetskaya, I.V., Fleming, Z.L., Panagi, M. and Stratmann, F.: CCN measurements at the Princess Elisabeth Antarctica research station during three austral summers. Atmospheric Chemistry and Physics, 19, 275-294, 2019.

Hirsikko, A., Bergman, T., Laakso, L., Maso, M.D., Riipinen, I., Hõrrak, U. and Kulmala, M.: Identification and classification of the formation of intermediate ions measured in boreal forest. Atmospheric Chemistry and Physics, 7, 201-210, 2007.

Huang, S., Wu, Z., Poulain, L., van Pinxteren, M., Merkel, M., Assmann, D., Herrmann, H., and Wiedensohler, A.: Source apportionment of the organic aerosol over the Atlantic Ocean from 53° N to 53° S: significant contributions from marine emissions and long-range transport. Atmospheric Chemistry and Physics, 18, 18043–18062, 2018.

Jayaratne, E.R., Pushpawela, B. and Morawska, L.: Temporal evolution of charged and neutral nanoparticle concentrations during atmospheric new particle formation events and its implications for ion-induced nucleation. Frontiers of Environmental Science & Engineering, 10, 13, 2016.

Jeffries, M.O. and Richter-Menge, J.: State of the climate in 2011: The Arctic. Bull. Am. Meteorol. Soc, 93, 127-148, 2012.

Jokinen, T., Sipilä, M., Kontkanen, J., Vakkari, V., Tisler, P., Duplissy, E.M., Junninen, H., Kangasluoma, J., Manninen, H.E., Petäjä, T. and Kulmala, M.: Ion-induced sulfuric acid–ammonia nucleation drives particle formation in coastal Antarctica. Science advances, 4, 9744, 2018.

Karl, M., Leck, C., Gross, A. and Pirjola, L.: A study of new particle formation in the marine boundary layer over the central Arctic Ocean using a flexible multicomponent aerosol dynamic model. Tellus B: Chemical and Physical Meteorology, 64, 17158, 2012.

Karl, M., Leck, C., Coz, E. and Heintzenberg, J.: Marine nanogels as a source of atmospheric nanoparticles in the high Arctic. Geophysical Research Letters, 40, 3738-3743, 2013.

Keene, W. C., Maring, H., Maben, J. R., Kieber, D. J., Pszenny, A. A. P., Dahl, E. E., Izaguirre, M. A., Davis, A. J., Long, M. S., Zhou, X., et al.: Chemical and Physical Characteristics of Nascent Aerosols Produced by Bursting Bubbles at a Model Air-Sea Interface. Journal of Geophysical Research: Atmospheres, 112, 2007.

Kerminen, V.M., Aurela, M., Hillamo, R.E. and Virkkula, A.: Formation of particulate MSA: deductions from size distribution measurements in the Finnish Arctic. Tellus B, 49, 159-171, 1997.

Kerminen, V.M., Paramonov, M., Anttila, T., Riipinen, I., Fountoukis, C., Korhonen, H., Asmi, E., Laakso, L., Lihavainen, H., Swietlicki, E. and Svenningsson, B.: Cloud condensation nuclei production associated with atmospheric nucleation: a synthesis based on existing literature and new results. Atmospheric Chemistry and Physics, 12, 12037-12059, 2012.

Kerminen, V.M., Chen, X., Vakkari, V., Petäjä, T., Kulmala, M. and Bianchi, F.: Atmospheric new particle formation and growth: review of field observations. Environmental Research Letters, 13, 103003, 2018.

Kim, J., Ahlm, L., Yli-Juuti, T., Lawler, M., Keskinen, H., Tröstl, J., Schobesberger, S., Duplissy, J., Amorim, A., Bianchi, F. and Donahue, N.M.: Hygroscopicity of nanoparticles produced from homogeneous nucleation in the CLOUD experiments. Atmospheric Chemistry and Physics, 16, 293-304, 2016.

Knudsen, E.M., Heinold, B., Dahlke, S., Bozem, H., Crewell, S., Gorodetskaya, I.V., Heygster, G., Kunkel, D., Maturilli, M., Mech, M. and Viceto, C.: Meteorological conditions during the ACLOUD/PASCAL field campaign near Svalbard in early summer 2017. Atmospheric Chemistry and Physics, 18, 17995-18022, 2018.

Köhler, H.: The nucleus in and the growth of hygroscopic droplets. Transactions of the Faraday Society, 32, 1152-1161, 1936.

Köllner, F., Schneider, J., Willis, M.D., Klimach, T., Helleis, F., Bozem, H., Kunkel, D., Hoor, P., Burkart, J., Leaitch, W.R. and Aliabadi, A.A.: Particulate trimethylamine in the summertime Canadian high Arctic lower troposphere. Atmospheric Chemistry and Physics, 17, 13747-13766, 2017.

Kulmala, M., Petäjä, T., Nieminen, T., Sipilä, M., Manninen, H.E., Lehtipalo, K., Dal Maso, M., Aalto, P.P., Junninen, H., Paasonen, P. and Riipinen, I.: Measurement of the nucleation of atmospheric aerosol particles. Nature protocols, 7, 1651, 2012.

Kulmala, M., Maso, M.D., Mäkelä, J.M., Pirjola, L., Väkevä, M., Aalto, P., Miikkulainen, P., Hämeri, K. and O'dowd, C.D.: On the formation, growth and composition of nucleation mode particles. Tellus B, 53, 479-490, 2001.

Kyrö, E.M., Kerminen, V.M., Virkkula, A., Maso, M.D., Parshintsev, J., Ruíz-Jimenez, J., Forsström, L., Manninen, H.E., Riekkola, M.L., Heinonen, P. and Kulmala, M.: Antarctic new particle formation from continental biogenic precursors. Atmospheric Chemistry and Physics, 13, 3527-3546, 2013.

Leaitch, W.R., Sharma, S., Huang, L., Toom-Sauntry, D., Chivulescu, A., Macdonald, A.M., Salzen, K. von ., Pierce, J.R., Bertram, A.K., Schroder, J.C., Shantz, N.C., Chang, R.Y.-W., and Norman, A.-L.: Dimethyl sulfide control of the clean summertime Arctic aerosol and cloud. Elem Sci Anth, 1, 2013.

Leaitch, W.R., Korolev, A., Aliabadi, A.A., Burkart, J., Willis, M.D., Abbatt, J.P., Bozem, H., Hoor, P., Köllner, F., Schneider, J. and Herber, A.: Effects of 20–100 nm particles on liquid clouds in the clean summertime Arctic. Atmospheric Chemistry and Physics, 16, 11107-11124, 2016.

Leaitch, W.R., Strapp, J.W., Isaac, G.A. and Hudson, J.G.: Cloud droplet nucleation and cloud scavenging of aerosol sulphate in polluted atmospheres. Tellus B: Chemical and Physical Meteorology, 38, 328-344, 1986.

Leck, C., Norman, M., Bigg, E.K. and Hillamo, R.: Chemical composition and sources of the high Arctic aerosol relevant for cloud formation. Journal of Geophysical Research: Atmospheres, 107, 2002.

Lehtinen, K.E., Dal Maso, M., Kulmala, M. and Kerminen, V.M.: Estimating nucleation rates from apparent particle formation rates and vice versa: Revised formulation of the Kerminen–Kulmala equation. Journal of Aerosol Science, 38, 988-994, 2007.

Levasseur, M.: Impact of Arctic meltdown on the microbial cycling of sulphur. Nature Geoscience, 6, 691, 2013.

Macke, A. and Flores, H.: The Expeditions PS106/1 and 2 of the Research Vessel POLARSTERN to the Arctic Ocean in 2017. Berichte zur Polar-und Meeresforschung= Reports on polar and marine research, 719, 2018.

Manninen, H.E., Nieminen, T., Asmi, E., Gagné, S., Häkkinen, S., Lehtipalo, K., Aalto, P., Vana, M., Mirme, A., Mirme, S. and Hõrrak, U.: EUCAARI ion spectrometer measurements at 12 European sites–analysis of new particle formation events. Atmospheric Chemistry and Physics, 10, 7907-7927, 2010.

Manninen, H.E., Franchin, A., Schobesberger, S., Hirsikko, A., Hakala, J., Skromulis, A., Kangasluoma, J., Ehn, M., Junninen, H., Mirme, A. and Mirme, S.: Characterisation of corona-generated ions used in a Neutral cluster and Air Ion Spectrometer (NAIS). Atmospheric Measurement Techniques, 4, 2767-2776, 2011.

Maslanik, J. and Stroeve, J.: Near-Real-Time DMSP SSMIS Daily Polar Gridded Sea Ice Concentrations, 1 Boulder, Colorado USA. NASA National Snow and Ice Data Center Distributed Active Archive Center. doi: https://doi.org/10.5067/U8C09DWVX9LM, 1999 [updated daily, accessed April 26, 2019].

Massling, A., Niedermeier, N., Hennig, T., Fors, E.O., Swietlicki, E., Ehn, M., Hameri, K., Villani, P., Laj, P., Good, N. and McFiggans, G.: Results and recommendations from an intercomparison of six Hygroscopicity-TDMA systems. Atmospheric Measurement Techniques, 2011.

Mauritsen, T., Sedlar, J., Tjernström, M., Leck, C., Martin, M., Shupe, M., Sjogren, S., Sierau, B., Persson, P.O.G., Brooks, I.M. and Swietlicki, E.: An Arctic CCN-limited cloud-aerosol regime. Atmospheric Chemistry and Physics, 11, 165-173, 2011.

Meier, W.N., Hovelsrud, G.K., van Oort, B.E., Key, J.R., Kovacs, K.M., Michel, C., Haas, C., Granskog, M.A., Gerland, S., Perovich, D.K. and Makshtas, A.: Arctic sea ice in transformation: A review of recent observed changes and impacts on biology and human activity. Reviews of Geophysics, 52, 185-217, 2014.

Merikanto, J., Spracklen, D.V., Mann, G.W., Pickering, S.J. and Carslaw, K.S.: Impact of nucleation on global CCN. Atmospheric Chemistry and Physics, 9, 8601-8616, 2009.

Mirme, S. and Mirme, A.: The mathematical principles and design of the NAIS–a spectrometer for the measurement of cluster ion and nanometer aerosol size distributions. Atmospheric Measurement Techniques, 6, 1061-1071, 2013.

Mirme, A., Tamm, E., Mordas, G., Vana, M., Uin, J., Mirme, S., Bernotas, T., Laakso, L., Hirsikko, A. and Kulmala, M.: A wide-range multi-channel Air Ion Spectrometer, 2007.

Miyazaki, Y., Kawamura, K. and Sawano, M.: Size distributions of organic nitrogen and carbon in remote marine aerosols: Evidence of marine biological origin based on their isotopic ratios. Geophysical Research Letters, 37, 2010.

Müller, K., Lehmann, S., Pinxteren, D.V., Gnauk, T., Niedermeier, N., Wiedensohler, A. and Herrmann, H.: Particle characterization at the Cape Verde atmospheric observatory during the 2007 RHaMBLe intensive. Atmospheric Chemistry and Physics, 10, 2709-2721, 2010.

Napari, I., Noppel, M., Vehkamäki, H. and Kulmala, M.: Parametrization of ternary nucleation rates for H2SO4-NH3-H2O vapors. Journal of Geophysical Research: Atmospheres, 107, 6, 2002.

Nguyen, Q.T., Glasius, M., Sørensen, L.L., Jensen, B., Skov, H., Birmili, W., Wiedensohler, A., Kristensson, A., Nøjgaard, J.K. and Massling, A.: Seasonal variation of atmospheric particle number concentrations, new particle formation and atmospheric oxidation capacity at the high Arctic site Villum Research Station, Station Nord. Atmospheric Chemistry and Physics, 16, 11319-11336, 2016.

Nicolaus, M.: Shipborne visual observations of Arctic sea ice during POLARSTERN cruise PS106. PANGAEA, https://doi.org/10.1594/PANGAEA.889264, 2018.

Nieminen, T., Kerminen, V.M., Petäjä, T., Aalto, P.P., Arshinov, M., Asmi, E., Baltensperger, U., Beddows, D., Beukes, J.P., Collins, D. and Ding, A.: Global analysis of continental boundary layer new particle formation based on long-term measurements. Atmospheric Chemistry and Physics, 18, 14737-14756, 2018.

Orellana, M.V., Matrai, P.A., Leck, C., Rauschenberg, C.D., Lee, A.M. and Coz, E.: Marine microgels as a source of cloud condensation nuclei in the high Arctic. Proceedings of the National Academy of Sciences, 108, 13612-13617, 2011.

Overland, J.E., Wood, K.R. and Wang, M.: Warm Arctic—cold continents: climate impacts of the newly open Arctic Sea. Polar Research, 30, 15787, 2011.

Park, K., Kim, G., Kim, J.S., Yoon, Y.J., Cho, H.J. and Ström, J.: Mixing state of size-selected submicrometer particles in the Arctic in May and September 2012. Environmental science and technology, 48, 909-919, 2013.

Park, K.T., Jang, S., Lee, K., Yoon, Y.J., Kim, M.S., Park, K., Cho, H.J., Kang, J.H., Udisti, R., Lee, B.Y. and Shin, K.H.: Observational evidence for the formation of DMS-derived aerosols during Arctic phytoplankton blooms. Atmospheric Chemistry and Physics, 17, 9665-9675, 2017.

Petters, M.D. and Kreidenweis, S.M.: A single parameter representation of hygroscopic growth and cloud condensation nucleus activity. Atmospheric Chemistry and Physics, 7, 1961-1971, 2007.

Pfeifer, S., Birmili, W., Schladitz, A., Müller, T., Nowak, A. and Wiedensohler, A.: A fast and easy-to-implement inversion algorithm for mobility particle size spectrometers considering particle number size distribution information outside of the detection range. Atmospheric Measurement Techniques, 7, 95-105, 2014.

Pichelstorfer, L., Stolzenburg, D., Ortega, J., Karl, T., Kokkola, H., Laakso, A., Lehtinen, K.E., Smith, J.N., McMurry, P.H. and Winkler, P.M.: Resolving nanoparticle growth mechanisms from size-and time-dependent growth rate analysis. Atmospheric Chemistry and Physics, 18, 1307-1323, 2018.

Pithan, F. and Mauritsen, T.: Arctic amplification dominated by temperature feedbacks in contemporary climate models. Nature Geoscience, 7, 181, 2014.

Polashenski, C., Golden, K.M., Perovich, D.K., Skyllingstad, E., Arnsten, A., Stwertka, C. and Wright, N.: Percolation blockage: A process that enables melt pond formation on first year Arctic sea ice. Journal of Geophysical Research: Oceans, 122, 413-440, 2017.

Praetorius, S., Rugenstein, M., Persad, G. and Caldeira, K.: Global and Arctic climate sensitivity enhanced by changes in North Pacific heat flux. Nature communications, 9, 3124, 2018.

Quinn, P. K., Collins, D. B., Grassian, V. H., Prather, K. A., Bates, T. S.: Chemistry and Related Properties of Freshly Emitted Sea Spray Aerosol. Chemical Reviews 115, 4383–4399, 2015.

Rampal, P., Weiss, J. and Marsan, D.: Positive trend in the mean speed and deformation rate of Arctic sea ice, 1979–2007. Journal of Geophysical Research: Oceans, 114, 2009.

Riccobono, F., Schobesberger, S., Scott, C.E., Dommen, J., Ortega, I.K., Rondo, L., Almeida, J., Amorim, A., Bianchi, F., Breitenlechner, M. and David, A.: Oxidation products of biogenic emissions contribute to nucleation of atmospheric particles. Science, 344, 717-721, 2014.

Roberts, G.C. and Nenes, A.: A continuous-flow streamwise thermal-gradient CCN chamber for atmospheric measurements. Aerosol Science and Technology, 39, 206-221, 2005.

Rothenberg, D. and Wang, C.: Metamodeling of droplet activation for global climate models. Journal of the Atmospheric Sciences, 73, 1255-1272, 2016.

Schobesberger, S., Junninen, H., Bianchi, F., Lönn, G., Ehn, M., Lehtipalo, K., Dommen, J., Ehrhart, S., Ortega, I.K., Franchin, A. and Nieminen, T.: Molecular understanding of atmospheric particle formation from sulfuric acid and large oxidized organic molecules. Proceedings of the National Academy of Sciences, 110, 17223-17228, 2013.

Screen, J.A. and Simmonds, I.: The central role of diminishing sea ice in recent Arctic temperature amplification. Nature, 464, 1334, 2010.

Serreze, M.C. and Barry, R.G.: Processes and impacts of Arctic amplification: A research synthesis. Global and planetary change, 77, 85-96, 2011.

Sipilä, M., Sarnela, N., Jokinen, T., Henschel, H., Junninen, H., Kontkanen, J., Richters, S., Kangasluoma, J., Franchin, A., Peräkylä, O. and Rissanen, M.P.: Molecular-scale evidence of aerosol particle formation via sequential addition of HIO3. Nature, 537, 532, 2016.

Smith, J.N., Barsanti, K.C., Friedli, H.R., Ehn, M., Kulmala, M., Collins, D.R., Scheckman, J.H., Williams, B.J. and McMurry, P.H.: Observations of aminium salts in atmospheric nanoparticles and possible climatic implications. Proceedings of the National Academy of Sciences, 107, 6634-6639, 2010.

Spielhagen, R.F., Werner, K., Sørensen, S.A., Zamelczyk, K., Kandiano, E., Budeus, G., Husum, K., Marchitto, T.M. and Hald, M.: Enhanced modern heat transfer to the Arctic by warm Atlantic water. Science, 331, 450-453, 2011.

Stefels, J., Steinke, M., Turner, S., Malin, G. and Belviso, S.: Environmental constraints on the production and removal of the climatically active gas dimethylsulphide (DMS) and implications for ecosystem modelling. Biogeochemistry, 83, 245-275, 2007.

Ström, J., Engvall, A.C., Delbart, F., Krejci, R. and Treffeisen, R.: On small particles in the Arctic summer boundary layer: observations at two different heights near Ny-Ålesund, Svalbard. Tellus B: Chemical and Physical Meteorology, 61, 473-482, 2009.

Taylor, P.C., Cai, M., Hu, A., Meehl, J., Washington, W. and Zhang, G.J.: A decomposition of feedback contributions to polar warming amplification. Journal of Climate, 26, 7023-7043, 2013.

Tremblay, S., Picard, J.-C., Bachelder, J. O., Lutsch, E., Strong, K., Fogal, P., Leaitch, W. R., Sharma, S., Kolonjari, F., Cox, C. J., Chang, R. Y.-W., and Hayes, P. L.: Characterization of aerosol growth events over Ellesmere Island during the summers of 2015 and 2016. Atmos. Chem. Phys., 19, 5589–5604, 2019.

Tritscher, T., Dommen, J., DeCarlo, P.F., Gysel, M., Barmet, P.B., Praplan, A.P., Weingartner, E., Prévôt, A.S.H., Riipinen, I., Donahue, N.M. and Baltensperger, U.: Volatility and hygroscopicity of aging secondary organic aerosol in a smog chamber. Atmospheric Chemistry and Physics, 11, 11477-11496, 2011.

Turpin, B.J. and Lim, H.J.: Species contributions to PM2.5 mass concentrations: Revisiting common assumptions for estimating organic mass. Aerosol Science & Technology, 35, 602-610, 2001.

Vakkari, V., Tiitta, P., Jaars, K., Croteau, P., Beukes, J.P., Josipovic, M., Kerminen, V.M., Kulmala, M., Venter, A.D., van Zyl, P.G. and Worsnop, D.R.: Reevaluating the contribution of sulfuric acid and the origin of organic compounds in atmospheric nanoparticle growth. Geophysical Research Letters, 42, 10-486, 2015.

Van Pinxteren, M., Barthel, S., Fomba, K. W., Müller, K., Von Tümpling, W., Herrmann, H.: The Influence of Environmental Drivers on the Enrichment of Organic Carbon in the Sea Surface Microlayer and in Submicron Aerosol Particles – Measurements from the Atlantic Ocean. Elementa: Science of the Anthropocene, 5, 35, 2017.

Vavrus, S.: The impact of cloud feedbacks on Arctic climate under greenhouse forcing. Journal of Climate, 17, 603-615, 2004.

Wagner, R., Manninen, H.E., Franchin, A., Lehtipalo, K., Mirme, S., Steiner, G., Petäjä, T. and Kulmala, M.: On the accuracy of ion measurements using a Neutral cluster and Air Ion Spectrometer, 2016.

Wagner, R., Yan, C., Lehtipalo, K., Duplissy, J., Nieminen, T., Kangasluoma, J., Ahonen, L.R., Dada, L., Kontkanen, J., Manninen, H.E. and Dias, A.: The role of ions in new particle formation in the CLOUD chamber. Atmospheric Chemistry and Physics, 17, 15181-15197, 2017.

Walsh, J.E.: Intensified warming of the Arctic: Causes and impacts on middle latitudes. Global and Planetary Change, 117, 52-63, 2014.

Weller, R., Schmidt, K., Teinilä, K. and Hillamo, R.: Natural new particle formation at the coastal Antarctic site Neumayer. Atmospheric Chemistry and Physics, 15, 11399-11410, 2015.

Wendisch, M., Macke, A., Ehrlich, A., Lüpkes, C., Mech, M., Chechin, D., Dethloff, K., Barientos, C., Bozem, H., Brückner, M. and Clemen, H.C.: The Arctic Cloud Puzzle: Using ACLOUD/PASCAL Multi-Platform Observations to Unravel the Role of Clouds and Aerosol Particles in Arctic Amplification. Bulletin of the American Meteorological Society, 2018.

Wentworth, G. R., Murphy, J. G., Croft, B., Martin, R. V., Pierce, J. R., Côté, J.-S., Courchesne, I., Tremblay, J.-É., Gagnon, J., Thomas, J. L., Sharma, S., Toom-Sauntry, D., Chivulescu, A., Levasseur, M., and Abbatt, J. P. D.: Ammonia in the summertime Arctic marine boundary layer: sources, sinks, and implications Atmos. Chem. Phys., 16, 1937–1953, 2016.

Wiedensohler, A.: An approximation of the bipolar charge distribution for particles in the submicron size range. Journal of Aerosol Science, 19, 387-389, 1988.

Wiedensohler, A., Covert, D.S., Swietlicki, E., Aalto, P., Heintzenberg, J. and Leck, C.: Occurrence of an ultrafine particle mode less than 20 nm in diameter in the marine boundary layer during Arctic summer and autumn. Tellus B, 48, 213-222, 1996.

Wiedensohler, A., Birmili, W., Nowak, A., Sonntag, A., Weinhold, K., Merkel, M., Wehner, B., Tuch, T., Pfeifer, S., Fiebig, M. and Fjæraa, A.M.: Mobility particle size spectrometers: harmonization of technical standards and data structure to facilitate high quality long-term observations of atmospheric particle number size distributions. Atmospheric Measurement Techniques, 5, 657-685, 2012.

Wiedensohlet, A., Orsini, D., Covert, D.S., Coffmann, D., Cantrell, W., Havlicek, M., Brechtel, F.J., Russell, L.M., Weber, R.J., Gras, J. and Hudson, J.G.: Intercomparison study of the size-dependent counting efficiency of 26 condensation particle counters. Aerosol Science and Technology, 27, 224-242, 1997.

Wiedensohler, A., Wiesner, A., Weinhold, K., Birmili, W., Hermann, M., Merkel, M., Müller, T., Pfeifer, S., Schmidt, A., Tuch, T. and Velarde, F.: Mobility particle size spectrometers: Calibration procedures and measurement uncertainties. Aerosol Science and Technology, 52, 146-164, 2018.

Willis, M.D., Burkart, J., Thomas, J.L., Köllner, F., Schneider, J., Bozem, H., Hoor, P.M., Aliabadi, A.A., Schulz, H., Herber, A.B. and Leaitch, W.R.: Growth of nucleation mode particles in the summertime Arctic: a case study. Atmospheric Chemistry and Physics, 16, 7663-7679, 2016.

Willis, M.D., Köllner, F., Burkart, J., Bozem, H., Thomas, J.L., Schneider, J., Aliabadi, A.A., Hoor, P.M., Schulz, H., Herber, A.B. and Leaitch, W.R.: Evidence for marine biogenic influence on summertime Arctic aerosol. Geophysical Research Letters, 44, 6460-6470, 2017.

Willis, M.D., Leaitch, W.R. and Abbatt, J.P.: Processes controlling the composition and abundance of Arctic aerosol. Reviews of Geophysics, 56, 621-671, 2018.

Yu, F.: Ion-mediated nucleation in the atmosphere: Key controlling parameters, implications, and look-up table. Journal of Geophysical Research: Atmospheres, 115, 2010.

Zhang, W., Miller, P.A., Jansson, C., Samuelsson, P., Mao, J. and Smith, B.: Self-Amplifying Feedbacks Accelerate Greening and Warming of the Arctic. Geophysical Research Letters, 45, 7102-7111, 2018.

Zhou, J., Swietlicki, E., Berg, O.H., Aalto, P.P., Hämeri, K., Nilsson, E.D. and Leck, C.: Hygroscopic properties of aerosol particles over the central Arctic Ocean during summer. Journal of Geophysical Research: Atmospheres, 106, 32111-32123, 2001.

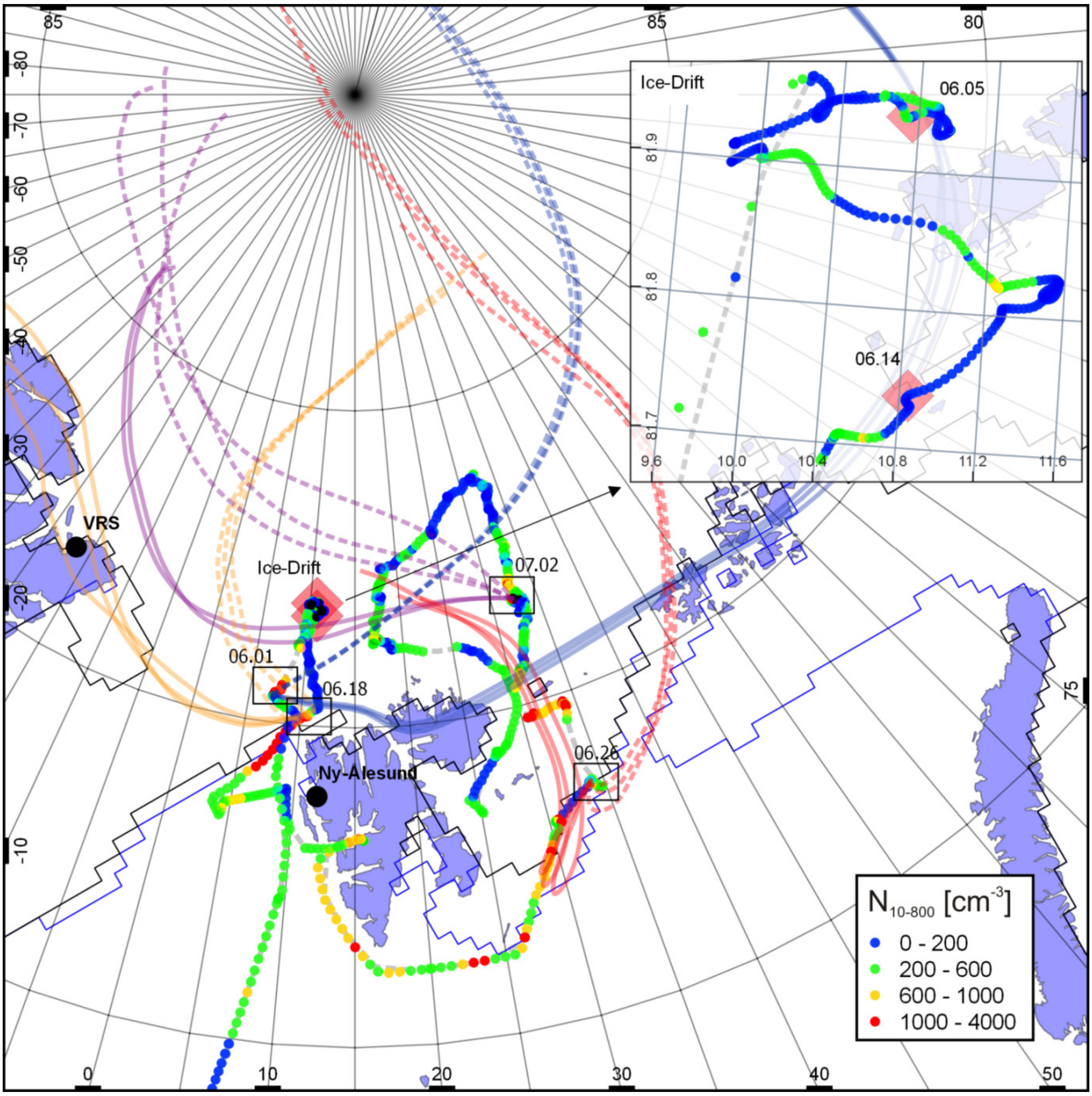

Figure 1: Cruise track and particle number concentration (integrated in a size range from 10 to 800 nm) during PASCAL and SiPCA expeditions. The days, which were picked to analyze NPF events and subsequent particle growth, are indicated with square boxes. Backward air mass trajectories (72 hours) were calculated using HYSPLIT (Draxler and Rolph, 2012), and are shown by solid (200 m a.s.l) and dotted (2000 m a.s.l) lines corresponding each NPF event. Ice-drift is shown in the insert. Thin blue and black lines are the observed ice-edge for June and July, 2017, respectively (Fetterer et al., 2002).

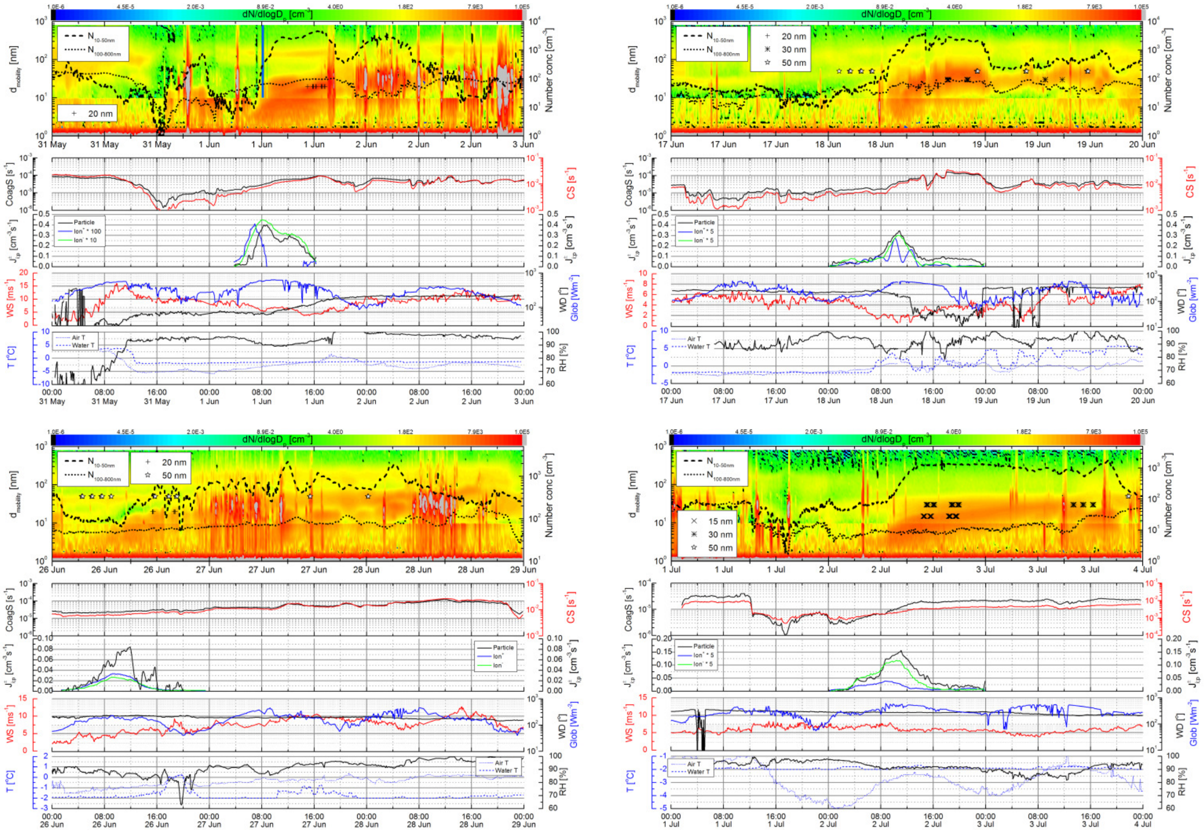

Figure 2: The NPF events observed during RV Polarstern cruise PS106. The PNSDs from NAIS (negative polarity) and MPSS are shown as contour plots. The color scale represents particle number concentration as *dN/dlogD$_p$*. Inside the contour plots, particle number concentration, integrated between two size ranges (10 to 50 nm and 100 to 800 nm) is shown with dashed and dotted black lines. The presence of corona charger ions (<2 nm, Manninen et al., 2011) can also be seen in NAIS data. This artefact was excluded from data analysis. Coagulation and condensation sinks, meteorological parameters (wind speed and direction, global radiation, temperature, and relative humidity), and formation rates (*J*) for each NPF event are shown in the panels below the contour plots. Note: sample contamination by ship exhaust was removed from data analysis, however, for better representation of particle growth, the contour plots include all the data (contamination not removed).

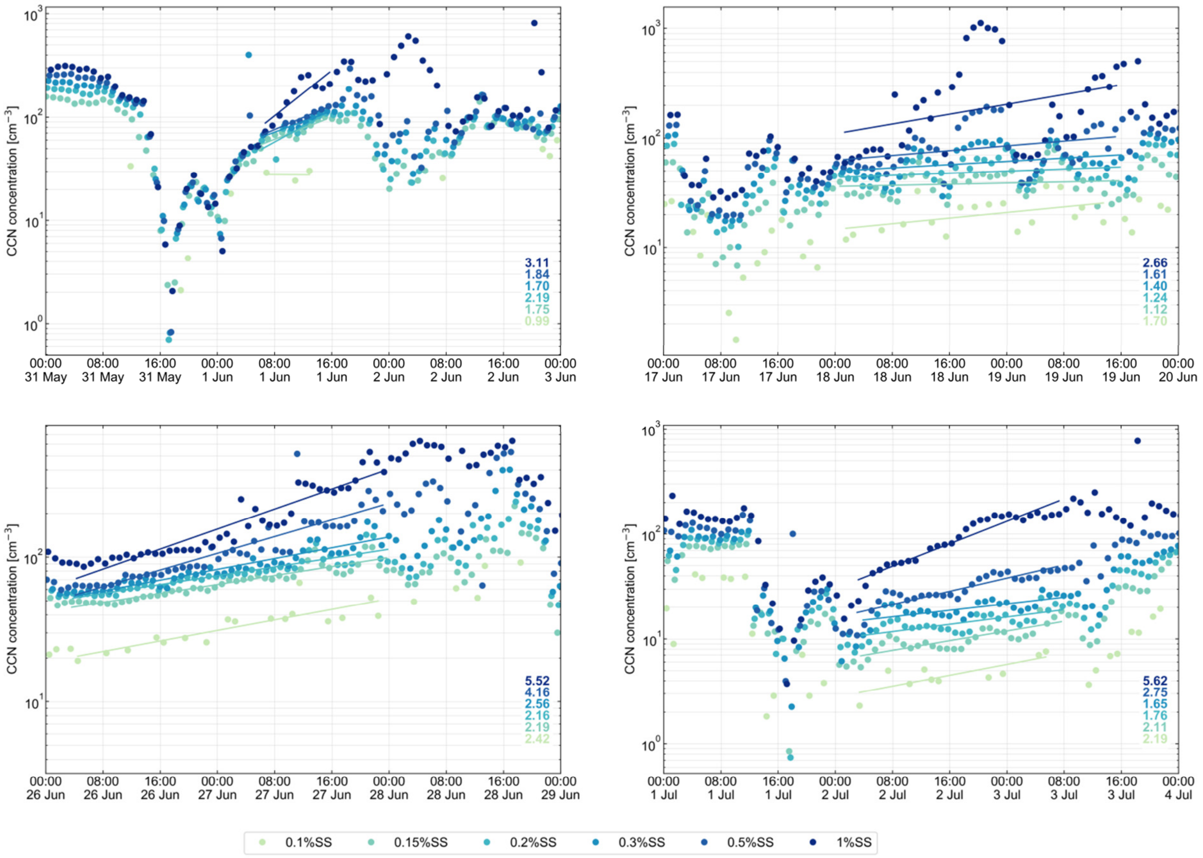

Figure 3: The CCN number concentration measured during NPF events (1 to 4). The lines and corresponding values show the increase in CCN concentrations (prior NPF vs. particles have grown to the Aitken mode).

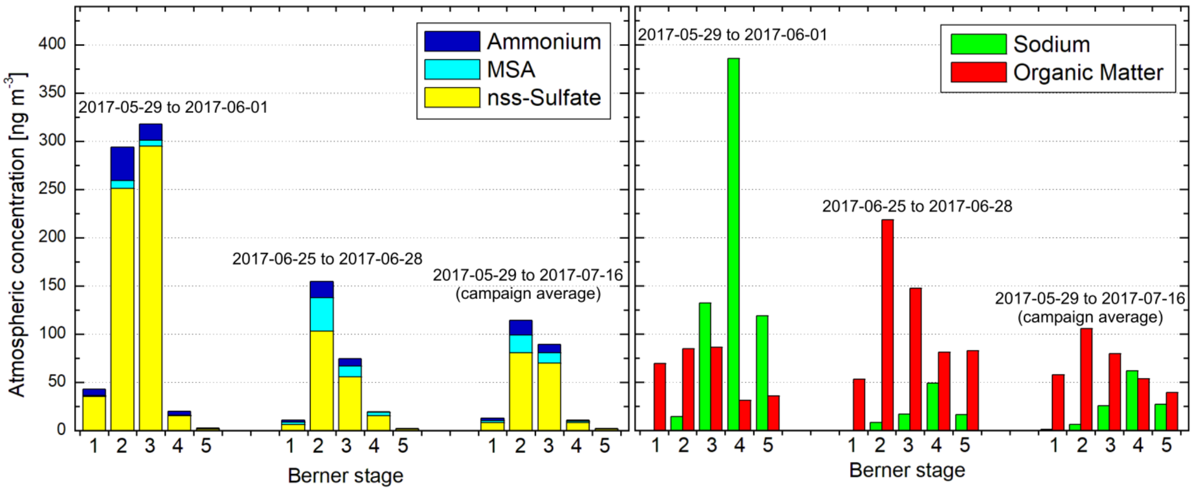

Figure 4: Size-resolved atmospheric concentrations for ammonium, MSA, nss-sulfate, sodium, and OM for two sampling periods and the whole campaign average. Stages 1, 2, 3, 4, and 5 corresponds to aerodynamic particle diameter ranges of 0.05 – 0.14, 0.14 – 0.42, 0.42 – 1.2, 1.2 – 3.5, and 3.5 – 10 µm, respectively.

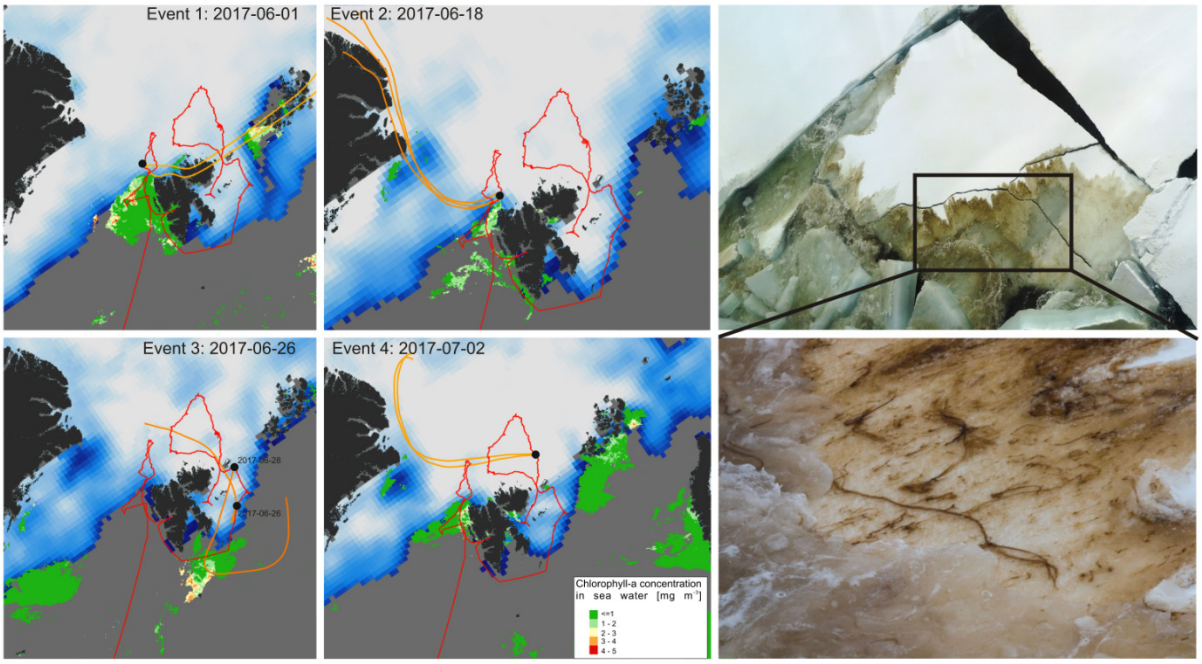

Figure 5: Sea ice concentration (white - 100%, dark blue - 1%; from NASA Worldview; Maslanik and Stroeve, 1999) and chlorophyll-a surface concentration (taken from http://marine.copernicus.eu, accessed 29 April, 2019) during NPF events (left). On the right - the ice alga and diatom *Melosira arctica* (right) observed from the ship deck during the NPF Event 1. RV Polarstern track and location during NPF event is indicated in red line and black circle, respectively. Orange lines mark 72 hour backward air mass trajectory at 200 m.a.s.l.

Table 1: Calculated parameters for observed NPF events during RV Polarstern cruise 106. The GR is obtained from NAIS size spectrum using the methods proposed by Kulmala et al. (2012) and Pichelstorfer et al (2018). J is the formation rate of 1.6-nm sized positive/negative ion clusters and 3-nm sized particles. Please note that in some instances the size range for GR and J calculations is different (due to measured PNSD). Nevertheless, we calculated both parameters from the smallest possible particle/ion size range. Value after "±" shows standard deviation.

Event	**Date (of 2017)**	**Ship position**	**GR [nm h^{-1}] (size range)**		
			Particle (3-7 nm)	Ion$^+$	Ion$^-$
1.	06-01	80.4N; 7.2S	1.2 ± 0.05	1.43 (1.6-4 nm)	0.66 (1.6-3 nm)
2.	06-18	80.2N; 10.7S	4.25 ± 0.89	3.30 (4-9 nm)	2.90 (1.6-3 nm)
3.	06-26	78.4N; 33.4S	0.62 ± 0.16	2.16 (2-6 nm)	1.22 (1.6-3 nm)
4.	07-02	81.6N; 33.3S	0.88 ± 0.01	3.43 (1.6-4 nm)	1.49 (2-3 nm)
			J [cm^{-3} s^{-1}]		
			Particle (J_3)	Ion$^+$	Ion$^-$
1.	06-01	80.4N; 7.2S	0.39±0.05	0.004 ($J_{1.6-}$)	0.045 ($J_{1.6-}$)
2.	06-18	80.2N; 10.7S	0.35±0.03	0.054 (J_{4-})	0.060 ($J_{1.6-}$)
3.	06-26	78.4N; 33.4S	0.08±0.01	0.033 (J_{2-})	0.026 ($J_{1.6-}$)
4.	07-02	81.6N; 33.3S	0.15±0.01	0.007 ($J_{1.6-}$)	0.023 (J_{2-})

Table 2: Hygroscopic growth factor (at 90% RH) and hygroscopicity parameter κ during NPF events. Here, Time of scans - a time window during which hygroscopicity distributions were measured; t_J - approx. time between the observed formation rate maximum and the measurements of HGF. In other words, t_J indicates how long before/after the NPF events the HGF was measured. For example, if $t_J = 7$, the HGF was measured 7 hours after the maximum in J. Negative t_J indicates the measurements of HGF prior NPF event; d_0 - selected diameter of dry particles; N_{scans} - number of scans; sd - standard deviation.

Time of scans	**t_J [h]**	**d_0 [nm]**	**HGF±sd**	**κ±sd**	**N_{scans}**
Event 1					
06.01 15:00 - 17:41	7.0	20	1.46±0.02	0.41±0.02	11
Event 2					
06.18 12:14 - 16:52	1.6	20	1.17±0.02	0.13±0.00	10
06.18 18:11 - 21:21	7.6	30	1.17±0.02	0.11±0.00	6
06.19 09:06 - 11:44	22.5	30	1.43±0.05	0.36±0.08	3
06.18 01:39 - 06:45	-8.9	50	1.36±0.08	0.24±0.07	10
06.18 22:40 - 22:50	12.1	50	1.26±0.04	0.16±0.04	3
06.19 06:07 - 06:18	19.5	50	1.25±0.01	0.16±0.00	3
06.19 15:31 - 15:42	29.0	50	1.33±0.01	0.21±0.00	3
Event 3					
06.26 15:18 - 18:47	6.1	20	1.16±0.01	0.12±0.02	6
06.26 04:29 - 19:04	-4.8	50	1.28±0.03	0.16±0.03	20
06.27 15:21 - 15:32	30.1	50	1.48±0.09	0.33±0.06	4
06.28 00:12 - 00:17	39.1	50	1.55±0.01	0.38±0.00	2
Event 4					
07.02 14:27 - 19:38	4.0	15	1.34±0.01	0.33±0.02	18
07.02 14:56 - 19:58	4.5	30	1.46±0.02	0.35±0.01	16
07.03 13:20 - 16:30	26.9	30	1.53±0.04	0.42±0.03	9
07.03 21:43 - 21:54	35.3	50	1.44±0.02	0.34±0.04	2

Table 3: Input parameters and the results from parcel model (Rothenberg and Wang, 2016). Here, P – pressure (Pascal), T – temperature (Kelvin), RH – relative humidity (%), GMD – geometric mean diameter of two modes fitted to PNSD (in nanometers); N – number concentration of particles in the mode (in particles per cubic centimeter), κ - hygroscopicity parameter kappa (derived for particle sizes indicated in bracket), σ - is the shape parameter (standard deviation of the log of the distribution), $N_{CCN,0.1}$ and $N_{CCN,3.2}$ is the number concentration of CCN at two different vertical wind velocities, 0.1 and 3.2 m s^{-1}. Note: κ for specific GMDs was adopted from the nearest value of measured 15, 20, 30, 50, and 150 nm particle hygroscopicity. For example, hygroscopicity of 20 nm particles was used as an input value for GMD of 16 nm mode particles.

Time	P [Pa]	T [K]	RH [%]	GMD [nm]	N [cm^{-3}]	κ	σ	$N_{CCN,0.1}$ [cm^{-3}]	$N_{CCN,3.2}$ [cm^{-3}]
2017-06-01 12:00-16:00	102715	271.5	92.0	16	3411	0.41(20)	1.4	0	1058
				144	112	0.52(150)	1.8	100	112
2017-06-18 12:00-16:00	100868	272.7	91.0	23	2574	0.13(20)	2.2	104	900
				194	33	0.28(150)	1.7	32	33
2017-06-18 20:00-21:00	100839	273.6	94.6	38	2614	0.11 (30)	1.9	156	1404
				184	44	0.25(150)	1.8	41	44
2017-06-19 08:00-12:00	100887	273.3	94.2	33	415	0.36(30)	1.9	43	327
				150	66	0.25(150)	2.7	47	64
2017-06-19 15:00-17:00	100958	272.7	97.3	44	491	0.21(50)	1.7	86	435
				162	31	0.25(150)	2.0	28	31
2017-06-26 04:00-12:00	100830	272.0	87.8	40	69	0.16(50)	1.8	0	0
				143	58	0.37(150)	2.0	0	0
2017-06-26 15:30-16:30	100772	272.4	85.0	13	588	0.12(20)	1.8	0	0
				151	66	0.37(150)	2.2	0	0
2017-06-28 00:00-01:00	100422	272.9	93.8	43	503	0.38(50)	1.8	55	448
				164	89	0.39(150)	2.2	69	88
2017-07-02 16:00-20:00	101417	270.4	91.7	13	1121	0.33(15)	1.8	17	344
				112	20	0.56(150)	2.1	18	20
2017-07-03 08:00-10:00	101382	271.4	84.4	25	814	0.42(30)	1.9	0	0
				101	27	0.65(150)	3.0	0	0
2017-07-03 21:00-23:00	101039	270.2	93.9	35	207	0.34(50)	2.0	40	178
				125	55	0.65(150)	1.9	50	55